



Hochschule Karlsruhe
Technik und Wirtschaft
UNIVERSITY OF APPLIED SCIENCES

Bachelor's Thesis

Development of a conditioned sensing Adapter for Hot Surface Ignition Systems

01.03.2017 – 01.08.2017

Student:

Alejandro Lombardía González; Matr.-Nr.: 60312

Supervisor Hochschule Karlsruhe:

Prof. Dr.-Ing. Maurice Kettner

Supervisor IKKU:

Fino Scholl, M. Sc.

Engine Technology Research Group of the Institute of Refrigeration, Air Conditioning and Environmental Engineering (IKKU)

Task of the Thesis

The aim of this bachelor's thesis is to design a conditioned sensing adapter for Hot Surface Ignition (HSI) Systems, which will be used to test different ceramic glow plugs (CGP) while they are under operation inside the engine. This new adapter must be able to measure both the temperature of the CGP's tip and the temperature at the inside of the adapter, while having a cooling system at the same time. In order to measure the temperature at the CGP's tip a pyrometer will be used, so the adapter must include a sapphire, it being the lens for the measuring device.

By doing so, new mathematical expressions can be derived for future applications since the temperature at the adapter's body and at the tip are known, and those mathematical expressions used until this day which made assumptions on which would be the temperature at the tip of the CGP, on this research department, will be now able to be checked.

This thesis also includes all the experiments required in order to ensure that the chosen design will work effectively and that it will not fail after short time of operation, the manufacturing plan that has to be followed in order to properly manufacture the needed parts for the assembly of the adapter, as well as the research for parts or tools needed to achieve the entire success of the project, from its design phase until its assembly phase.

Declaration of Originality

I hereby declare that this thesis and the work reported herein was composed by and originated entirely from me. Information derived from the published and unpublished work of others has been acknowledged in the text and references are given in the list of sources.

Place and Date

Signature

Alejandro Lombardía González

Acknowledgments

I would like to offer my gratitude to the Hochschule Karlsruhe, my supervisor in the Hochschule Karlsruhe, Prof. Dr.-Ing. Maurice Kettner, and my supervisor at the IKKU, Fino Scholl, M. Sc., for the opportunity they gave me to work on this project and for their assistance throughout the development of this bachelor's thesis.

I would like to thank my tutor and coordinator at the EPI-Gijón (University of Oviedo), Prof. Miguel Ángel José Prieto for making possible this experience and for his understanding and help.

I dedicate a special gratitude to my family, which has made a big effort to give me the opportunity to study this Mechanical Engineer degree and has always supported me with their love, sacrifice and trust.

I dedicate also, a special gratitude to my girlfriend Laura, who has always trusted and supported me, not only for this project but for everything we have experienced since we first met.

Karlsruhe, August 2017

Alejandro Lombardía González

Resumen del proyecto en español

Título: Desarrollo de un adaptador con refrigeración para sistemas de ignición de superficie caliente (bujías incandescentes)

Realizado por: Alejandro Lombardía González

Lugar y fecha: Hochschule Karlsruhe Technik und Wirtschaft; curso 2016 / 2017.

El objetivo de este proyecto es diseñar un adaptador con refrigeración para bujías incandescentes, el cuál será usado para probar diferentes bujías cerámicas de incandescencia cuando estén trabajando en los motores de la Universidad. Este nuevo adaptador ha de ser capaz, además, de medir la temperatura de la punta de la bujía y las temperaturas dentro del mismo. Con el fin de medir la temperatura de la punta de la bujía se utilizará un pirómetro, que estará conectado a un zafiro dentro del adaptador que funcionará como lente para el mismo. Una vez el proyecto esté finalizado, las expresiones matemáticas derivadas hasta entonces, las cuales partían de suposiciones acerca de estas temperaturas, podrían ser comprobadas, y así poder derivar nuevas expresiones.

Este proyecto además incluye todos los experimentos científicos llevados a cabo en el laboratorio, para probar el funcionamiento de las bujías y para cerciorarse de que el modelo elegido para el nuevo adaptador funcionará correctamente y no fallará a las pocas horas de funcionamiento; además, incluye también toda la investigación realizada en busca de partes, herramientas o software necesario para el desarrollo del nuevo adaptador, desde su fase de diseño hasta la fase de montaje una vez fabricado.

Una vez finalizada la documentación inicial para conocer el funcionamiento de las bujías incandescentes, la fase experimental dio comienzo. Esta fase experimental formó parte de un proyecto de investigación, *Analysis of the Thermo-electrical Behaviour of Ceramic Glow Plugs by Alejandro Lombardía González*, en el cual las bujías cerámicas serían sometidas a pruebas para extraer la máxima información posible de ellas y, de ese modo conocer sus comportamientos eléctricos y térmicos.

Como primer paso para esta fase de investigación inicial, una mesa de ensayos fue construida en el laboratorio de manera que se pudiesen asegurar la reproducibilidad de los resultados. Para la construcción de esta mesa de ensayos fue necesario: un bloque metálico para simular el bloque motor donde las bujías y el adaptador estarían colocadas; las propias bujías; una fuente de alimentación con el circuito eléctrico necesario para alimentar la bujía; y cables coaxiales conectados a los ordenadores del laboratorio para extraer la información gracias al software de los mismos. En esta fase de investigación, el software utilizado fue: LabVIEW , DEWESoft, ADbasic. Gracias a los programas, que habían sido creados previamente a este proyecto, se pudieron realizar los experimentos de una forma más automática. La mesa de ensayos creada para los experimentos se puede ver en la siguiente imagen.

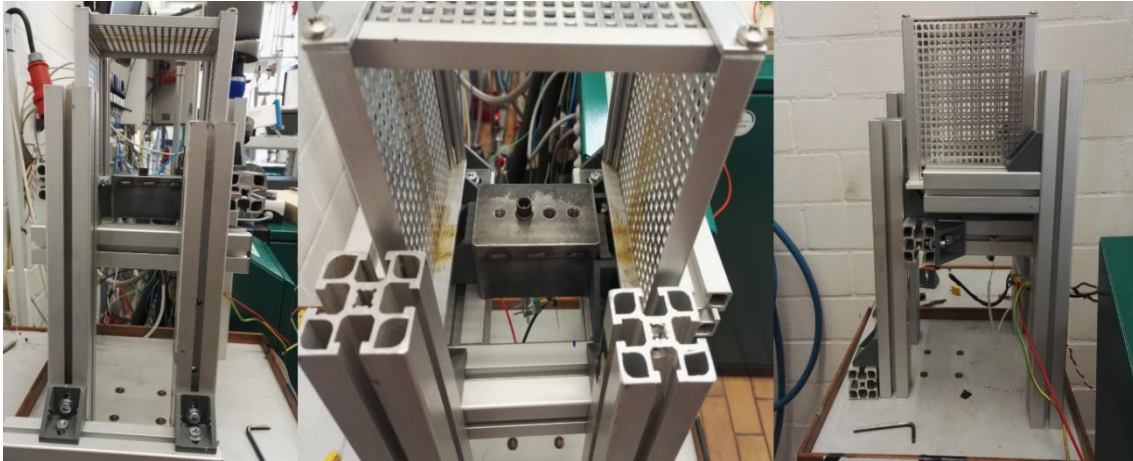


Ilustración 1. Mesa de ensayos construida para el desarrollo de los distintos experimentos del proyecto.

El primer experimento que se llevó a cabo fue para conocer la resistencia en frío de las bujías con y sin el adaptador; la resistencia en frío R_0 indica la resistencia eléctrica de una bujía de incandescencia tiene por sí sola, la resistencia eléctrica que tiene cuando un voltaje muy pequeño se aplica hasta condiciones de estacionarias o cuando un voltaje es aplicado durante un breve periodo de tiempo. Para obtener estos valores de R_0 , se llevaron a cabo dos pruebas, cuya eficiencia y comparabilidad había sido probada previamente en el proyecto de investigación mencionado antes, por un lado, se aplicaría un voltaje a las bujías de 5V durante 5ms, y por otro, se aplicaría un voltaje de 0.5 V hasta alcanzar condiciones estacionarias. Dado que todos los resultados obtenidos no son relevantes para el desarrollo del proyecto, a continuación, se muestran unos ejemplos para contextualizar mejor la comparación con el siguiente experimento: la resistencia en frío para la bujía número 1 sin adaptador fue de 195 m Ω , la resistencia en frío de la misma bujía con el adaptador fue de 211.4 m Ω ; la resistencia en frío para la bujía número 16 sin adaptador fue de 202.1m Ω mientras que su resistencia en frío con el adaptador fue de 211.2 m Ω .

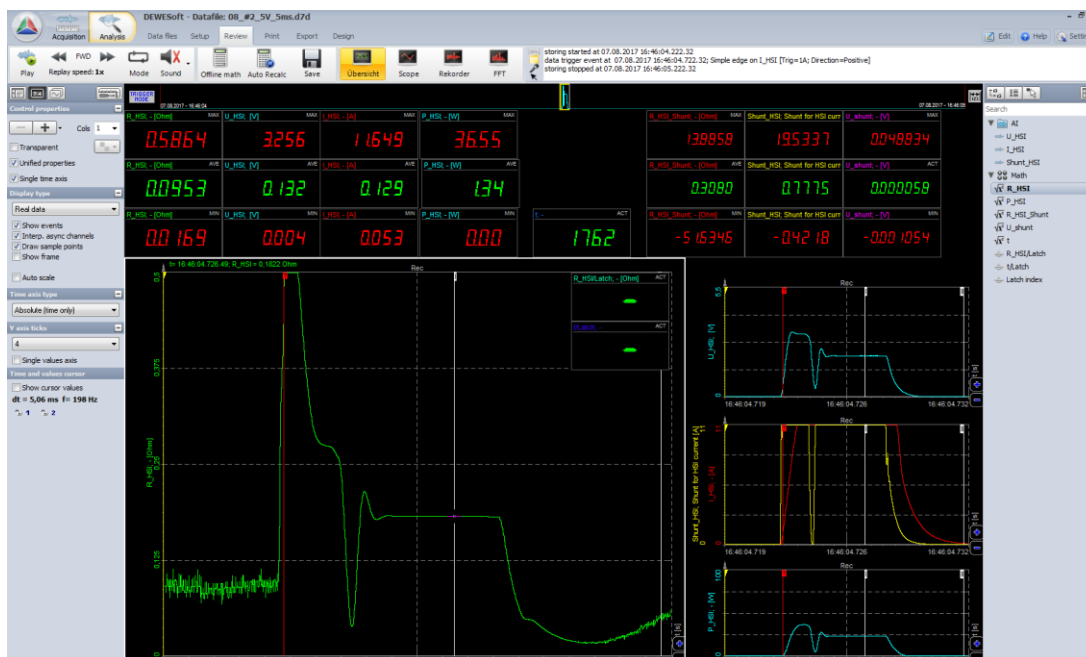


Ilustración 2. Ejemplo de gráfica obtenida en DEWESoft al analizar la resistencia en frío con el método de 5V.

Lo importante para este trabajo de fin de grado, era localizar la fuente de esta resistencia en frío debido a que esta misma sería la encargada a su vez, de generar la resistencia eléctrica total de la bujía, o gran parte de ella, siendo esta a su vez el foco de calor que se debería refrigerar. Para poder localizar este foco de resistencia una bujía fue dividida en dos, en su parte cerámica y en su parte metálica, como se puede ver en la siguiente foto.



Ilustración 3. En la parte superior la parte cerámica (situada dentro del casquillo metálico), en la inferior la parte metálica de una bujía.

Debido a que la resistencia de esta pequeña parte metálica se suponía muy pequeña, un voltaje de tan sólo 0.05 V durante 5 ms fue aplicado, a temperatura ambiente y otro test calentando esta parte hasta llegar a una temperatura cercana a 130 °C, simulando de esta manera las condiciones de trabajo en el motor. Una vez los experimentos fueron finalizados, se concluyó que la mayor

parte de la Resistencia estaba generada en la parte cerámica de la bujía, ya que la parte metálica de la misma sólo había mostrado una resistencia de aproximadamente $5.5 \text{ m}\Omega$, incluso cuando estaba bajo el efecto de la temperatura, cuando la resistencia en frío de una bujía está en un rango comprendido entre $180 \text{ m}\Omega$ y $220 \text{ m}\Omega$. Si se compara este valor con la resistencia en frío obtenida previamente, se puede concluir que la parte en la que la refrigeración del adaptador se debería centrar sería en la parte cerámica de la bujía.

El segundo experimento que fue llevado a cabo serviría para demostrar la relación que hay entre la resistencia en frío de la bujía y las temperaturas del propio adaptador, para ello se utilizaría el adaptador que había sido utilizado hasta entonces, el cuál contaba con tres termopares situados en línea en distintos puntos del interior del adaptador, y cuya posición está indicada en la siguiente foto.

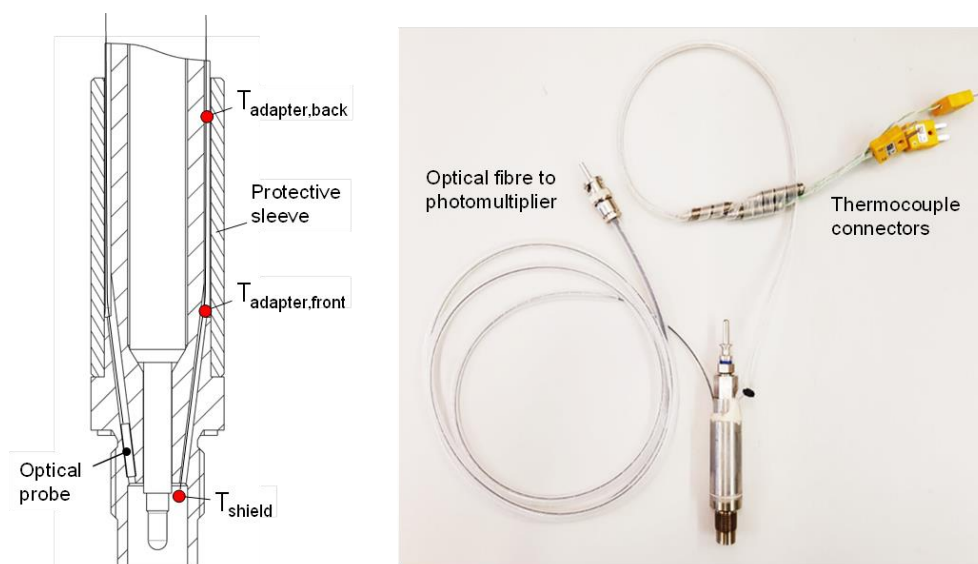


Ilustración 4. Localización de los puntos de temperatura en la izquierda, adaptador actual en la derecha

Para el primer experimento, el cuerpo del adaptador fue calentado con una pistola de aire caliente hasta que las temperaturas de los termopares llegasen a condiciones estacionarias, gracias a que la pistola de aire caliente permitía la regulación de su caudal y temperatura, numerosos puntos pudieron ser evaluados. Como se puede ver en la siguiente gráfica, una vez concluido el experimento se observó que no sólo la resistencia de la bujía tenía una relación directa con la temperatura del adaptador, sino que esta relación era lineal, hecho que facilitaría la derivación matemática que se llevará a cabo en futuros proyectos.

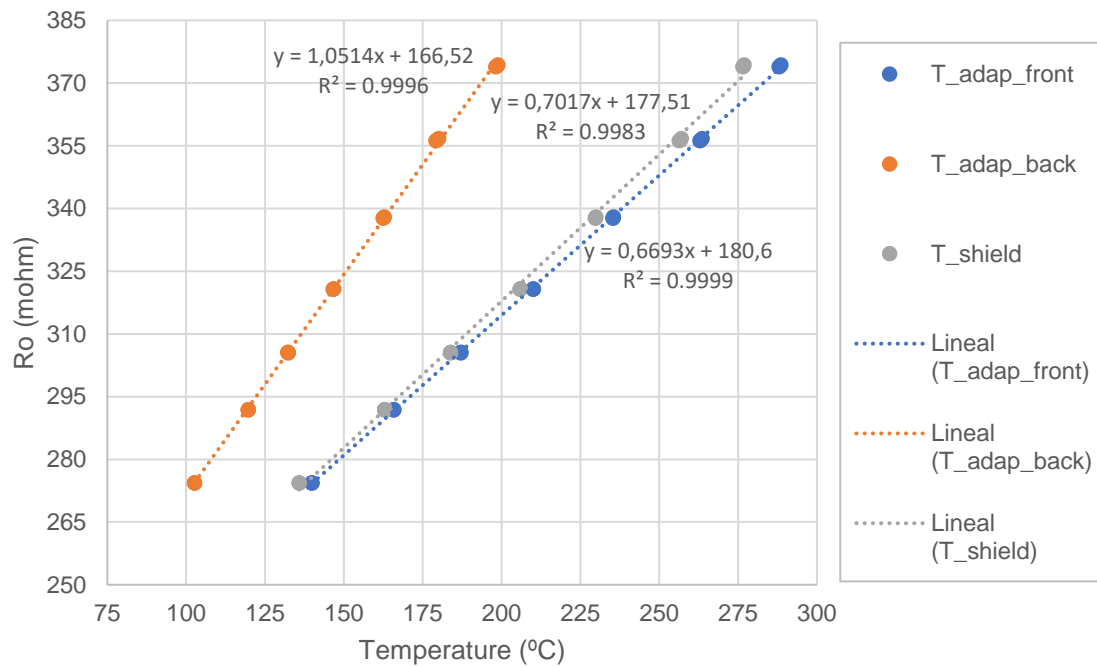


Ilustración 5. Variación de la resistencia en frío con la temperatura del adaptador.

Para el siguiente experimento, el cuerpo del adaptador se calentó de nuevo, esta vez hasta condiciones estacionarias a la máxima temperatura que se podía lograr con la pistola de aire caliente disponible; una vez estas condiciones fueron alcanzadas la pistola de aire caliente se apagó, de manera que las temperaturas del adaptador comenzaron a descender, durante este descenso la resistencia de la bujía fue medida, para comprobar la relación una vez más entre temperatura y resistencia. Para solventar cualquier duda acerca de ello, la temperatura denominada T_{shield} , no aparece en la siguiente gráfica de resultados, debido a que, por cuestiones ajenas a este proyecto, el termopar encargado de medir esta temperatura se rompió durante otro experimento, algo que en realidad no es importante para este proyecto, ya que las temperaturas importantes son aquellas que se encuentran en el adaptador.

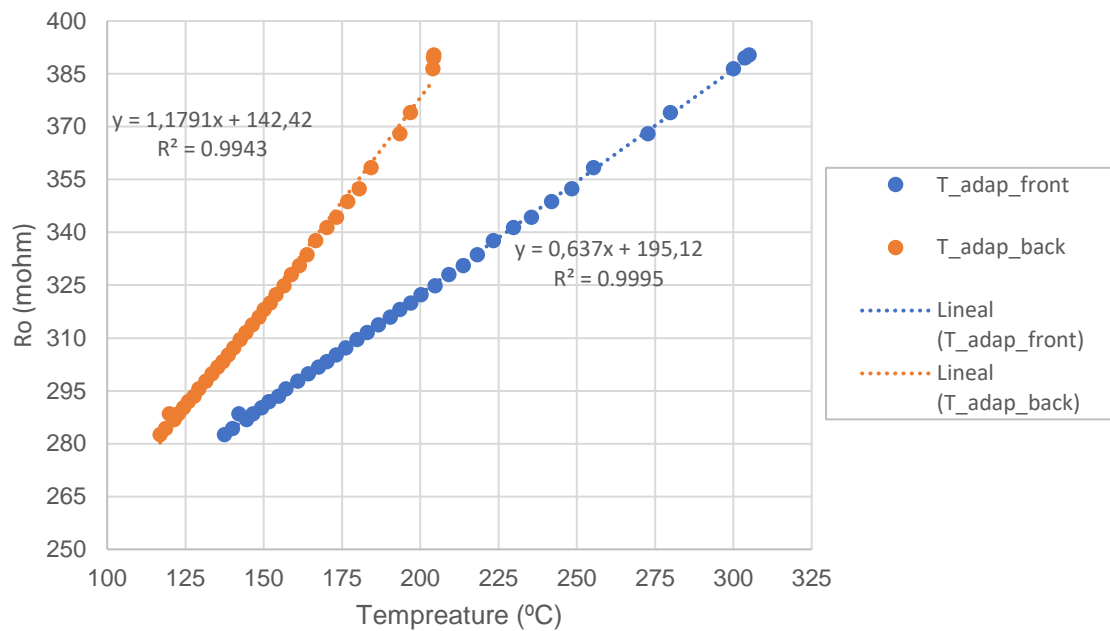


Ilustración 6. Variación de la resistencia en frío cuando se deja el adaptador enfriar.

Una vez más la relación lineal entre resistencia y temperatura habrían sido demostrados.

Como último experimento de investigación, se buscó obtener la distribución de temperaturas en la bujía, para poder lograr esto se utilizó una termo cámara (FLIR T460) para sacar fotos térmicas a la bujía mientras estaba situada en la mesa de ensayos previamente mencionada, a diferentes voltajes. En este experimento se probará, la relación que hay entre la resistencia eléctrica de la bujía R_{HSI} para diferentes voltajes, y cuatro temperaturas que fueron capturadas con la cámara térmica como muestran las siguientes fotos.

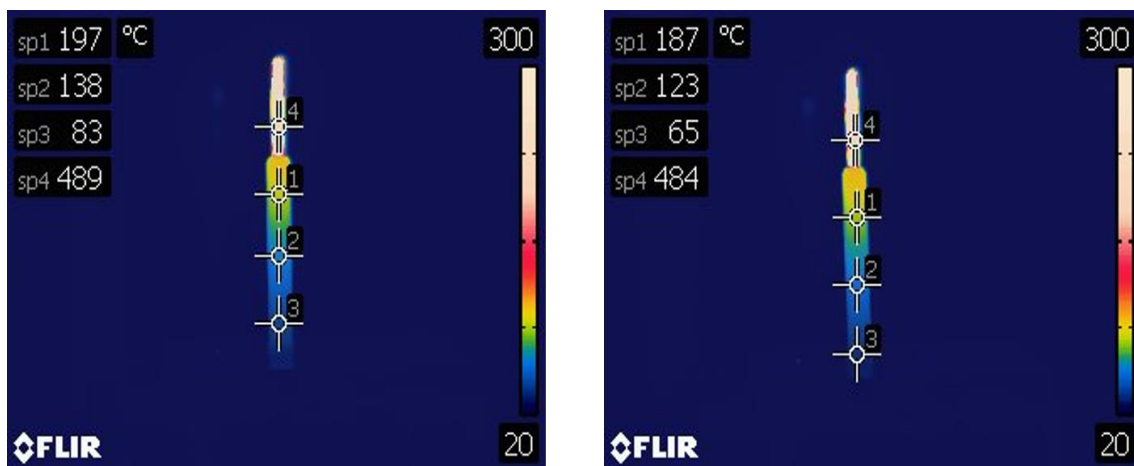


Ilustración 7. Ejemplos de fotografías térmicas obtenidas para ambas bujías utilizadas en estos experimentos. Se observan también los 4 puntos de temperatura medidos.

En este experimento se probaron dos bujías distintas para poder extraer información proveniente de distintas fuentes (designadas por bujía número #10 y bujía número #19 respectivamente). Los resultados del experimento están resumidos en la siguiente gráfica.

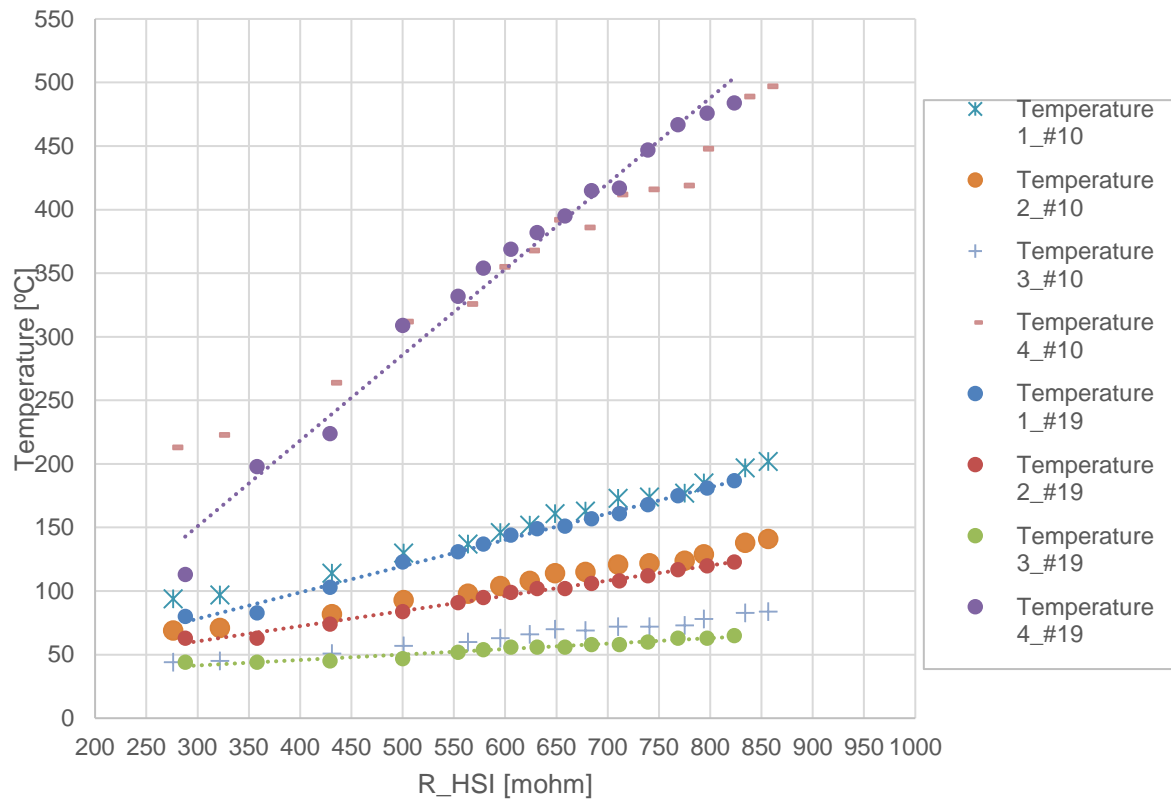


Ilustración 8. Relación entre la resistencia de la bujía y los cuatro puntos de temperatura medidos con la cámara térmica.

Como se puede observar, la relación lineal entre resistencia eléctrica y temperatura quedarían una vez más probadas.

Como conclusión de estos experimentos, se puede observar que la mayor parte de resistencia eléctrica y por tanto calor, generados en la bujía están localizados en su parte inferior (la parte de cerámica), por tanto, sería suficiente si el método de refrigeración se centrara en esta zona de la bujía. Además, se extrae también que, si gracias al método de refrigeración las temperaturas del adaptador pudiesen ser controladas incluso bajo funcionamiento, el comportamiento eléctrico de la bujía lo sería también, al estar tan fuertemente relacionados.

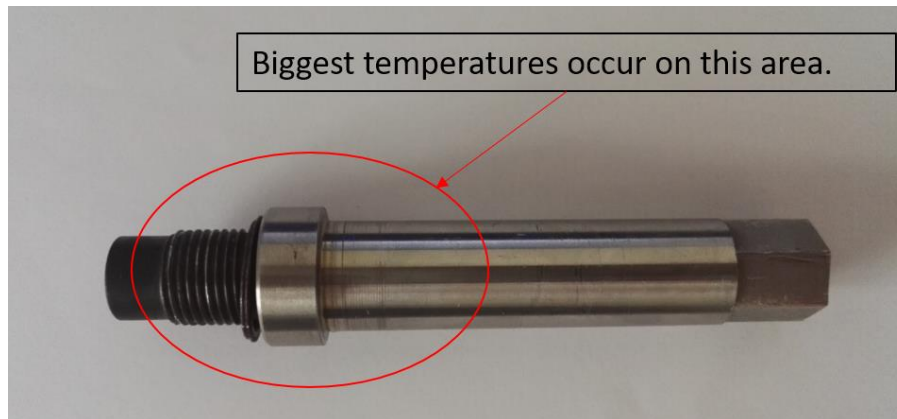


Ilustración 9. Zona en la que habría que aplicar la refrigeración para el nuevo adaptador, señalada sobre uno de los adaptadores antiguos utilizados.

Una vez concluidos los experimentos, la fase de diseño podría comenzar. Para empezar, el diseño del adaptador anterior fue estudiado cuidadosamente para localizar fallos, puntos fuertes y características a mejorar, ya que el objetivo de este proyecto era diseñar un adaptador que funcionase perfectamente durante largas horas de operación, pero no tenía por qué ser distinto al adaptador que había previamente.

Uno de los grandes fallos del adaptador diseñado previamente, es que el zafiro estaba incrustado en el adaptador sin salir completamente, dejando un hueco entre la cara externa del zafiro y la superficie exterior, hueco que, tras horas de operación, se iría llenando poco a poco de partículas dificultando la función del pirómetro. Por ello, basándose en la reflexión de la luz en el zafiro, el siguiente concepto para el mismo fue seleccionado.

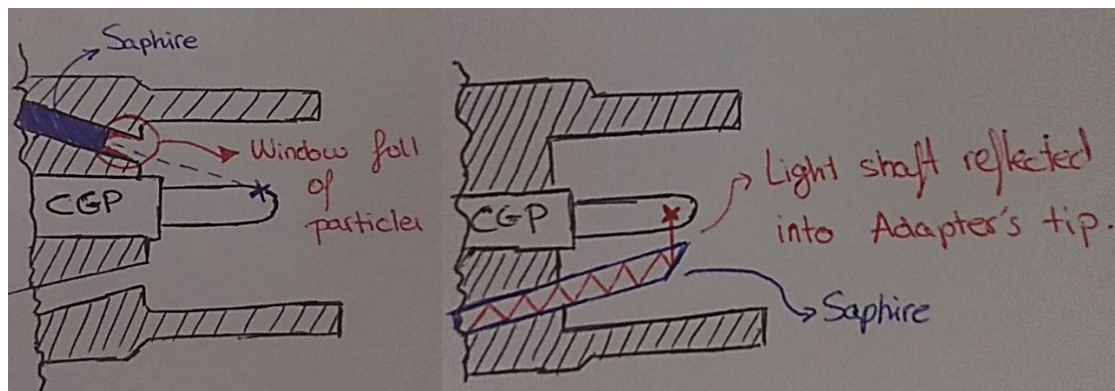


Ilustración 10. En la izquierda método utilizado previamente para medir la temperatura de la punta, puede verse la zona en la que se depositaban las partículas; a la derecha método seleccionado para el futuro adaptador, utilizando la reflexión de la luz para medir.

Otro problema fácilmente reconocible del adaptador era el material previamente seleccionado, acero inoxidable, el cual tiene una conductividad térmica relativamente baja para el objetivo del adaptador, debido a ello se cambió el material del adaptador por la aleación Nickel 99.2 LC con una conductividad térmica de $k = 78.5 \text{ W/(mK)}$, unas 5 veces superior a la del acero inoxidable, favoreciendo de esta manera la disipación de calor en el adaptador.

La limitación de espacio para este proyecto fue una de las grandes dificultades, ya que, el diámetro exterior máximo para el adaptador venía dado por el hueco del bloque motor en el que trabajaría, en este caso 20 mm lo cual dejaba muy poco espacio para añadir características que favoreciesen tanto la medición como la refrigeración. Aun así, la intención del nuevo adaptador sería la de incluir termopares más distribuidos, a unas profundidades controladas, para poder crear un gradiente de temperatura cuando la bujía estuviese funcionando dentro del motor.

Una vez realizadas estas consideraciones previas, las características del adaptador fueron diseccionadas, dando varias opciones de diseño para cada una de estas características. Una vez esto fue generado, gracias a la combinación de las opciones disponibles, varios modelos fueron creados, para más tarde ser evaluados de manera crítica eligiendo el más recomendable para este proyecto.

Al evaluar las opciones para el método de refrigeración, se dividieron las opciones diseñadas en dos: modelos refrigerados por agua y modelos refrigerados por aire a presión. Como resumen de las opciones se presentan los siguientes tres modelos:

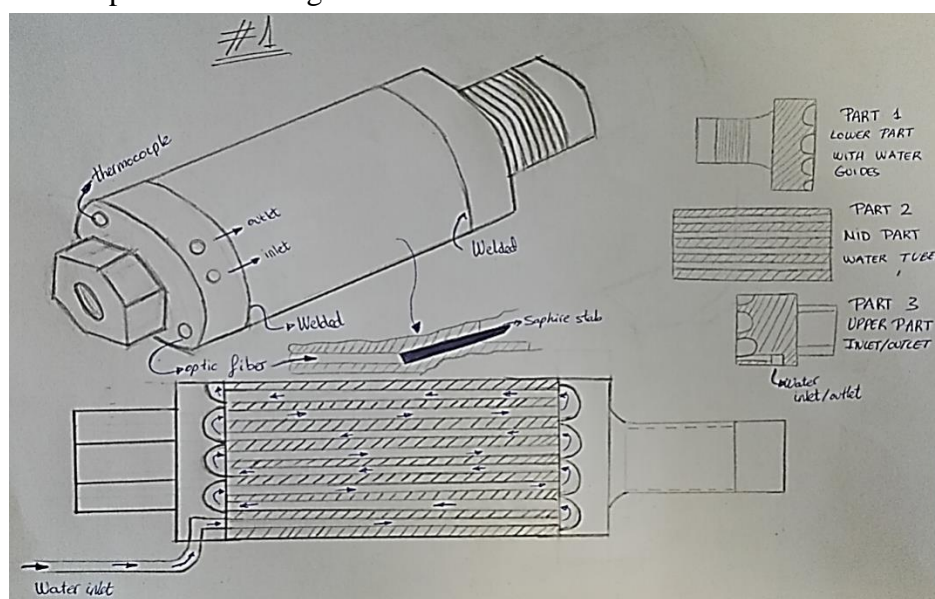


Ilustración 11. Se muestra una de las opciones seleccionadas, en este caso el Modelo 1 refrigerado por agua con bahías en su interior.

Para este modelo, el adaptador estaría dividido en tres partes distintas las cuáles irían soldadas por soldadura láser en su superficie exterior. Gracias a las cavidades que se pueden ver en el dibujo del modelo, el agua circularía por el interior del adaptador refrigerando el mismo. Una de las desventajas de este adaptador sería que, debido a la limitación de espacio no se podrían añadir muchos termopares ya que las cavidades interiores estarían dedicadas casi en su totalidad a los conductos por los que el agua circularía, además tendría el problema de no poder soldar interiormente, lo que provocaría la incertidumbre de si el agua se filtraría al interior del adaptador o no, una vez funcionado.

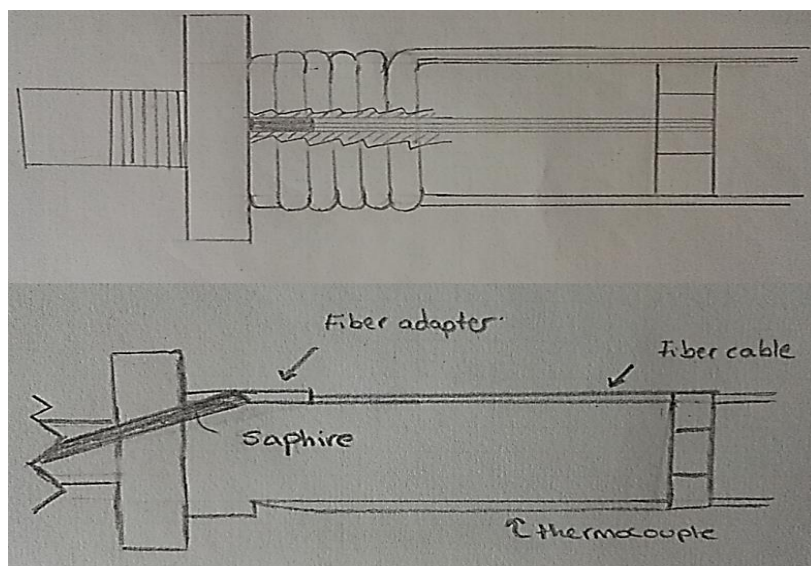


Ilustración 12. Se muestra otra de las opciones seleccionadas, en este caso el Modelo 5 refrigerado por agua con una bobina de cobre en su exterior.

Para este modelo el método de refrigeración vendría dado por una bobina de cobre enrollada en la superficie exterior del adaptador como se indica en el dibujo, el agua circularía por ella disipando calor fácilmente, debido a que las propias tuberías serían de cobre cuya conductividad térmica es enorme. La propia bobina de cobre funcionaría como capa protectora a su vez para los termopares y la fibra óptica que va conectada al zafiro, lo que haría que este modelo sólo requiriese de dos partes extras: la bobina de cobre y el adaptador que conecta fibra óptica y zafiro, como puede verse en la imagen.

Tras evaluar los modelos en los que el agua sería el medio refrigerante, el último modelo presentado en este resumen salió elegido, el modelo número 5, gracias a su simplicidad a la hora de fabricarse, y a tener espacio suficiente para la incursión de al menos tres termopares a distintas profundidades.

Para las opciones que utilizarían aire comprimido como refrigerante sólo se diseñó un concepto, debido a que, lo necesario para refrigerar el adaptador con aire comprimido mientras está en el bloque motor sería simplemente, una tubería conectada a la alimentación, y que el aire pasase por una válvula de control de flujo, de manera que éste se pudiese controlar, una vez realizado este simple circuito, la salida de la tubería se colocaría apuntando al adaptador de éste modo logrando su refrigeración.

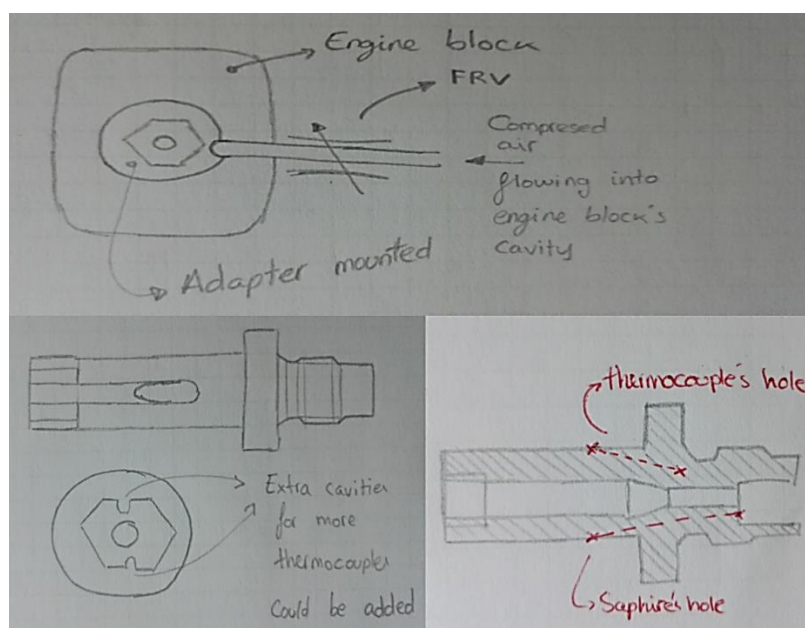


Ilustración 13. Idea inicial seleccionada para el modelo cuya refrigeración se llevaría a cabo por agua.

Debido a que el método de refrigeración estaría situado en el exterior del propio adaptador, no habría problema para disponer de varios termopares distribuidos a lo largo del mismo. En este modelo sí sería necesario una funda protectora para tanto los termopares como la fibra óptica. Para poder escoger la mejor solución entre estas dos, se llevaron a cabo varios experimentos, para probar la efectividad de la refrigeración con agua y la efectividad de la refrigeración con aire comprimido. Para ello, se compraron tuberías de cobre para fabricar la bobina de cobre por la que el agua ha de circular, y más tarde el adaptador con esta bobina fue situado en la mesa de ensayos utilizada anteriormente, y la bobina conectada a la unidad de refrigeración disponible en el laboratorio (cuyo flujo máximo era: $\dot{v}_{max} = 9.44 \times 10^{-6} \frac{m^3}{s}$). Una vez el adaptador estaba listo para probarse, la bujía fue sometida a 3 puntos distintos de voltaje, 3V, 4V y 5.4 V (siendo este el punto en el que la bujía alcanza su temperatura estándar de funcionamiento). Una vez las máximas temperaturas para cada voltaje fueron alcanzadas la bomba fue encendida, y el agua circulando por la bobina refrigeró dichas temperaturas a la temperatura mínima posible con este método. Los resultados finales están resumidos en la siguiente gráfica.

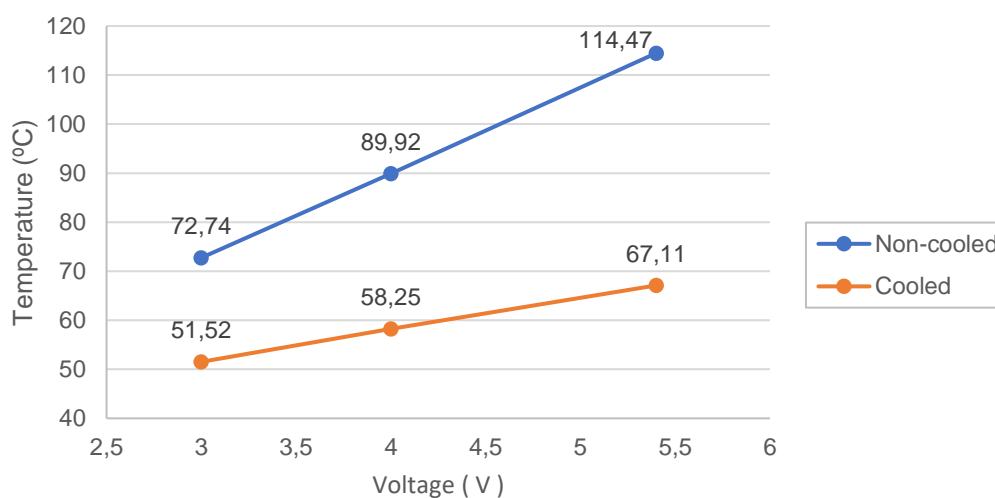


Ilustración 14. Resultados obtenidos al realizar el primer experimento con la bobina de cobre conectada a la unidad de refrigeración.

Como se puede observar la refrigeración obtenida en la parte delantera del adaptador (donde está la parte cerámica de la bujía) fue bastante pobre. Dado que las tuberías de cobres utilizadas en este experimento fueron más grandes, de las que se usarían en el modelo real, la superficie de contacto también estaría siendo más pequeña y por tanto estaríamos disipando menos calor del que se disiparía realmente; debido a esto, el adaptador se cubrió con pasta de cobre para aprovechar la máxima superficie de contacto, incluso mayor de la que se lograría con las tuberías del modelo real, una vez hecho esto el mismo experimento se llevó a cabo.

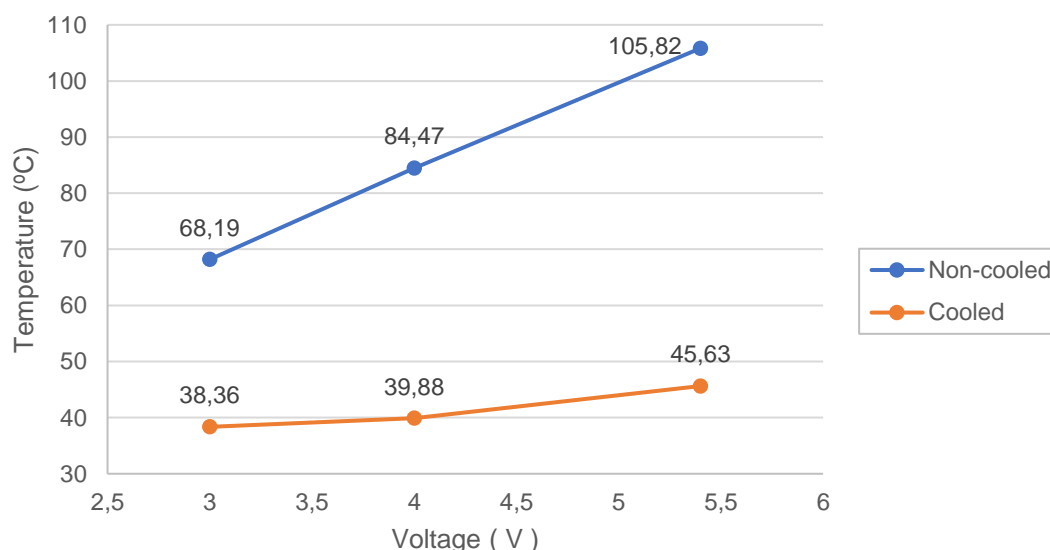


Ilustración 15. Resultados del experimento al aplicar la pasta de cobre sobre el adaptador.

Los resultados obtenidos esta vez fueron, lógicamente, mejores que los anteriores, pero lejos de lo esperado, ya que se buscaba una refrigeración capaz de llevar la temperatura delantera del

adaptador a 100°C cuando la bujía estuviese sometida a 5.4V, lejos de los 155°C finalmente obtenidos.

Debido a que la resistencia térmica del bloque metálico que simula al bloque motor de la mesa de ensayos, era menor que la resistencia térmica del propio adaptador, gran parte de calor saldría por el punto de contacto que hay entre el bloque y el adaptador, creando en esa zona las altas temperaturas (justo la zona que recoge la temperatura delantera del adaptador); debido a esto, aunque se consiguiese refrigerar la parte trasera del adaptador, nunca se conseguiría refrigerar más la temperatura delantera debido a la baja resistencia térmica del bloque. No sólo eso, sino que las temperaturas obtenidas durante los ensayos son mucho menores que las que se obtendrían dentro del motor, las cuales serían del orden de 250°C – 300 °C para la parte delantera, debido a que éste estaría en un entorno cerrado, así que la refrigeración que se conseguiría en el bloque motor sería aún menor que la mostrada durante los ensayos.

Para probar la refrigeración por aire, la pistola de aire comprimido del laboratorio fue situada a una distancia pequeña del propio adaptador montado en la mesa de ensayos, una vez hecho esto la bujía fue sometida a 5.4 V y llevada condiciones estacionarias de nuevo, para alcanzar la máxima temperatura posible y probar de esta manera la efectividad de este método. Cuando las condiciones estacionarias fueron alcanzadas, la pistola de aire comprimido fue activada con el máximo flujo disponible y los siguientes resultados fueron obtenidos.

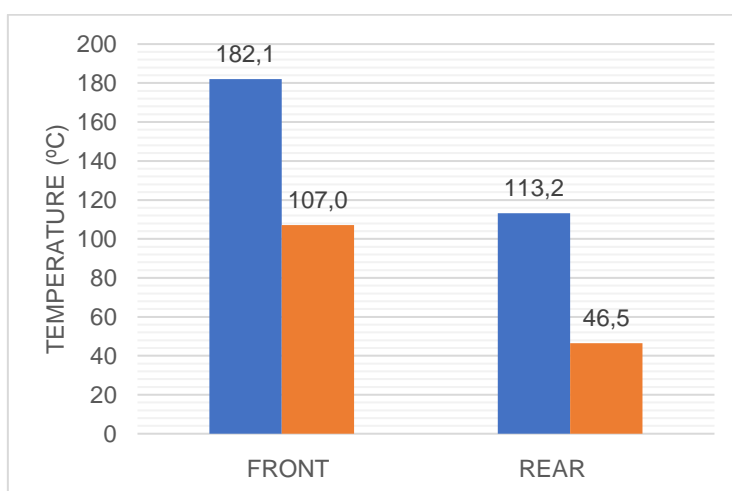


Ilustración 16. Resultados obtenidos al aplicar aire comprimido directamente sobre el adaptador. En azul las temperaturas máximas alcanzadas, y en naranja las temperaturas obtenidas al aplicar la refrigeración.

Como se puede observar en la gráfica anterior, los resultados son claramente mejores que aquellos obtenidos con la refrigeración por agua, aunque aún lejos de los 100°C objetivos. Debido a que no hay espacio suficiente en el adaptador, para disponer de una refrigeración por agua más cercana a la propia bujía, y a su vez de termopares y zafiro para el pirómetro, este método de refrigeración se descartó, escogiendo así refrigerar el adaptador con aire comprimido, el cual había mostrado unos resultados muy superiores.

Tras la realización de estos experimentos, la fase de diseño en 3D dio comienzo, y tras varios modelos realizados con el programa Pro-Engineer, se llegó a la siguiente solución para el adaptador y las distintas partes necesarias:

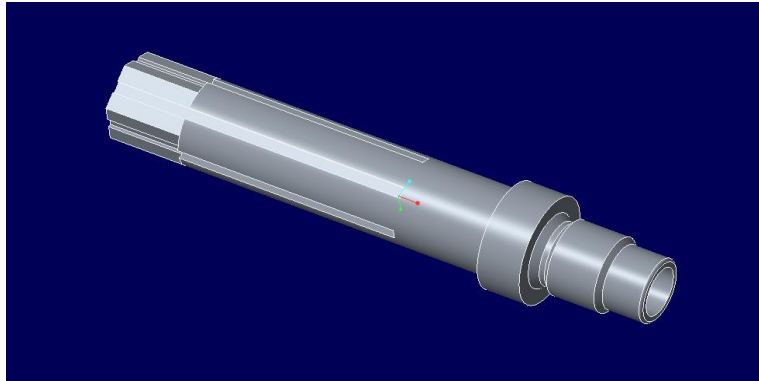


Ilustración 17. Modelo 3D de la solución elegida para el adaptador.

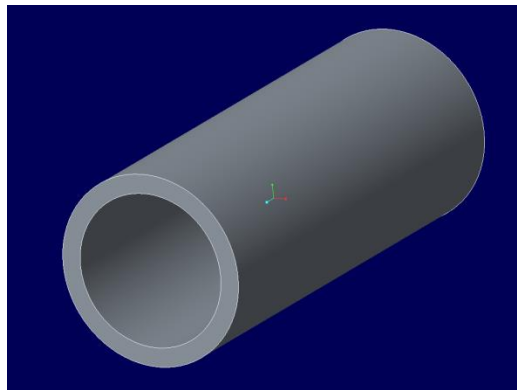


Ilustración 18. Modelo 3D para la funda protectora del adaptador.

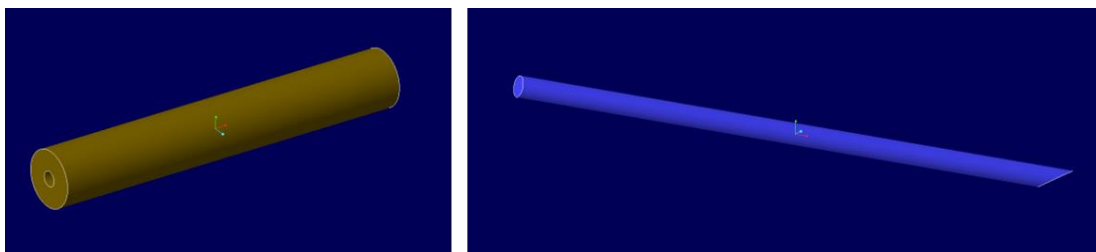


Ilustración 19. En la izquierda adaptador para conectar el zafiro y la fibra óptica; en la derecha modelo 3D del zafiro necesario para el adaptador.

Una vez diseñado el modelo en 3D, se comenzó a diseñar su plan de fabricación, el cual estaría dividido en varias fases: primero se fabricaría un adaptador sin las características utilizadas para las mediciones (agujeros y fresados para el zafiro y los termopares), una vez hecho esto se fabricaría la funda protectora que cubriría el adaptador para finalmente mecanizar las características necesarias para insertar en el adaptador el zafiro y los termopares.

Una vez realizadas las primeras ideas de este plan de fabricación, se habló con el taller de la universidad y allí se comentó la dificultad de mecanizar los agujeros para los termopares y el zafiro, debido a la inclinación y longitud que tendrían. La primera idea fue mecanizarlos por el método de mecanizado por electro erosión, pero por cuestiones ajenas al proyecto, no se podía realizar dentro de la Universidad, imposibilitando el uso de este método por el alto coste que supondría hacerlo en una empresa externa; luego estos agujeros se deberían de mecanizar por taladrado. La taladradora del taller de la Universidad fue diseñada en 3D para comprobar que no habría colisiones cuando los agujeros fuesen mecanizados, y una vez comprobado esto se volvió a hablar con el taller, llegando a la conclusión que para facilitar el centrado de las brocas de la taladradora, se deberían fresar unas superficies extras, creando de esta manera un plano perpendicular al eje de los agujeros, lo que facilitaría mucho la realización de los taladros. Debido a estos cambios, el modelo final del adaptador quedaría como se muestra en las siguientes imágenes:

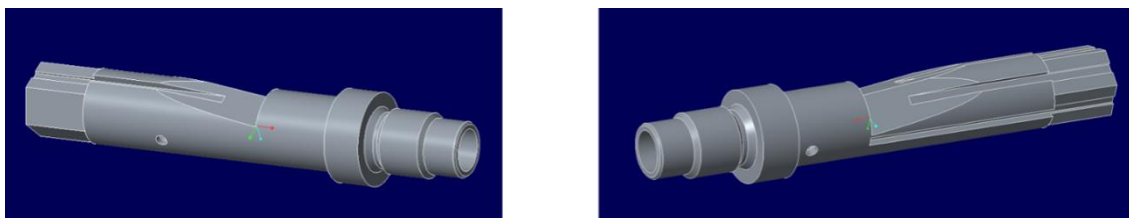


Ilustración 20. Modelo 3D de la versión final del adaptador dónde se pueden ver los fresados extra necesarios para fabricar los agujeros en la taladradora.

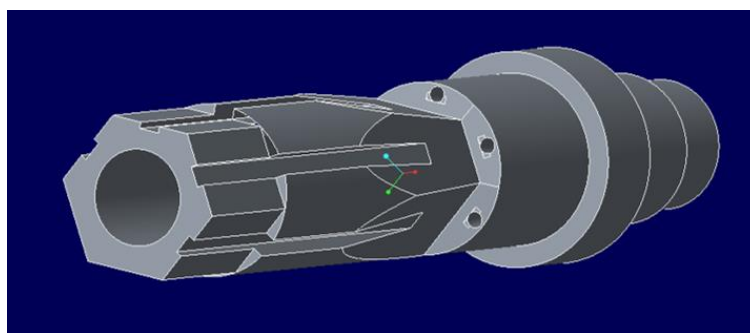


Ilustración 21. Vista trasera del adaptador, se observan los diferentes agujeros mecanizados.

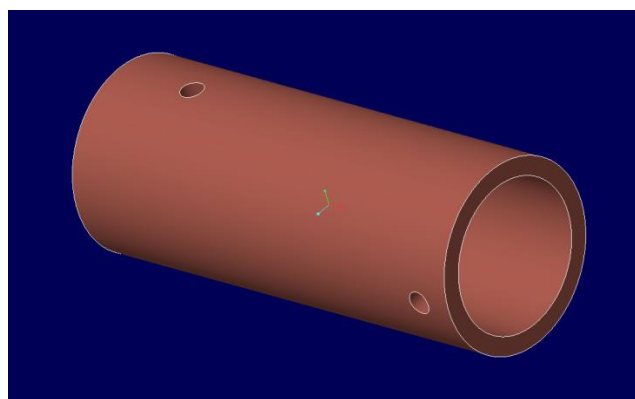


Ilustración 22. Modelo 3D final de la funda protectora del adaptador.

Como se puede observar se añadieron dos agujeros para poder colocar la funda del adaptador simplemente atornillando un par de pequeños tornillos, en lugar de utilizar pegamento como se usó en los antiguos modelos. En cuanto al adaptador de la fibra óptica y el zafiro, sus diseños no sufrieron modificaciones.

Una vez estudiados todos los posibles cambios al diseño final, se idearon también los pasos que se deberían seguir una vez todas las piezas estuviesen fabricadas para montar el adaptador en su totalidad.

Algo importante sería que de la punta de la bujía a la superficie del adaptador que le sigue inmediatamente, deberían haber 10 mm cuando la bujía fuese insertada aplicando un momento de 10 Nm, por ello el zafiro debería estar situado a esa altura para ser capaces de medir la temperatura de la punta exactamente, debido a esto, un bloque de 10 mm debería ser utilizado como referencia a la hora de introducir el zafiro en su agujero (el cual estaría relleno de pegamento para fijar el zafiro completamente). Todo esto se puede observar claramente en el documento incluido en el *Apéndice B* donde se recogen los dos planes de fabricación que se idearon.

A continuación, se muestran fotos del resultado final del diseño.

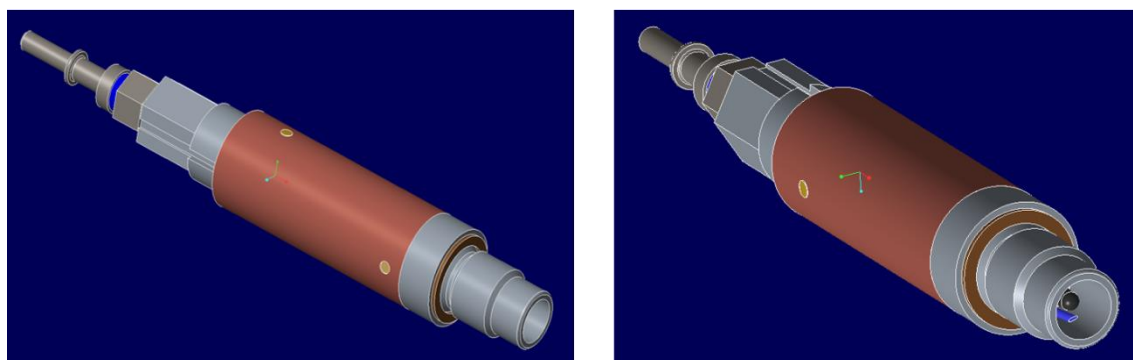


Ilustración 23. Resultado final del modelo 3D totalmente montado con la bujía situada en su posición correcta.

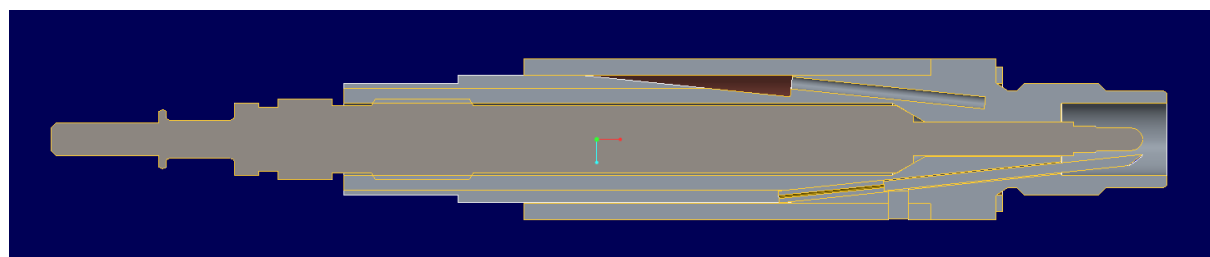


Ilustración 24. Vista de sección del conjunto final del adaptador.

Index

Task of the Thesis	II
Declaration of Originality	III
Acknowledgments	IV
Resumen del proyecto en español	V
Index	XXI
List of Abbreviations	XXIII
Symbols Directory	XXIV
1 Introduction	26
1.1 Goals of the thesis	26
1.2 Strategy followed for the development of the adapter	26
1.3 Introduction to glow plugs	27
1.3.1 General concepts about glow plugs	27
1.3.2 Classification of glow plugs	29
2 Experimental research	32
2.1 Set up for the trials	32
2.2 CGP Tests: Cold resistance	34
2.3 CGP Tests: Cold resistance dependency on temperature of the adapter	37
2.4 CGP Tests: Temperature distribution	42
2.5 Useful conclusions for the adapter design	45
3 Development of the new adapter's design	47
3.1 Initial considerations for the new adapter's design	47
3.2 Design options for the adapter	52
3.2.1 Water cooled: Model N°1	54
3.2.2 Water cooled: Model N°2	55
3.2.3 Water cooled: Model N°3	56
3.2.4 Water cooled: Model N°4	57
3.2.5 Water cooled: Model N°5	58
3.2.6 Air cooled: Model N°6	59
3.3 Evaluation of the different options for the new adapter's design with water as cooling medium	60
3.3.1 Cooling medium tests: Water	62
3.3.2 Cooling medium tests: Air	70
3.4 Chosen Design	72
4 Manufacturing Plan	75
4.1 Adapter without the measuring techniques	75

4.2	Extra Parts for the final assembly	76
4.3	Adapter with all the required characteristics.....	77
5	Assembly of the adapter	81
6	Conclusions	84
	Summary	85
	Bibliography.....	87
	Table of Figures	89
	Appendix A: Technical drawings.....	92
	Appendix B: Manufacturing Plan	101

List of Abbreviations

Abbreviation	Meaning
CGP	Ceramic Glow Plug
FCV	Flow Control Valve
FRV	Flow Regulating Valve
HSI	Hot Surface Systems
MgO	Magnesium Oxide
NHTC	Ceramic high-temperature Glow Plug
PTC	Positive temperature coefficient
SRC	Self-Regulating Ceramic Glow Plug
SRM	Self-Regulating quick start

Symbols Directory

Symbol	Units	Description
U	[V]	Voltage
I	[A]	Current
R	[Ω]	Electrical Resistance
P	[W]	Power
U_{HSI}	[V]	Voltage of the Glow Plug
I_{HSI}	[A]	Current of the Glow Plug
R_{HSI}	[Ω]	Electrical Resistance of the Glow Plug
P_{HSI}	[W]	Power of the Glow Plug
R_h	[Ω]	Heating resistance in a Glow Plug
R_l	[Ω]	Limiting or controlling resistance of a Glow Plug
dR	[Ω]	Differential of Resistance
R_0	[Ω]	Cold Resistance of a Glow Plug
R_{block}	[K/W]	Thermal Resistance of the metallic block that simulates the engine block
T_i	[K] ; [°C]	Temperature of a point
dT	[K] ; [°C]	Differential of temperature
T_{phi_m}	[K] ; [°C]	Ambient temperature
T_{adap_front}	[K] ; [°C]	Temperature measured at the front of the Adapter
T_{adap_back}	[K] ; [°C]	Temperature measured at the back of the Adapter
T_{shield}	[K] ; [°C]	Temperature measured at the Shield of the Adapter
T_{inlet}	[K] ; [°C]	Temperature at the inlet of the circuit
T_{outlet}	[K] ; [°C]	Temperature at the outlet of the circuit
P_0	[mbar]	Ambient pressure
ε	[-]	Emissivity of a surface or object
k	[W/mK]	Thermal conductivity of a material
M	[Nm]	Torque
V_i	[m ³]	Volume measured
V_m	[m ³]	Average volume

t	[s]	Time
\dot{v}_{max}	[m ³ /s]	Maximum flow rate delivered by the pump
Q_{water}	[W]	Heat produced by the water
\dot{m}_w	[kg/s]	Mass flow rate of the water
$c_{p,water}$	[J/kgK]	Thermal capacity of the water
ρ_{water}	[kg/m ³]	Density of the water
\varnothing	[mm]	Diameter
L_i	[mm]	Depth of the holes in the technical drawings
Ω_i	[°]	Angle used in the technical drawings

1 Introduction

As a first step of the project, the goals of it were completely understand, the strategy which I would follow to design the final adapter was defined and a general overview of glow plugs was obtained in order to understand the very basics of them. The first steps of this thesis were the same ones as those developed in the research project: *Analysis of the Thermo-electrical Behaviour of Ceramic Glow Plugs by Alejandro Lombardía González*.

1.1 Goals of the thesis

As it was said, the goal of this project was to design a conditioned sensing adapter for HSI Systems, that would be used in following research experiments where different CGPs would be tested in the engines.

The new adapter should be able to measure the temperature at its body and also, the temperature at the CGP's tip while this last is working in the engine. In order to do so a pyrometer would be connected to a sapphire included on the adapter, and to measure its body's temperature some thermocouples should be included; all of this while having a cooling system able to reduce the temperature on the adapter itself.

This project includes all the research for literature, experiments carried out to understand the behaviour of the CGPs and extract useful information for the new adapter, its design with the analysis of all the possible solutions found, the analysis of the different cooling systems which could be a valid option for this device, the manufacturing plan for the adapter which would help to find possible corrections to the chosen solution for its design and the needed extra parts, when included, and the steps required to correctly assemble all the parts of the adapter.

1.2 Strategy followed for the development of the adapter

This bachelor's thesis followed the same structure as any project or product development, dividing all the steps in different phases in order to follow a path that allowed to correct any potential failure before being too late for its correction. See *Figure 1*.

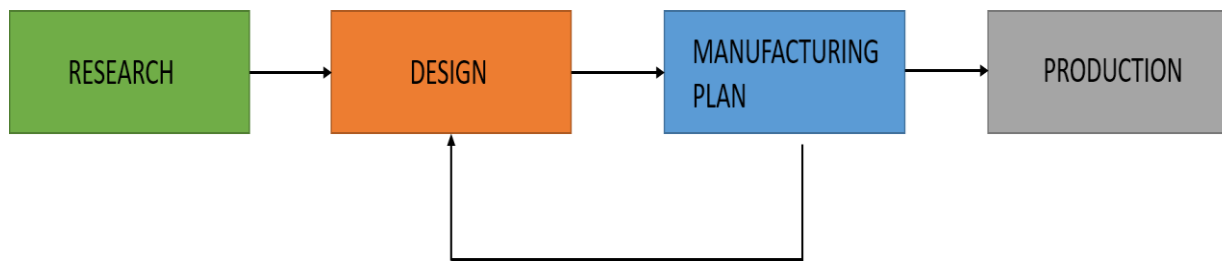


Figure 1. General structure in product development

As any other product development process, this project will start with a research on glow plugs to obtain a general overview of them, once this is completed the next step will be to realize scientific experiments to understand how these glow plugs behave under working conditions, and furthermore, to try out any experimental trial which could be useful for the development of the new adapter.

After extracting all the possible information about the experimental research, the design phase can start, where all the useful data obtained is combined to look for all of the possible solutions to discuss finally which could be the best one on this specific case. Once the solution is chosen, since the part has to be manufactured, a manufacturing plan is created in order to detect any possible failure that design could have with respect its manufacturing process, if that would be the case, the design should be reviewed in order to look for a better solution that could fit the manufacturing processes available. Once every step is fulfilled and , only if they are successfully achieved, the production of the new product can start.

1.3 Introduction to glow plugs

As a first step to the project, a general overview of the glow plugs was needed in order to fully understand the devices that I was going to work with. Information given by several manufacturers is summarized in the next chapters of this project.

1.3.1 General concepts about glow plugs

A glow plug is a device that heats up the air-fuel mixture in the Diesel engines' combustion chamber with a two fold objective. The first is to facilitate the startup even at low external temperatures, the central function of glow plugs is to provide additional energy for the start. The second is to reduce pollution emissions by favoring combustion (The glow plug's heat development optimizes the combustion, so that the development of smoke and other emissions is reduced) [2].

Glow plugs are installed in the cylinder head, examples of the exact placement of the glow plugs can be seen on *Figure 2*.

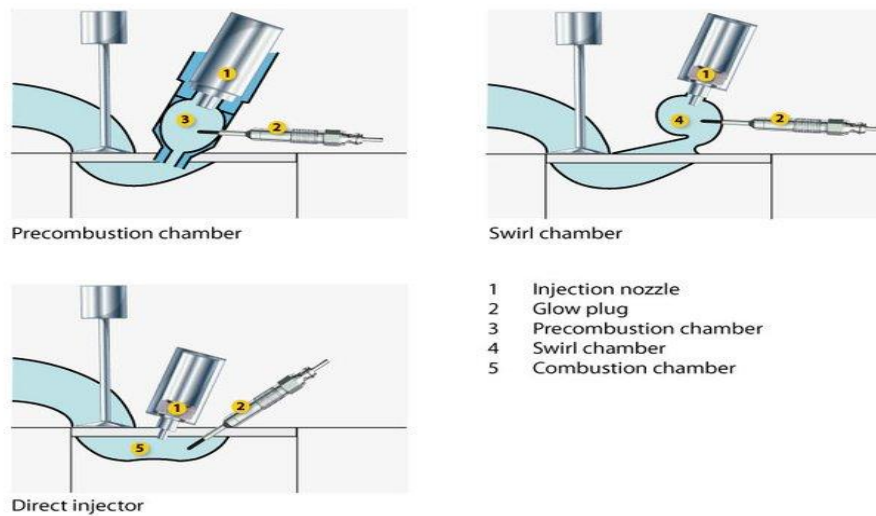


Figure 2. Different examples of locations for a glow plug [11]

The glow rod extends into the hot zone and/or the precombustion chambers. However, the glow rod should be positioned exactly at the edge of the mixture. In this way, it can provide the heat exactly where it is needed. However, it may in no case extend too far into the combustion chamber, because the preparation of the fuel and thus the formation of an ignitable fuel-air mixture would not be guaranteed.



Figure 3. Example of a Glow Plug [10]

Glow Plugs are also a possible ignition source for direct injected natural gas engines. This ignition assistance application is much different than the cold start assist function for which most glow plugs have been designed. In the cold start application, the glow plug is simply heating the air in the cylinder. In the cycle-by-cycle ignition assist application, the glow plug needs to achieve high surface temperatures at specific times in the engine cycle to provide a localized source of ignition. Whereas a simple lumped heat capacitance model is a satisfactory representation of the glow plug for the air heating situation, a much more complex situation exists for hot surface ignition. [7]

1.3.2 Classification of glow plugs

Glow plugs are basically differentiated between metal rod glow plugs and Ceramic Glow Plugs (CGP); although in this project the CGP are the used ones, a general overview of both types of glow plugs will be given.

A heating coil in the glow rod of a metal rod Glow plug produces the necessary heat, while, the CGPs come without a metal glow tube, instead, their heating element is encased in a special type of ceramic. Normally, ceramic glow plugs reach the necessary operating temperature very quickly, and they are usually more compact, making all of these features a really big advantage for modern engines. [10]

Metal Glow Plugs: The self-regulating quick-start glow plug (SRM glow plug) is amongst the most frequently used glow plug types. It is comprised of the components that can be seen on *Figure 4*. The interior of the glow tube is filled with an extremely compressed, special magnesium oxide which has good insulating properties. [10]

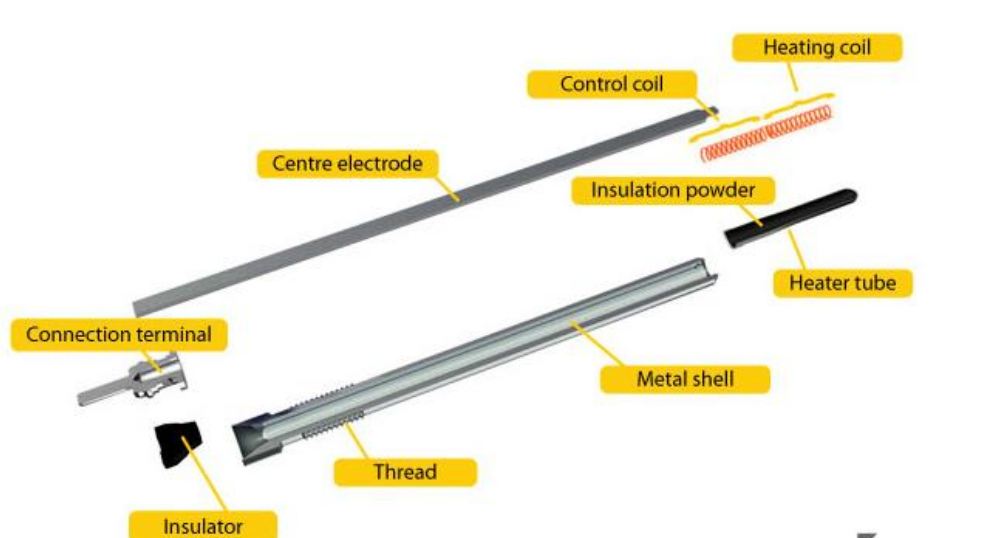


Figure 4. Exploded view of a Metal Glow Plug [10]

The different parts that can be seen on the previous figure are:

- Heating coil: The heating coil of a self-regulating quick-start glow plug is made of metal. As soon as the glow plug is supplied with current it begins to glow and thereby heats up its surroundings. By using different wire diameters or lengths for the construction of heating coils, the heating behaviour changes, thus influencing how quickly the glow plug glows.
- Insulating filler: The inside of the glow tube is filled with an extremely compact, special powder: MgO. Magnesium oxide is electrically insulating and is an outstanding heat conductor. The insulation filling fulfils two important functions: It protects the coils

from impact and vibrations and guarantees an optimal transmission of the produced heat.

- Heating tube: The heating tube of a metal rod glow plug is made of a heat-resistant alloy. In combination with the insulation filling, it ensures that the coils inside are not subjected to the combustion and shockwaves resulting from combustion without protection.
- Regulating Coil: The control coil is welded to the current-carrying central electrode and the heating coil. As the temperature increases, the electrical resistance of the control coil also increases. In this manner, it reduces the current flow to the heating coil depending on the temperature.
- Central electrode: The battery voltage reaches the coils through the central electrode.
- Thread: The thread of a high-quality glow plug is always rolled and never cut. This way, damage to the glow plug bore in the cylinder head is prevented.
- Connection: The battery voltage is applied at the current connection.

Metal glow plugs are mainly divided in: Standard rod glow plugs, Rapid Start glow plugs, Self-Regulating rod glow plugs and Quick Glow system. Since they are not the focus of this project the exact differences between them are not relevant for the development of the thesis.

Ceramic glow plugs: The heating coil of a CGP has an especially high melting point. It is also sheathed in silicon nitride, an extremely rugged ceramic material. The combination of the heating coil and ceramic sheath enable higher temperatures and extremely short preheating times due to excellent thermal conductivity. Also, CGPs have a more compact design. This is important, because there is very little free space in today's engines, which will be one of the limitations for the development of this project. The components for this type of glow plug can be seen on *Figure 5. Exploded view of a SRC -CGP*

CGPs are mainly divided in two big families:

- Self-Regulating CGPs (SRC): They are equipped similarly to the self-regulating metal rod glow plugs, with one heating coil and one control coil. Since the electrical resistance of the control coil increases as the temperature increases and thereby limits the current flow, this glow plug requires practically no external control. This glow plug type heats up to over 1100 °C in 3 seconds and then independently regulates the temperature to below 1000 °C. [10]
- Ceramic high-temperature glow plugs (NHTC glow plug): They have a fully ceramic heating element. It reaches an operating temperature of 1000 °C in two seconds and can afterglow for up to ten minutes at temperatures up to 1350 °C. That means: It glows in push phases or during the regeneration phase of the particle filter and thereby minimizes the particle emissions during this time. The NHTC ceramic glow plug was specially

developed by the industry to enable automobile manufacturers to comply with the Euro 4 and Euro 5 emissions standards. One of the goals of these standards is to reduce the compression ratio in diesel engines. NHTC glow plugs reach a temperature of 1000 °C in less than two seconds and can after-glow for more than ten minutes at temperatures of up to 1350 °C. Optimal combustion is assured even with low compression ratios. In addition, the NHTC glow plug can glow intermediately to prevent cooling of the particle filter in deceleration phases. [10]

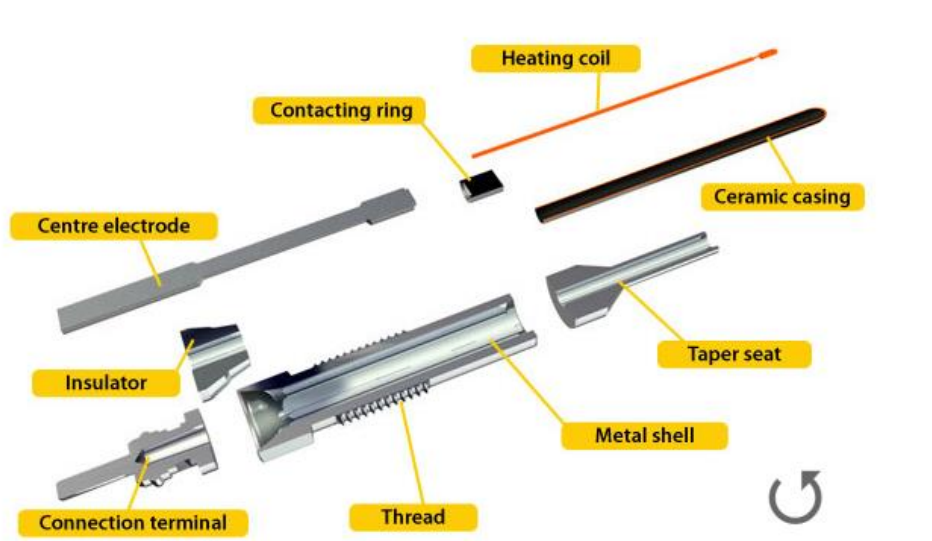


Figure 5. Exploded view of a SRC-CGP [10]

The different parts that can be seen on the previous figure are:

- Heating coil: Like metal rod glow plugs, conventional CGP also have a metal heating coil, however, their melting point is especially high, which enables higher glow temperatures and faster heating.
- Ceramic liner: The heating coil or heating element of a CGP is encased by a highly-resistant ceramic material: silicon nitrite. It protects the coil from the elevated temperatures and vibrations and is also an outstanding heat conductor, so the heat which arises is quickly released in the combustion chamber.
- Regulating coil: Metal control coils, like those used in self-regulating glow plugs, increase their electrical resistance as temperatures increase (PTC Behaviour). In this way, the current flow is minimized and the glow plug is protected from overheating.
- Central electrode: The battery voltage reaches the coils through the central electrode.
- Insulator: The thread of a high-quality glow plug is always rolled and never cut. This way, damage to the glow plug bore in the cylinder is prevented.
- Connecting bolt: The battery voltage is applied at the current connection.

2 Experimental research

The initial data acquisition for this bachelor thesis was carried out by the development of a research project, *Analysis of the Thermo-electrical Behaviour of Ceramic Glow Plugs* by *Alejandro Lombardía González*, where the CGPs were tested in order to extract the maximum possible information about their behaviour. All of the knowledge that was acquired doing this research project, have carried an important task on this thesis, since they were the base for the correct development of the new adapter design.

By the end of these experiments, the CGP's electrical and thermal behaviour were understood, so a proper design could be derived from this information. In order to achieve this previous important aspects, a test bench was created at the start of the semester for carrying out all of the needed tests, both for the initial research and also for the cooling tests which will come later.

2.1 Set up for the trials

In order to carry out all the needed tests, the repeatability of results had to be ensured, to do so, a test bench was constructed. This test bench, ensured that the results shown were reproducible, since the CGPs and all the elements of the test bench were placed every time on the same spot and also the same power sources were used. In order to control the electrical and thermal behaviour of the CGPs tested, the circuit shown in the next figure was constructed.

See *Figure 6*.

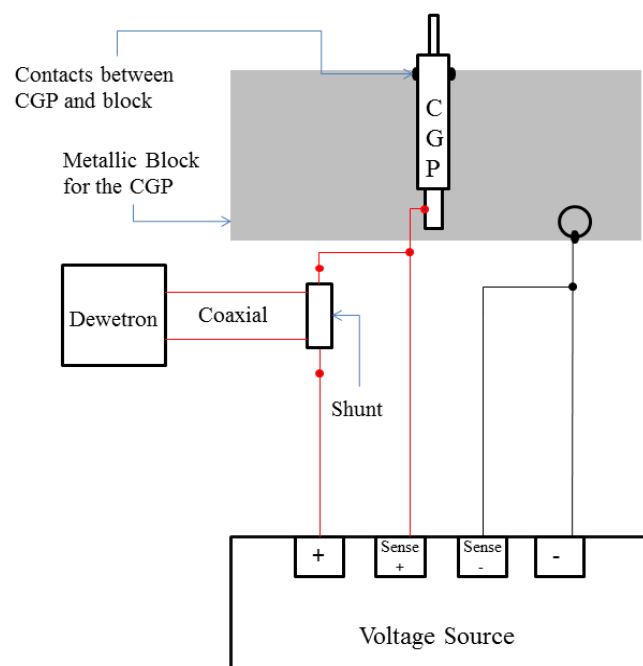


Figure 6. Scheme of the circuit [9]

The metallic block which can be seen on the *Figure 6*, simulates the engine block where the CGP will work on.

Once the needed circuit was designed, it was time to construct a structure to support all the needed elements to perform the tests, and as it has been said, to ensure the repeatability of those. In order to achieve that, a test bench was constructed using alluminum profiles to build a custom structure where the metallic block (with the CGP) would always be on the same position. An important factor to take into account was that the test bench had to ensure the facility of assembling and disassembling the CGPs and all the electrical componetes when needed. The final test bench is shown in the next figure. See *Figure 7*.

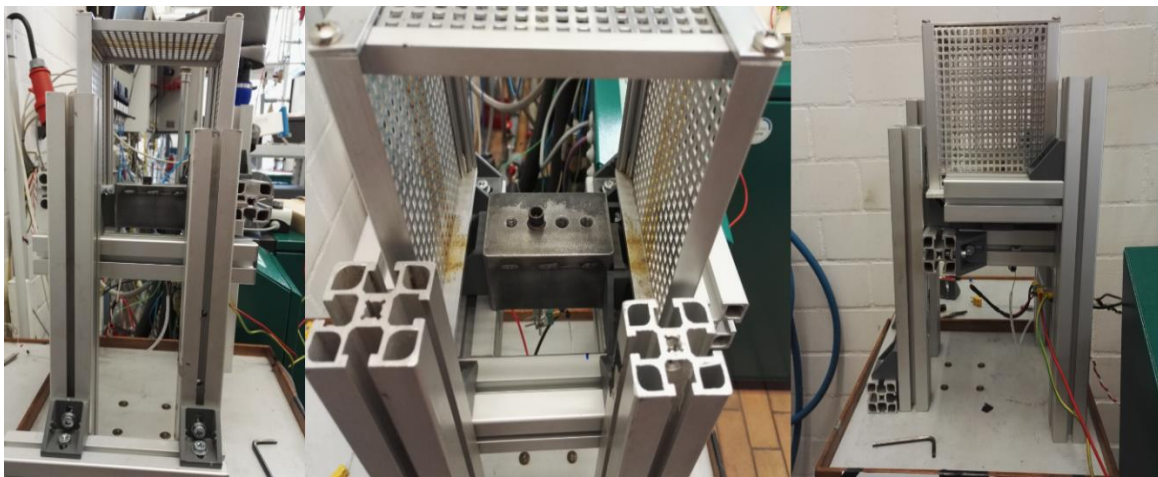


Figure 7. Three views of the Test Bench used [9]

This structure fulfilled all the requirements for the test bench, and for security reasons a metallic cage was added in order to prevent any possible risk that may occur when the CGP was tested under operation conditions, because of the high temperatures that it would achieve.

Finally the basic elements required for the test bench were: the alluminum structure, both the metallic block and metallic cage, and all the electrical components to create the circuit mentioned above.

For the data adquisition, and the realization of the experiments a lot of software was needed, and so the required Hardware that goes with it. Specifically, LabVIEW and DEWESoft were used as well as some specific programmes developed for carrying out each of the needed tests in an automatic way. In order to fulfill this task, the Adwin-Gold II and the ADwin-Pro II (shown in the next figures), with the help of their software ADbasic (where the specific programmes were programmed), were used. [9]



Figure 8. On the left, ADwin-Gold II, On the Right, ADwin-PRO II [9]

2.2 CGP Tests: Cold resistance

The Cold Resistance of a CGP (R_0) indicates the Electrical Resistance that a CGP has by itself, meaning, the Resistance that it has when applying a really low voltage or by applying a voltage over a really short period of time. The R_0 is an indicator also for the state of a CGP, when the CGP has a lot of hours under operation conditions, its R_0 will change due to aging.

In order to obtain the values of R_0 , two different tests were carried out, one applying 5 V during 5 ms and another one applying 0.5 V until steady state conditions were reached. As it was experimentally proven in the *Analysis of the Thermo-electrical Behaviour of Ceramic Glow Plugs* by Alejandro Lombardía González, mentioned before, both tests gave similar results and thus they can be compared.

As an example some R_0 values, for different CGP with and without Adapter, are shown.

Comment	R_0 obtained in DEWESoft
Test	R_0 (mohm)
CGP#1_5V_test_without_Adapter	189,9
CGP#1_0.05V_test_without_Adapter	195
CGP#1_5V_test_with_Adapter	178,4
CGP#1_0.5V_test_with_Adapter	211,4
CGP#16_5V_test_without_Adapter	197,1
CGP#16_0.5V_test_without_Adapter	202,1
CGP#16_5V_test_with_Adapter	198,2
CGP#16_0.5V_test_with_Adapter	211,2

Table 1. Example of different values of Cold resistances obtained while the CGPs were mounted with and without the Adapter [9]

For this bachelor's thesis the concern about the R_0 of the CGP was to find out where this value was mainly produced, because if the Electrical Resistance of the CGP was produced all over it, it would mean that the adapter would need a cooling system that covered all the length of the CGP. In order to understand how R_0 and thus the Resistance of the CGP were distributed, a CGP was split into two parts: an inner metallic lead (the metallic part of the CGP) and the ceramic part of the CGP. See *Figure 9* and *Figure 10*.



Figure 9. Ceramic part of a CGP located at the inside of this shell [9]



Figure 10. Inner metallic lead of a CGP [9]

It was assumed, thanks to previous information, that the inner metallic lead of the CGP had a really low value of resistance in comparison with the one of the ceramic part. Since the inner metallic lead was the part with the connector of the CGP, it was really easy to prove this assumption. By connecting the upper extreme of this inner metallic lead to a really small voltage (0.05 V during 5 ms, because a high voltage could potentially damage the part if the resistance is as low as expected) and the lower extreme to ground, letting this way the current flow and thus producing the desired value of resistance. [9]

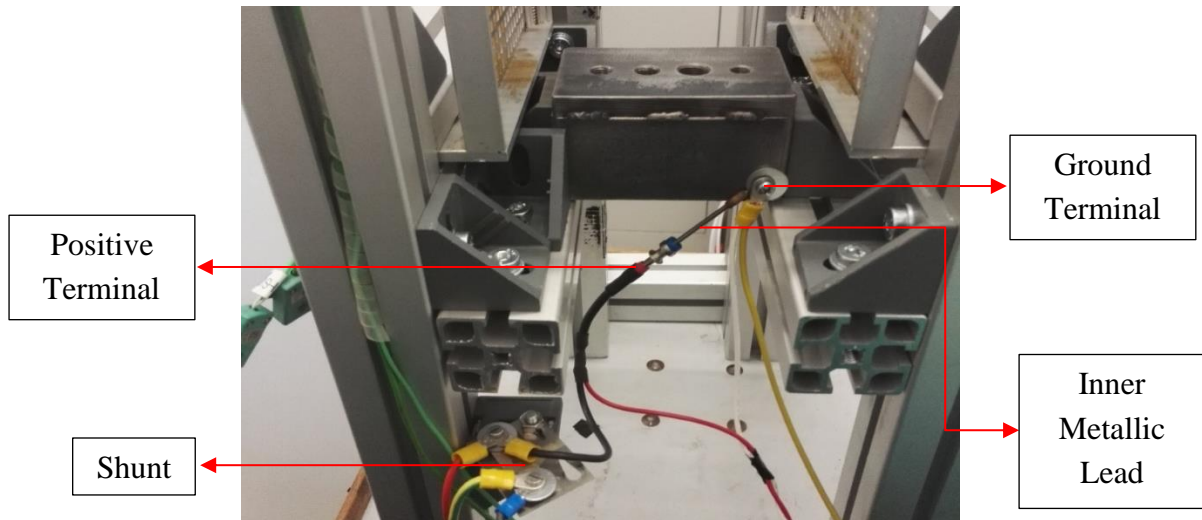


Figure 11. Inner Metallic Lead connected for the tests

To simulate the working conditions, the inner metallic lead was heat up to 130°C with the help of a hot air tool, in order to see if an increase of Temperature would cause a really big impact on its Resistance value.



Figure 12. Hot air tool used on the experiments; Steinel Professional HG 2120E [16]

The following data, shown in *Table 2*, were obtained:

Comment	R_0 obtained in DEWESoft	Ambient Temperature
Test	R_0 (mohm)	T_{phi_m} (°C)
01_Inner_Met_Lead	5,2	22.2
02_Inner_Met_Lead	5,1	22.5
03_Inner_Met_Lead	5,2	22.5
04_InnerMetLead_HeatUp_130C	5,8	22.7
05_InnerMetLead_HeatUp_130C	5,6	22.7
06_InnerMetLead_HeatUp_130C	5,7	22.7

Table 2. R_0 values for the inner metallic lead [9]

As expected, the R_0 of the inner metallic lead was really small, even when heated up (there is an increase of only 6 m Ω when heated around 100 °C), thus it could be said that the highest amount of Resistance is located on the ceramic part of the CGP; or in other words, the heat production of the CGP is mainly located at its ceramic part.

2.3 CGP Tests: Cold resistance dependency on temperature of the adapter

The aim of this experiment was to show, in a scientific way, the dependency of the Cold Resistance of a CGP on the temperature of the adapter's body, in order to do so, two experiments were carried out. The adapter that was used on this experiments had three thermocouples placed on three different spots inside its body, these temperatures were used as reference for all the following experiments.

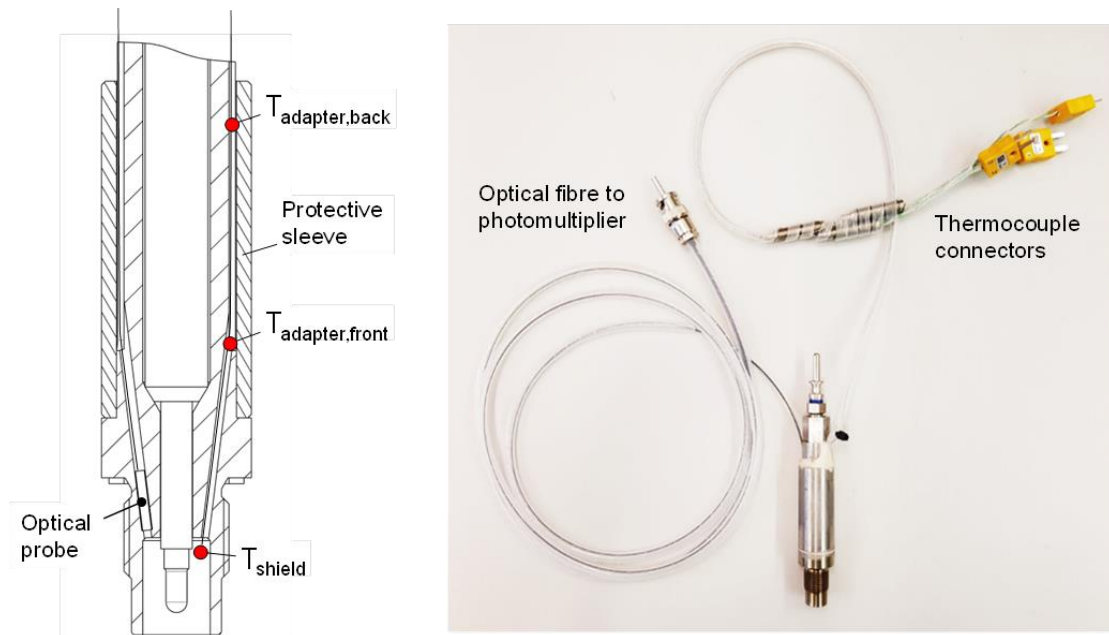


Figure 13. Location of the three measuring points

For the first experiment, the adapter's body is heated with the hot air tool shown in *Figure 12*, since this hot air tool allowed the user to vary the temperature range by moving a wheel and adapting its flow (this information is later expressed as level 2 or 3 for the air flow, and the position of the wheel), several points were measured applying different temperature levels of this tool.

HG 2120 E settings			
Airflow rate stage 2 low airflow rate		Airflow rate stage 3 high airflow rate	
Thumbwheel	Temperature approx.	Thumbwheel	Temperature approx.
1	80 °C	1	80 °C
2	110 °C	2	110 °C
3	190 °C	3	180 °C
4	280 °C	4	260 °C
5	360 °C	5	340 °C
6	440 °C	6	420 °C
7	500 °C	7	480 °C
8	570 °C	8	560 °C
9	630 °C	9	630 °C

Table 3. Temperature ranges of the hot air tool used in the experiments [16]

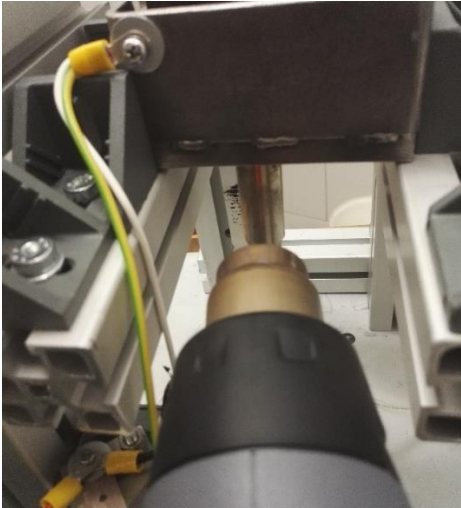


Figure 14. Hot air tool heating up the adapter

Once the Adapter’s body reached a constant temperature, the exact same cold resistance tests, previously done, were carried out and the information extracted. For this experiment the T_{adap_front} was taken as reference to know when the adapter have reached consant temperature. In the next table a summary of the results of this experiments are shown:

Comment	P_0 (mbar)	T_{phi_m} (°C)	R_0 (mohm)	T_{adap_front} (°C)	T_{adap_back} (°C)	T_{shield} (°C)
01_ R_0 _level2_wheel4	1000,2	24,5	274,4	139,8	102,6	135,8
02_ R_0 _level2_wheel4	1000,2	24,5	274,4	139,8	102,6	135,8
03_ R_0 _level2_wheel5	999,7	24,3	291,9	165,8	119,6	162,8
04_ R_0 _level2_wheel5	999,7	24,3	291,8	165,8	119,7	162,9
05_ R_0 _level2_wheel6	999,7	24,5	305,6	187	132,2	183,8
06_ R_0 _level2_wheel6	999,7	24,5	305,5	187	132,3	183,8
07_ R_0 _level2_wheel7	999,6	24,4	320,7	209,9	146,5	205,9
08_ R_0 _level2_wheel7	999,66	24,4	320,8	210	146,6	205,9
09_ R_0 _level2_wheel8	999,5	24,4	337,7	235,2	162,4	229,7
10_ R_0 _level2_wheel8	999,5	24,4	337,8	235,3	162,6	229,8
11_ R_0 _level2_wheel9	999,5	24,5	356,2	262,8	179,1	256,3
12_ R_0 _level2_wheel9	999,5	24,5	356,4	263,2	179,6	256,6
13_ R_0 _level3_wheel9	999,4	24,5	374,1	288,3	198,5	276,7
14_ R_0 _level3_wheel9	999,4	24,5	374,4	288,5	198,9	276,9

Table 4. Example of R_0 values when the Adapter is heated up [9]

Just by taking a look on these results, it can be said that there is a strong dependency of R_0 on the adapter's temperature. These results are plot now in a graph to clearly see the type of dependency.

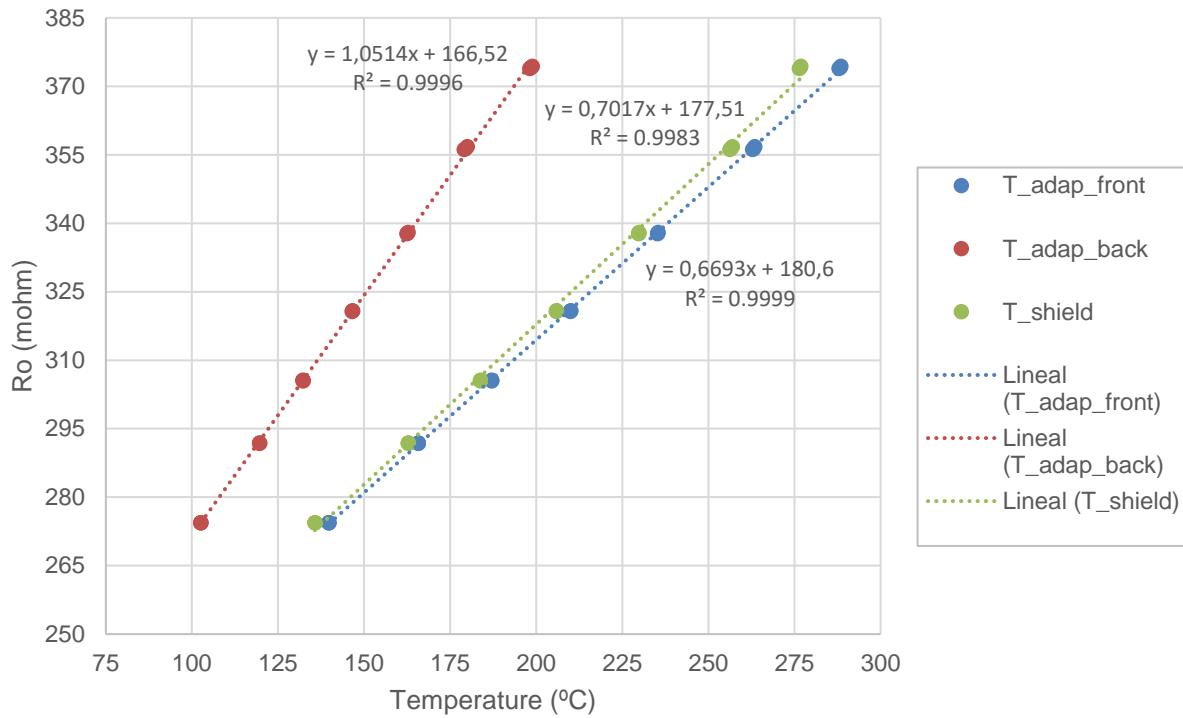


Figure 15. Ro variation with temperature of the adapter [9]

Thanks to this graph it is shown not only the strong dependency of the cold resistance of the CGP with the adapter’s temperatures, but also it has been proven that it is a linear dependency, which will be very useful for the mathematical derivations needed for future researchs.

For the second experiment, the adapter’s body was heated up again with the hot air tool until steady state conditions at the maximum available temperature were reached. Once this had happened, the hot air tool was turned off and thus the adapter’s temperatures started to drop, while these temperatures were dropping the cold resistance of the CGP was measured in order to see the dependency on this process. As a remark, the thermocouple encharged of measuring the T_{shield} broke during the realization of the experiments and since it could not be replaced the experiments were done without taking into account the value of this temperature.

Since the amount of measured points is huge, only the maximum temperature point, the minimum temperature point and some intermediate values are going to be shown on the following table:

Comment	P_0 (mbar)	T_{phi_m} (°C)	R_0 (mohm)	T_{adap_front} (°C)	T_{adap_back} (°C)
01_ R_0 _Max_Temperature	1001,9	24	390,4	304,9	204,3
02_ R_0 _Max_Temperature	1001,9	24	389,6	303,6	204,1
03_ R_0 _Intermediate_Temp	1001,9	24,1	322,3	200,2	153,9
04_ R_0 _Intermediate_Temp	1001,9	24,1	320	196,9	152,1
05_ R_0 _Min_Temperature	1001,9	24,2	284,3	140,1	118,6
06_ R_0 _Min_Temperature	1001,9	24,2	282,6	137,4	116,9

Table 5. Example of measurements while the temperature was decreasing [9]

As before, it can be clearly seen a strong dependency of the cold resistance with the temperature. For the hole set of measured points, the dependency of the cold resistance with the temperatures can be easily seen on the following graph:

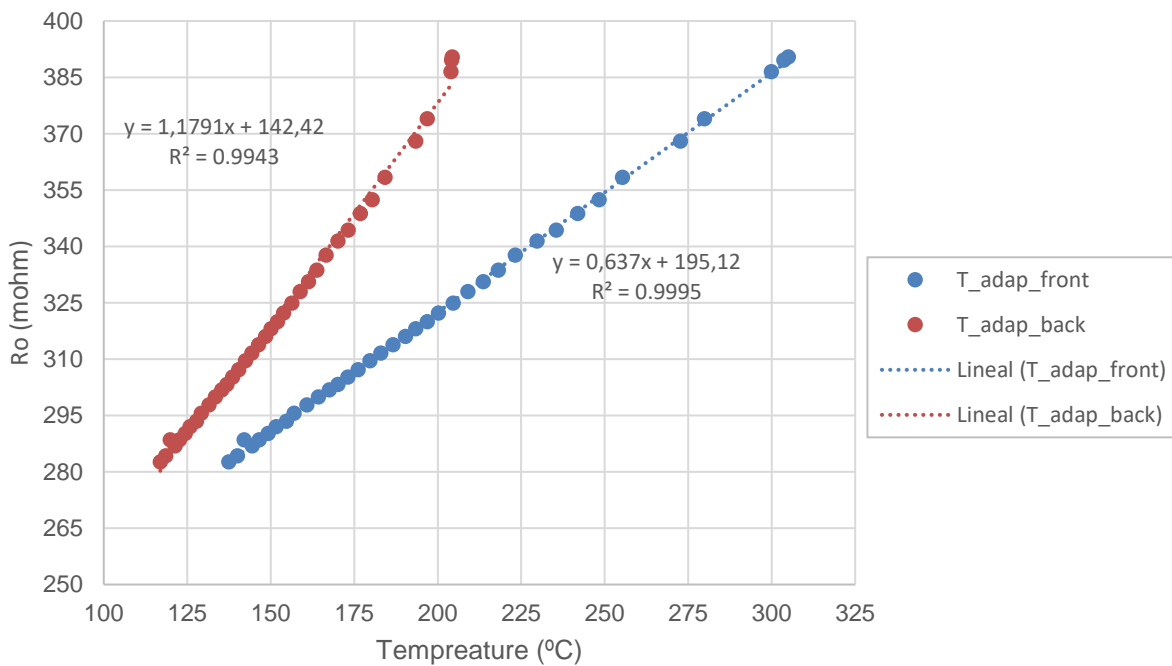


Figure 16. R_0 variation when adapter's temperatures decreases [9]

The linear dependency of the cold resistance value with the adapter's temperatures is once again proven. This confirms this dependency and sets a strong basis for further researches and mathematical derivations.

2.4 CGP Tests: Temperature distribution

The maximum temperature of the CGP while working is found at its tip, from that point the temperature starts to drop all over the CGP's body creating a temperature gradient. This gradient of temperatures is a really big source of information when thinking about cooling the adapter of the CGP, since this gradient will be the same one that will appear when the CGP is inserted into the adapter.

It has been shown before, that the temperature of the rear part of the adapter is always lower than that of the front part, as it is expected, thus being the main source of heat the front part of the adapter when the CGP is inserted into it. In order to fully understand and to prove this behaviour an experiment was carried out with the help of the thermal camera shown in the next figure. See *Figure 17*.



Figure 17. Thermal camera FLIR T460 used on this project [8]

For the procedure of this experiment, the thermal camera was placed, as it is shown in the next figure, at a fixed distance of the CGP in order to obtain always the same photos, and since the results of the thermal camera vary depending on the distance between its lens and the focus of the heat, this was a key point for the correct development of the experiment.



Figure 18. Experiment set up for the thermal camera [9]

At the beginning, the CGP body was painted in black, as shown in the previous figure, in order to obtain photos with a better resolution in terms of temperature ranges, and also the thermal camera was adjusted to obtain good resolution photos of a ceramic surface by applying a emissivity coefficient of $\epsilon = 0.9$. Also a matte plate was added at the rear part of the test bench in order to avoid any possible light reflexion that could lead of wrong results. As it can be seen in *Figure 18. Experiment set up for the thermal camera*, at the screen of the camera, the thermal camera gave the opportunity to record the temperature of specific points defined by the user, generating this way, the temperature gradient that was under study (an example of the points recorded with the camera to generate the gradient is shown in the next figure). Furthermore, a dependency between the electrical resistance of the CGP and its temperatures was extracted. [9]

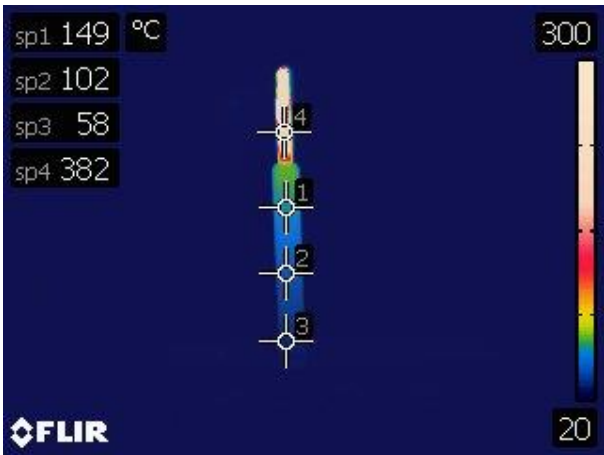


Figure 19. Thermal images of the CGP working showing the four used temperature points [9]

The point named as number 4, was really difficult to approach due to the small width of that part of the CGP, since the zoom was needed to obtain good pictures of the CGP the values of the point number 4 were really difficult to be obtained exactly by this methodology, but anyways, finally really good results were obtained.

This experiment was also part of the research project mentioned before, *Analysis of the Thermo-electrical Behaviour of Ceramic Glow Plugs by Alejandro Lombardía González*, thus a lot of points were evaluated for two different CGPs. This working points covered a range between 1 V and 5.6 V, having information this way of the CGP with a really low voltage applied and also, at the mainly working point of 5.4 V. Since all the data extracted from this experiment is not relevant to the aim of this project, on the following figures and tables some examples are given in order to create a general overview of the information obtained after the experiment.

As mentioned before, two CGPs were evaluated, number 10 and number 19, obtaining the following results. See *Figure 20* and *Table 6*.

Comment	U_{HSI} (V)	R_{HSI} (mohm)	T_1 (°C)	T_2 (°C)	T_3 (°C)	T_4 (°C)
01_CGP_#10	1,996	431,1	114	82	51	264
02_CGP_#10	4,504	740,1	174	122	72	415
03_CGP_#10	5,417	834,1	197	138	83	489
04_CGP_#19	1,995	429,1	103	74	45	224
05_CGP_#19	4,545	739,1	168	112	60	447
06_CGP_#19	5,390	823,5	187	123	65	484

Table 6. Example of data obtained at the end of the experiment with the thermal camera [9]

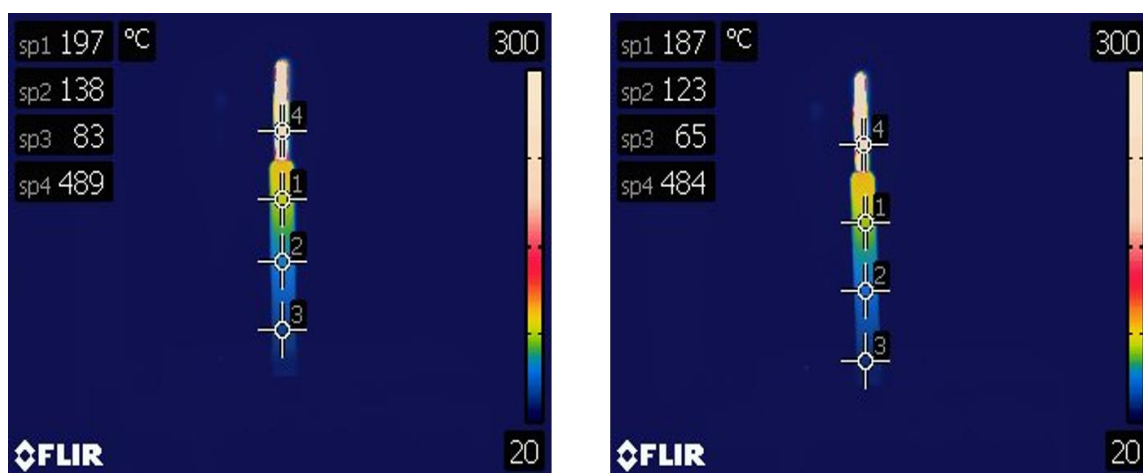


Figure 20. Thermal images at 5.4V: on the left CGP #10, on the right CGP #19 [9]

As it can be observed from the table above, there are differences, as it is expected, between both CGPs but both share something in common that is the dependency between R_{HSI} and all the

temperatures measured with the thermal camera; as it was mentioned before, the CGPs follow a PTC behavior when they are applied a voltage. In the next graph the variation of temperature and resistance with the voltage applied for the whole set of evaluated points is shown.

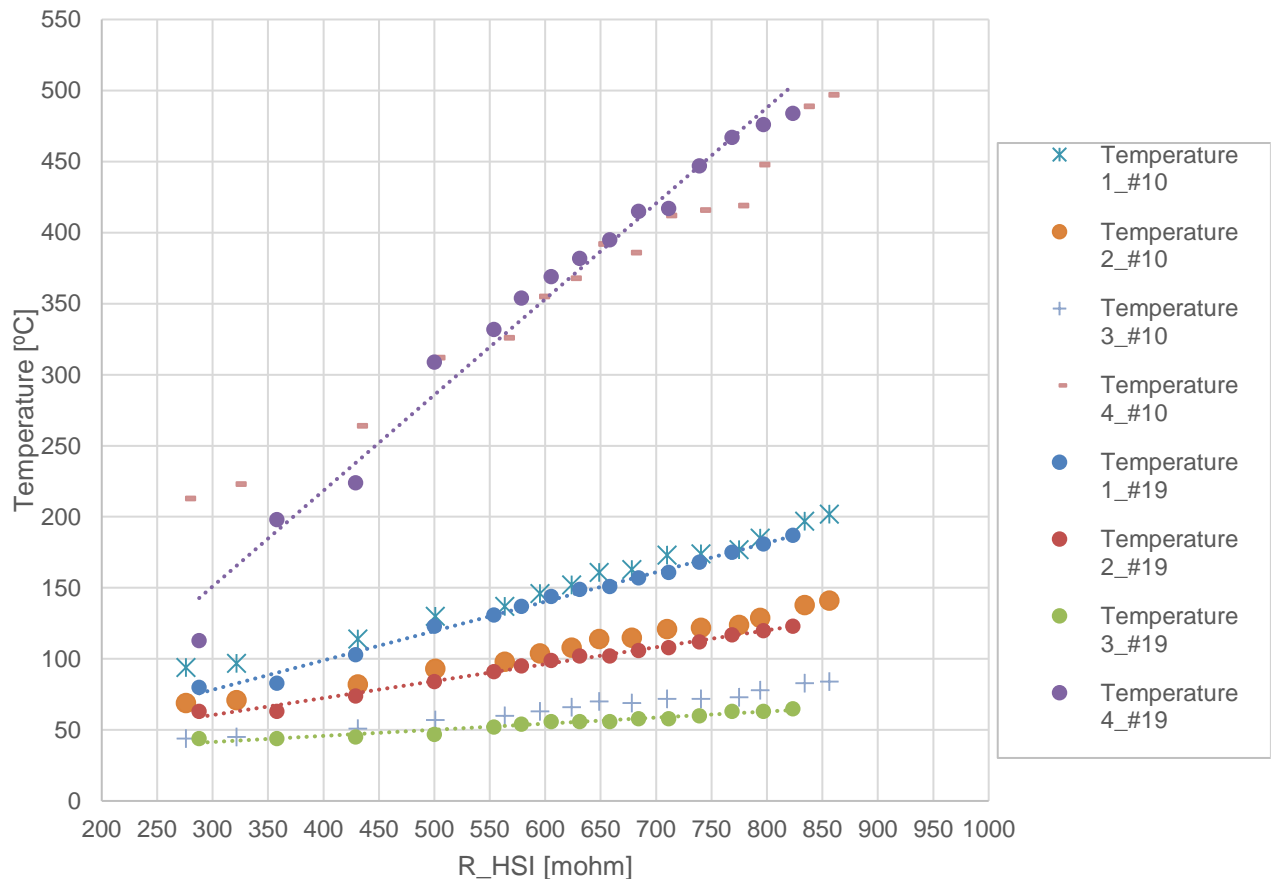


Figure 21. Electrical resistance variation with the temperature of the CGPs for both glow plugs tested [9]

One more time, a linear dependency between Electrical Resistance and temperature of the CGP can be observed. In this case an important remark is the huge difference of temperature between the point 4 and point 1, shown in *Figure 19*, but having not a big distance between both points.

2.5 Useful conclusions for the adapter design

With the development of this initial research, useful information for the design of the new adapter can be extracted.

First of all, it has been proven that only the ceramic part of a CGP has a real influence on the total electrical resistance of the CGP, thus this ceramic part is the cause of the heat generation.

For the cooling of the adapter, this ceramic part would be the one that really needs to be cooled or controlled. In order to reduce the operating temperatures of the adapter during operation, this ceramic part will be the focus of the cooling system.

It has also been shown that by controlling the temperature of the adapter the electrical behaviour of the CGP can be easily derived, thanks to its linear dependency, thus if the cooling system is able to achieve a constant temperature of the adapter while being under working conditions, for future researches, exact mathematical expressions for the Electro-thermal behaviour of the CGP can be derived and the ones obtained previously to this project can now be proven.

As a final remark for these experiments, the difference of temperature obtained between points 1 and 4 shown in *CGP Tests: Temperature distribution*, confirms that the lower part of the adapter, being this the one which is connected to the positive voltage, is not going to be hot at all in comparison with the part closer to the tip of the CGP, meaning that the cooling system that has to be found and designed for this project would not have to focus on the entire adapter but it will be enough if it is able to control and cool the main source of temperature, which is the one where T_{adap_front} is located, as shown in *Figure 13*. A graphical explanation of this last conclusion is shown in the next figure. See *Figure 22*.

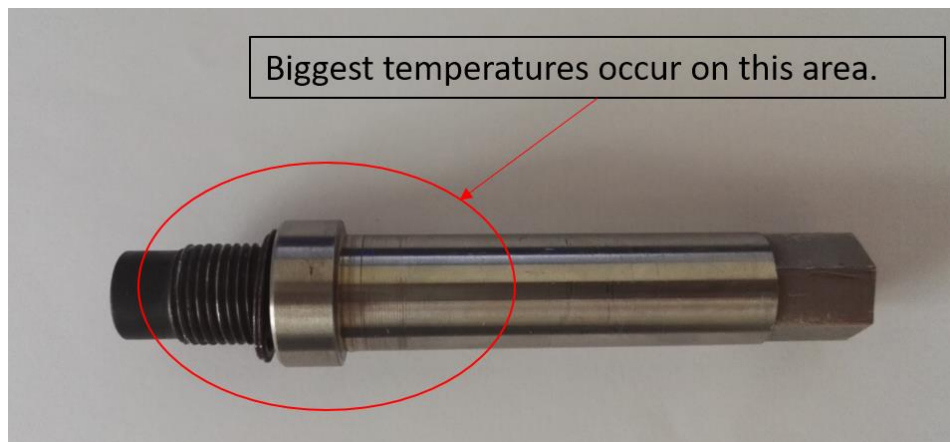


Figure 22. Biggest Temperatures' generation area shown in an old adapter

3 Development of the new adapter's design

After performing all the previous experimental research a decent amount of data was obtained, which is summarized in the previous point of this project, and thus the design phase could start. Before starting to think about the new design right away, the previous design was analyzed, looking for its failures in order to correct them; furthermore, all the requirements of this project were once more carefully analyzed combining this information with all the data extracted experimentally.

In this section all the development of the adapter is presented, from the analysis of data until the chosen final solution.

3.1 Initial considerations for the new adapter's design

The first step in order to be able to design a new adapter, was to analyze the actual design of it, to extract useful information as the failures that were found while working with it; to achieve this I used as a source of information the Master's thesis: *Entwicklung von Auswertestrategien und Durchführung von Versuchen unter Verwendung von kontrollierter Oberflächen-zündung in stationären Erdgasmotoren* by Javier Rio Sastre; using the 3D model of this adapter all of its characteristics were extracted and thus, improvements were found. See *Figure 23*.

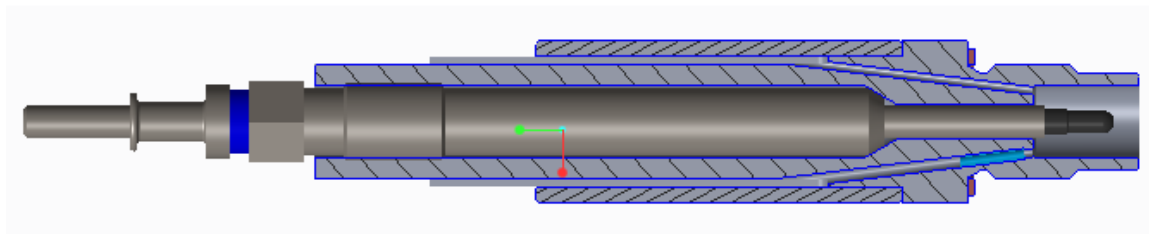


Figure 23. 3D model of the adapter's assembly used until this project [13]

To begin with, the material used for the construction of this adapter was stainless steel (1.4301), with only a thermal conductivity $k = 16.2 \text{ W/(mK)}$ which is really low for one of the aims of this project, cooling down the adapter while being under operation conditions. With this low thermal conductivity the heat dissipation that could potentially be achieved would be lower than that achieved with a material with higher thermal conductivity, and since the mechanical properties of the material are not important for this project, since the adapter is not going to be subjected to big mechanical stresses, one of the first changes for the new adapter will be the selection of a new material.

As can be seen in the next figure, the sapphire used as lens in this adapter to measure the tip's temperature of the glow plug was placed far away from it. See *Figure 24*.

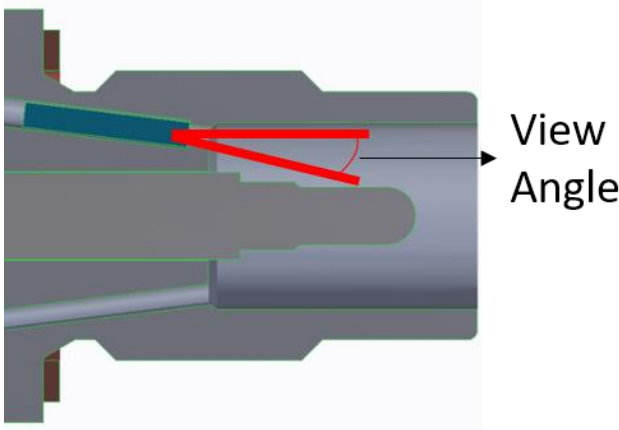


Figure 24. Method used for measure the tip's temperature in the old Adapter [13]

The following drawing shows that the small gap between the outer surface of the adapter and the sapphire, acted like a window were the light shaft had to pass through in order to reach the measuring point at the tip. This small gap, or window, was a really big problem while working with the adapter after some hours of operation, because particles generated in the combustion chamber were deposited on this small window thus, causing the gap to be completely or partially covered by them and finally obstructing the vision of the adapter's tip. See Figure 25.

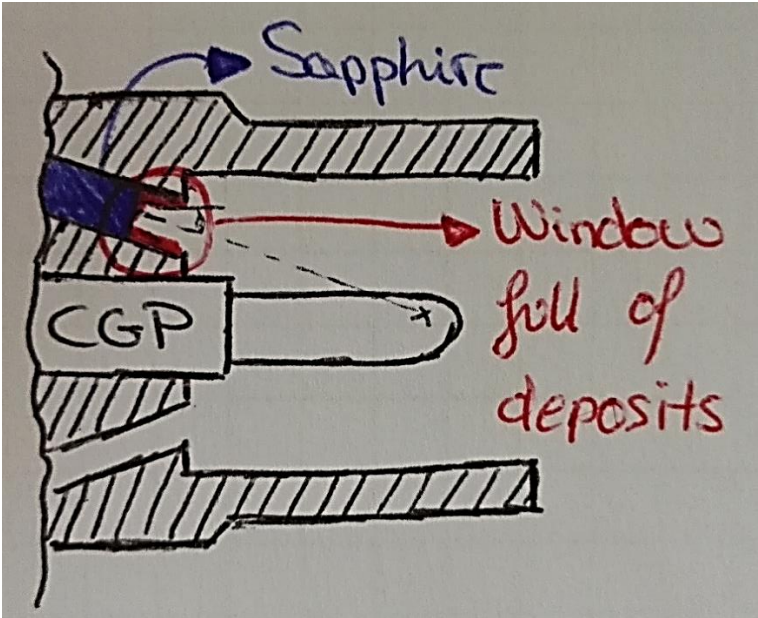


Figure 25. Scheme of the old sapphire's design with the deposition of particles problem

In order to solve this problem, the design for the sapphire had to be changed, and instead of having an small sapphire inserted into the adapter, the solution studied was to have a longer

sapphire placed next to the adapter's tip with an angle that allow us to directly measure the desired temperature ,while not having to deal with the deposition of particles. Thanks to the angle of the sapphire's outer surface, the light shaft reflected on this surface would give us the right measurement of the tip's temperature. See *Figure 26*.

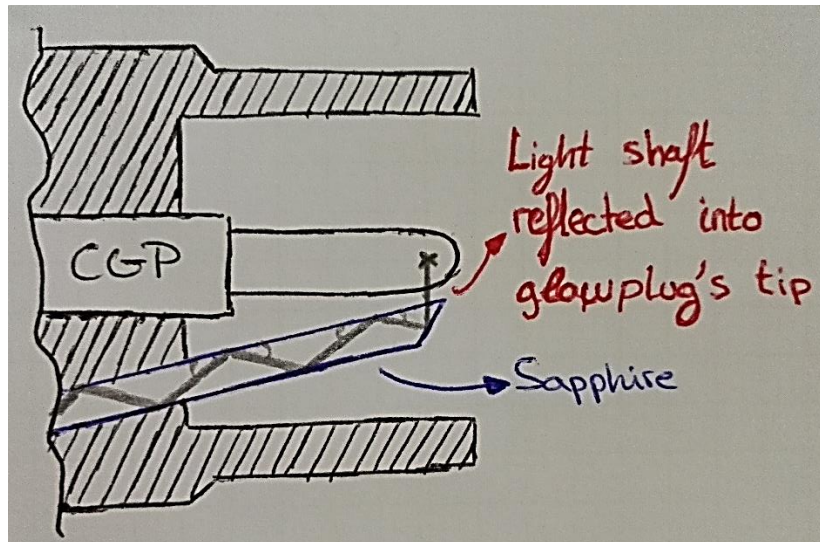


Figure 26. New concept for the sapphire design

Other of the problems found on the old design was that the optical fiber, which was connecting the pyrometer with the sapphire, was glued into the adapter making this way really difficult the possibility of changing it if it was needed.

As shown in *Figure 13* and at *Figure 23*, the three measuring points of temperature inside the adapter were on the same cavity, the thermocouples were glued on three different locations to measure three different points of temperature. While this was a valid solution, the aim of this project is to fully measure and extract all the information possible, about the CGP behaviour and thus its adapter's behaviour. In order to do so, while looking for the best solution for adding a cooling system to the adapter, including more thermocouples in a more distributed way is going to be studied, if this fact can be achieved then a proper gradient of temperature could be created.

The biggest restriction on this project was the space available where the adapter had to be inserted in. See *Figure 27*.

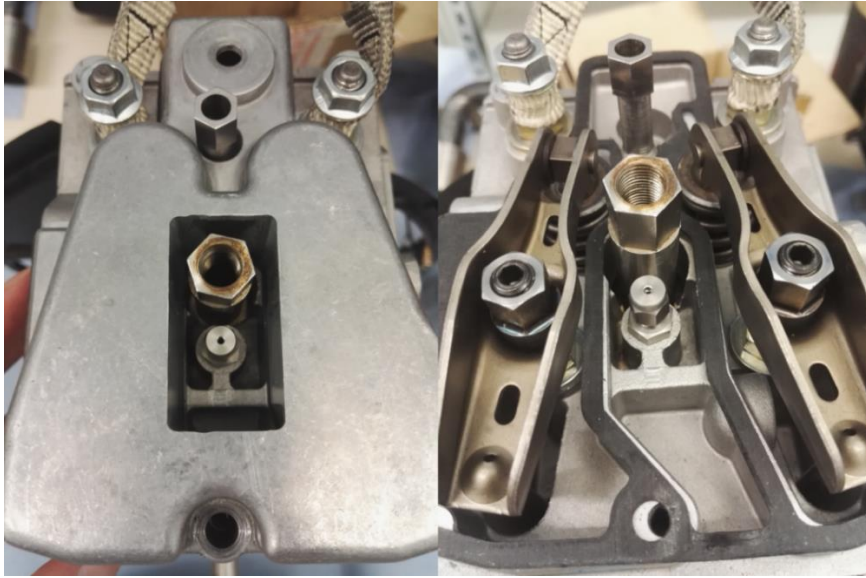


Figure 27. Old adapter placed in an engine block

As can be seen on this last figure, there is not much room left when the adapter is placed in the engine block. After measuring the gap where the adapter is placed in, it was found that the maximum outer diameter available was $\varnothing = 20$ mm. This is shown in the next scheme.

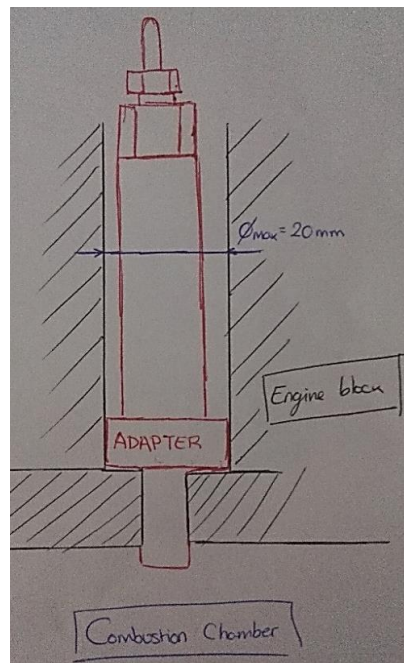


Figure 28. Scheme of adapter placed in the engine block

Some of the dimensions of the lower part of the adapter, the one closer to the combustion chamber, are given by the engine block's design and thus they could not be really changed.

The inner dimensions of the adapter could not be changed neither since they are defined by the CGPs, like for example the thread length in the upper part of the adapter where the CGP would be screwed in or the inner diameters for the different sections of the CGP.

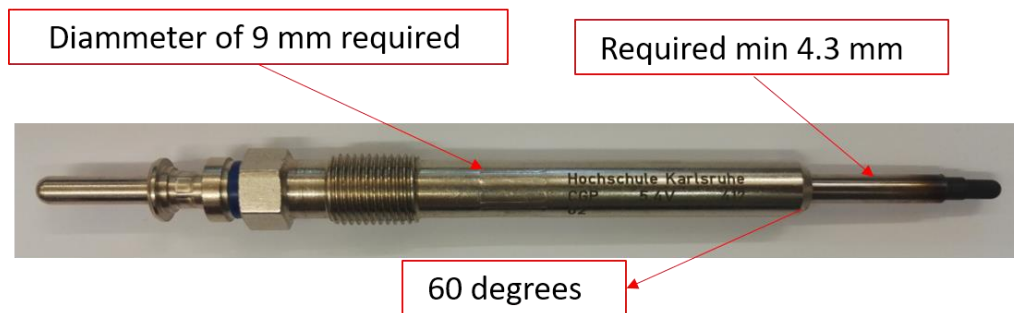


Figure 29. Important features of the CGP to take into account when designing the adapter

A closer look on the inner design of the adapter was taken, and by taking a look also on the CGPs that were tested with this Adapter a really big problem was detected.



Figure 30. Marks on the CGP after operation in the Adapter

In the last figure it can be observed that the CGP had some marks in form of rings on its metallic body caused when operating inside the adapter, this marks were done because of the lack of concentricity of the inner diameters of the adapter, causing the CGP to be in contact with the inner walls of the adapter when it was screwed into it. The concentricity of this inner characteristics would be ensured on the design of the new adapter and the diameter of this area of the adapter would be redesigned in order to look for one that will not cause these types of problems in the future.

In order to understand why these marks were produced, the CGPs available at the lab were measured to get the average diameter of that spot shown in *Figure 30*. The average diameter obtained was $\varnothing = 4.15$ mm, in order to ensure that this problem would not happen again, the diameter that can be seen on the next figure, obtained from the technical drawing of the previous adapter, with a value of 4.3 mm was decided to be changed for 4.4 mm in order to have some extra space and furthermore, a geometrical tolerance of concentricity was added for those diameters.

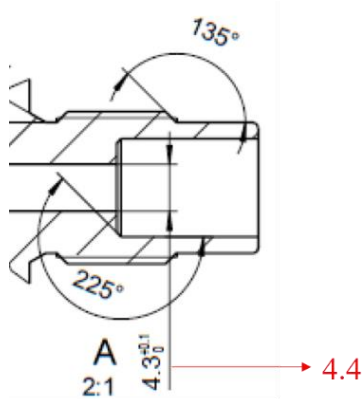


Figure 31. Diameter that was changed to ensure that the marks will not happen again

With all of this information extracted analyzing the old adapter design, the engine block and the data extracted from the initial research done for the development of this project, a path for the new adapter's designed was created and thus, the brainstorming about the possible new designs could start.

3.2 Design options for the adapter

Once the old adapter was completely evaluated, it could be said that the initial ideas for the new adapter's design could be based on it but some changes needed to be applied as it has been discussed.

Different options for each characteristic of the new adapter were discussed and are shown in the following table:

	Option A	Option B	Option C
Adapter itself split into several parts	YES	NO	
Symmetry of the Adapter	Completely symmetrical	Partially symmetrical	Asymmetrical
Cooling medium	Water	Compressed Air	
Method used for cooling	Copper coiling	Manufactured fluid guiding	Direct exposition
Fluid supply	Pump	Refrigeration Unit	Air supply
Temperature Measurement	Thermocouples		
Tip temperature measurement	Saphire with fiber optic		
Number of cavities for thermocouples	Single	Multiple	
Protection for optics / temperature measurement devices	Completely covered by adapter	Metallic Shell	Copper Coiling
Method for inserting the optic fiber in the Adapter (contact with the Saphire)	Glued adapter	Threaded Adapter	Interference Fit
Connection method for the thermocouples	Glued	Interference fit	
Material	Steel alloy	Nickel Alloy	

Figure 32. Options for each characteristic studied for the design of the new adapter

As it has been said before, the old material of the adapter did not meet the requirements of heat disipation that a cooling system would need, therefore the material needed to be changed. In order to facilitate the selection of the best solution based on the different options that are going to be presented, a Nickel alloy was selected to be the material for the new adapter, specifically Nickel 99.2 LC alloy which has a thermal conductivity of $k = 78.5 \text{ W/(mK)}$ [17] which is almost 5 times of the one of the previous used material. Furthermore, this Nickel alloy does not have any problem when it needs to be machined or welded, it works perfectly at high temperatures, and since the mechanical properties of the material are not trully important for

this project this alloy fits really good the new adapter's design, so all of the models that were discussed were meant to be made out of Nickel 99.2 LC.

By combining the characteristics that have been presented in the last figure, some options for the new adapter's design were developed. And they were divided in to two big groups, models that used water as cooling medium and models which used compressed air as cooling medium, being this two the only available cooling mediums for the development of this project.

3.2.1 Water cooled: Model N°1

This adapter would be split into 3 different parts, as shown in the figure below. This model would have holes on its mid part, that would work as water pipes so the water would be flowing inside the adapter, close to the CGP and to the area where T_{adap_front} is located. Both low and upper part would have some cavities so the water would flow up and down, driven by these cavities. The outer diameter of the adapter would be constant and equal to 20 mm in order to have the maximum available space on its inside part. See *Figure 33*.

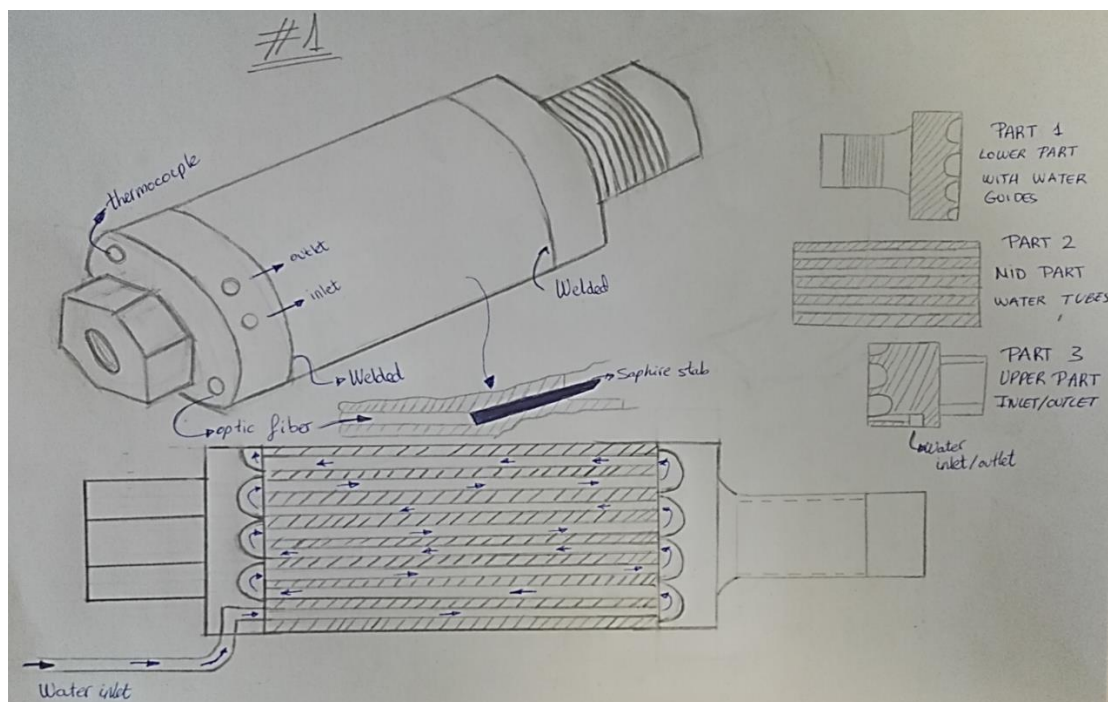


Figure 33. Model N°1; On the right part the different parts of the adapter can be seen, on the lower part the water flow sketch can be seen

As it can be seen on the figure above, the three parts would be assemble by welding them all along their outer surface.

The sapphire stab would be a long one, and it would be in contact with the optical fiber as exposed there; this optical fiber would be out of the adapter thanks to the upper hole, and the same for the thermocouple inserted. To add more thermocouples could be study when designing the part, it would depend on the available space. For the cooling system, just two pipes for the inlet and outlet would be needed, as well as the sufficient water flow rate.

3.2.2 Water cooled: Model N°2

By studying the first model shown, it was noticed that by only welding the outer surface of the parts, the water that would be flowing inside the adapter might filter into the CGP cavity, which would be unacceptable; but this fact could not be confirmed unless the part would be manufacture. In order to correct this possible failure, this new model was designed.

See *Figure 34*.

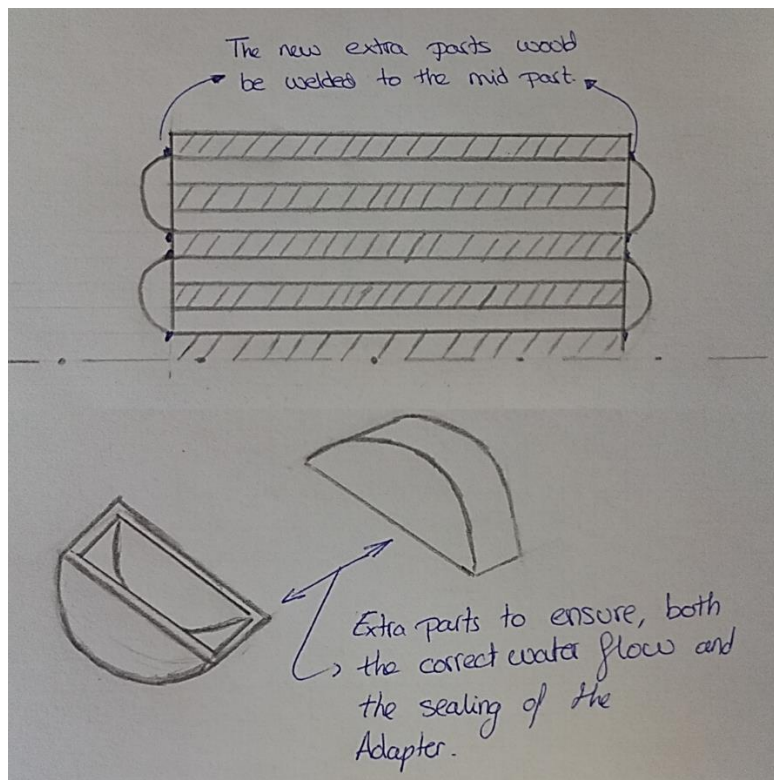


Figure 34. Model N°2; Extra parts for this model

The complete assembly of this model would look the same as the one before, thus it is not shown on the last sketch. By adding the parts that are shown in the figure above, an inner sealing for the water would be achieved, since these little parts would need to be welded to the mid part of the adapter, and afterwards the outer surface of it would be welded again.

Everything would remain the same as before, just the cavities on the lower and upper part should be bigger this time, in order for those little parts to fit inside them.

For the sapphire and thermocouples everything would remain the same, with the possible complication that the addition of more thermocouples may be impossible this time, since the cavities of both upper and lower part should be bigger this time.

3.2.3 Water cooled: Model N°3

In this model, the cooling system would be carried out by an external copper coil where the water could flow through, being in contact with the outer surface of the adapter, and since the copper has a really high conductivity, and so does the Nickel alloy chosen, the heat disipation would be really high.

As it was discussed, there is no need for cooling the entire adapter, only the area where the ceramic part of the CGP is located would need to be cooled. The sketch of the model is shown in the next figure. See *.Figure 35*.

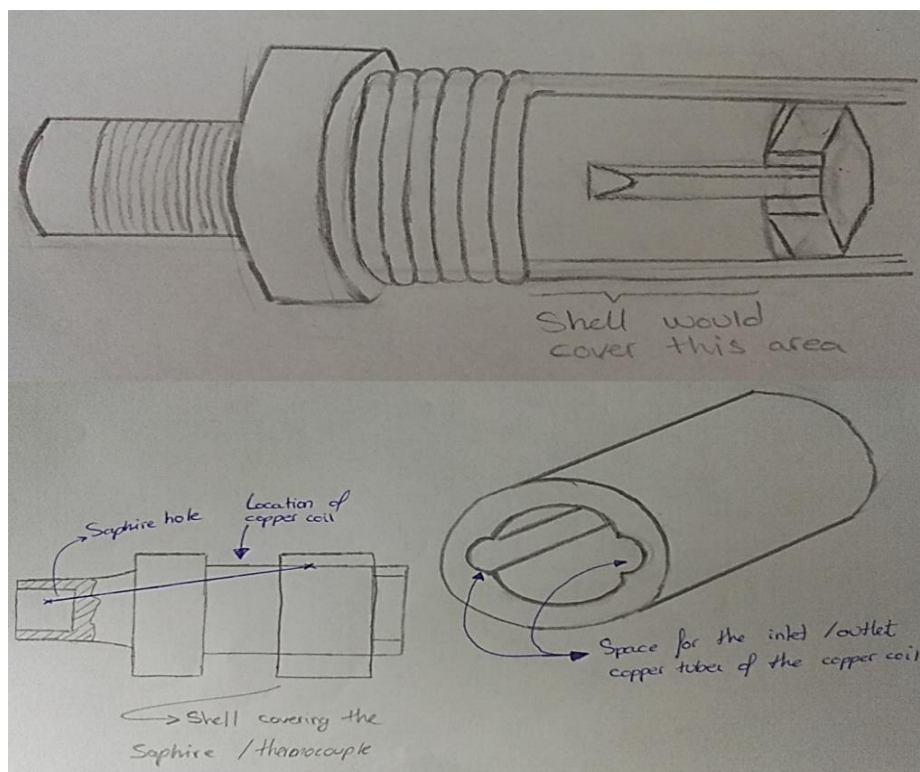


Figure 35. Model N°3; On the upper part the adapter with the copper coil; on the lower part the shell needed and the sketch for the sapphire's hole

As it can be seen, the copper coil would be placed as closer as possible to the area of T_{adap_front} ; while the hole for the sapphire would begin on the upper part of the adapter (same would be the case for the single or multiple holes for thermocouples that could be included on this adapter's model), thus needing some protective sleeve that would cover these cavities, this

would be done by the shell shown in the sketch. The reason of the shell having those „ears“ on its inner surface, would be to have sufficient space for the copper coil's inlet and outlet.

The biggest problem with this model would be the space limitation that the adapter has; for example, if the shell had a thickness on its wider wall of 2 mm this would mean that the maximum possible diameter for the copper tubes would be 1 mm, since the adapter has a diameter of 16 mm on its thin part and 20 mm on its thicker one.

For the sapphire connection the concept would be the same as before, one long sapphire stab connected thanks to an adapter for the optical fiber, that would be inserted on its hole.

3.2.4 Water cooled: Model N°4

This solution is based on the one shown before. This time, the adapter would be machined in order to have external cavities for the copper coil, allowing us this time to use bigger copper tubes that would be easier to bend and to obtain. See *Figure 36*.

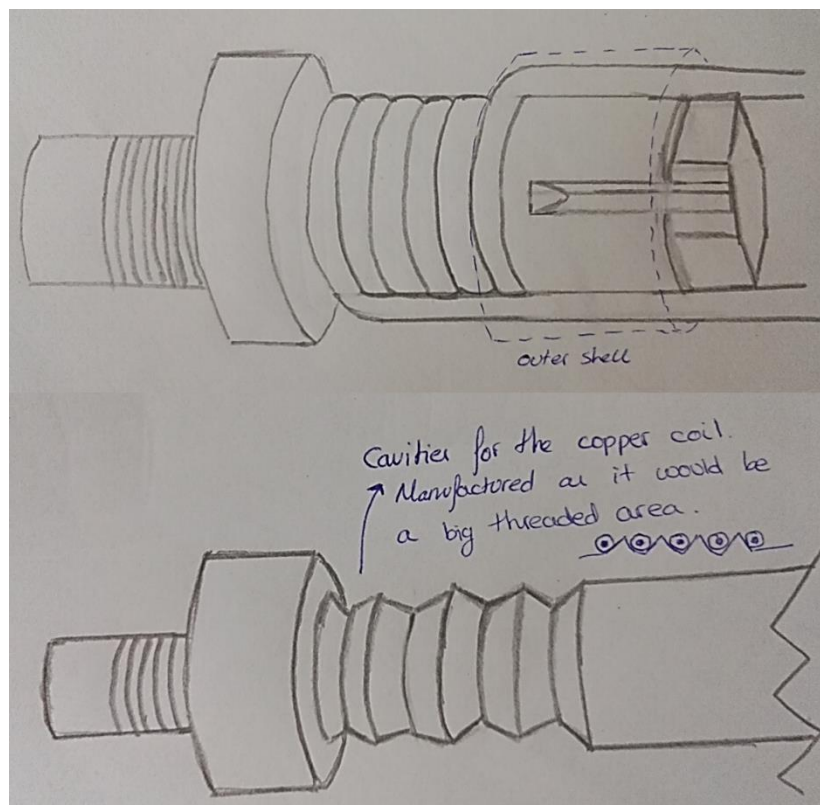


Figure 36. Model N°4; On the upper part the adapter with the copper coil is shown; on the lower part the machined surface of the adapter without the copper coil

By doing so, the copper coil itself would have copper tubes of a certain diameter, while the inlet and outlet of the coil could have smaller diameters (as a possibility it would not need to be

made out of copper, plastic pipes could be used to connect the inlet and outlet of the copper coil) in order to be able to include the same shell as before, since it would be needed because the sapphire and thermocouples designed would not change, and thus they would need a protective sleeve.

3.2.5 Water cooled: Model N°5

Based on the rest of the models that include a copper coil for the cooling system, this model would have the advantage of not having a Shell to act like a protective sleeve for the thermocouples and Sapphire, due to the fact that the holes for the thermocouples and sapphire would be shorter (easier manufacturing process), so copper coil itself would act as this protective sleeve. See *Figure 37*.

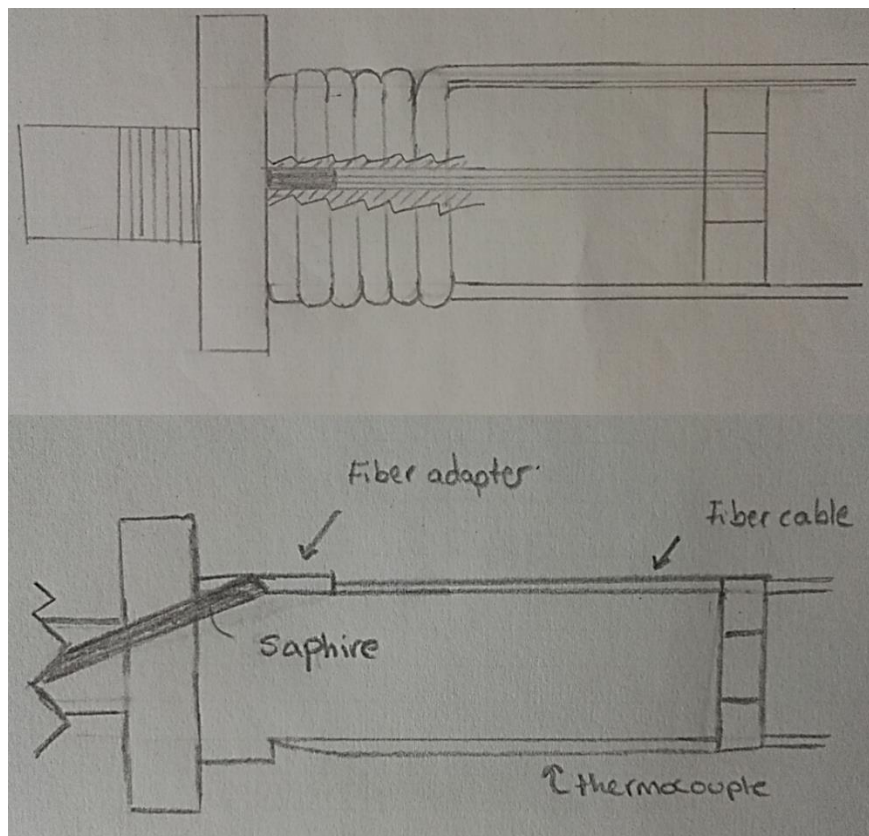


Figure 37. Model N°5; On the upper part the adapter with the copper coil is shown; on the lower part the measurement techniques

The advantage of this would be that the optical fiber would not be as hot, since the copper coil would be cooling it as well, which it was not a requirement of the project but it would be a nice feature to have. Another advantage would be that there would be more space available to place thermocouples, and for the complete assembly less parts would be needed since there would

not be shell this time. As a drawback, again 1 mm copper tubes would be used, since there would not be more space for placing bigger ones.

3.2.6 Air cooled: Model N°6

In this Model for the new adapter's design, compressed air would be used as a cooling medium for it. In order to do so, a pipe inserted into the engine block's cavity where the Adapter is mounted would let the compressed air flow directly into the adapter's body. By adding a flow control valve (FCV) the flow rate of this compressed air could be controlled if desired.

Since this model does not need any extra features for including the cooling system on the Adapter, all the space available on the Adapter could be used to add as many thermocouples as we could in order to create the desired gradient of temperatures.

See *Figure 38*.

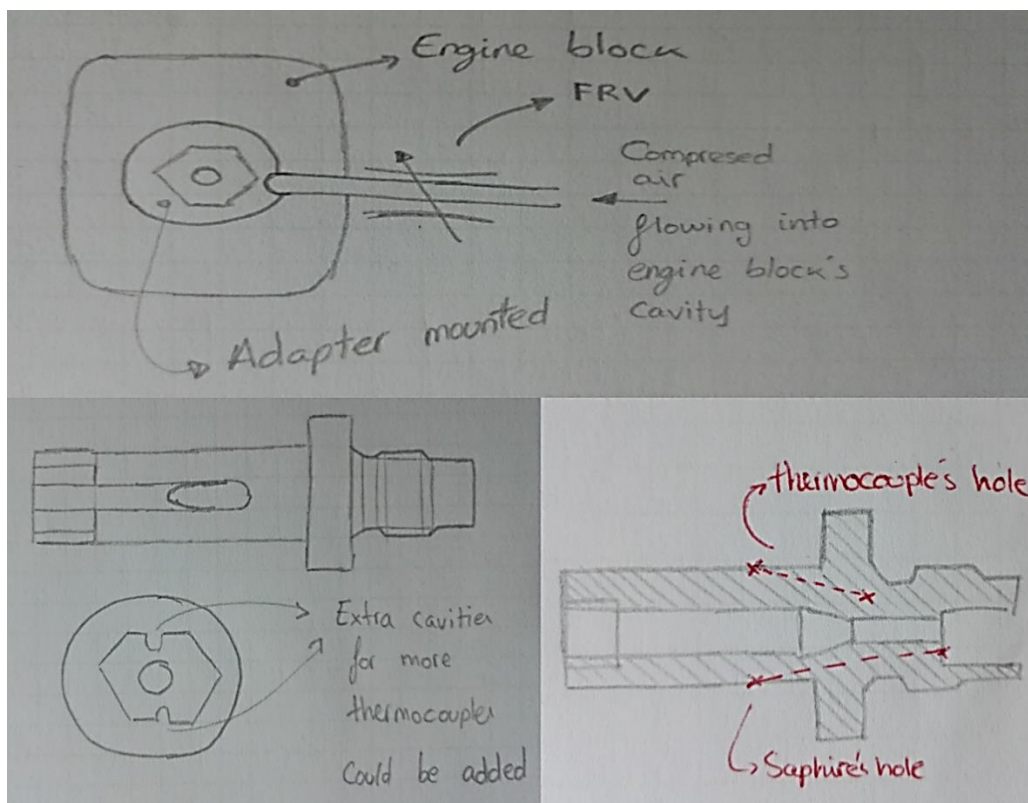


Figure 38. Model N°6; in the upper part the pipe with the FCV is shown entering the engine block's cavity; on the lower part the possible design for the adapter is shown.

As stated before, the method for measuring the tip's temperature of the CGP would not change, the sapphire will be inserted into a hole specifically designed for its dimensions which will be drilled all over the length of the adapter, but this time some extra features for thermocouples could be added since the difficulty of manufacturing this adapter would not be as high as the

ones previously mentioned, because of the lack of specific characteristics for the cooling system, so several thermocouples could be added at different depths to create a temperature gradient.

3.3 Evaluation of the different options for the new adapter's design with water as cooling medium

In order to have a fair discussion about which could be the best choice for the new adapter, again, the discussion about which would be this design was split between options with water as cooling medium and options with air compressed as cooling medium.

Since the design with compressed air as cooling medium was the only one of its type, being simple and functional in all cases, there will not be any discussion about it, but experimental trials were carried out in order to show the effectiveness of both cooling methods, thus choosing between them once the experiments were concluded.

For the options that had to do with water as cooling medium, some criteria was defined in order to be able to choose which was the best possible solution for this project. This criteria is shown in the next figure. See *Figure 39*.

	Model n° 1	Model n°2	Model n°3	Model n°4	Model n°5	Weight
Difficulty of the Manufacturing process for the adapter itself	0	0	2	1	2	1
Difficulty of the Manufacturing process for the cooling system	0	0	2	2	2	1,5
Difficulty of the Manufacturing process for optics / thermocouples	0	0	1	0	2	2
Difficulty of the assembly (lot of assembly planes ,tools involved,...)	0	0	1	1	2	1,5
Difficulty to mount / dismount it into the combustion chamber.	2	2	1	1	1	1,5
Sealing (water of the cooling system)	0	2	2	2	1	2
Optic fiber can be easily removed / replaced	2	2	0	0	1	1,5
Easy comparison of results wrt the last adapter, due to not having big changes.	0	0	2	1	2	1,5
Need of extra parts (cooling , sealing)	1	0	0	0	0	1,5
Durability	2	2	1	1	1	2

0=Difficult , NO, not taken into account

1=Standard, YES

2=Easy, Really good solved

0= Yes ; 1= NO

Result	11,5	14	19	14,5	22
--------	------	----	----	------	----

Figure 39. Comparisson of models which water as cooling medium

As a result of this evaluation the option, between the ones that had water as cooling medium, that fit the best into the requirements of this project was the *Water cooled: Model N°5*, due to its simplicity of design while having all the measurement characteristics needed and ensuring that water will not flow into the system which could provoke a really big failure of the system. This option was one of those which included a copper coil made out of copper pipes, and it was selected as better option in comparison with *Water cooled: Model N°3* and *Water cooled: Model N°4* due to the fact that it has no extra parts or extra features that needed to be manufactured in order to include the copper coiling. Due to the fact, that this design would not include a shell for protecting the optical fiber and thermocouples, bigger copper tubes, than the ones used on the other designs, could be used, increasing this way the contact surface between adapter's body and copper coil which will cause an increase of heat disipation.

Now that both cooling methodology had a chosen option was time to prove which method satisfied better the cooling requirements, which was to reduce the temperatures of the area at T_{adapt_front} , shown in *Figure 13*, to a value as low as possible with the equipment available at

the laboratory. In order to do so, several trials were carried out for both cooling mediums, both water and compressed air.

The results of these trials are exposed over the following sections of this project.

3.3.1 Cooling medium tests: Water

The test bench and all the equipment mentioned in the *Experimental research* for the development of the experiments were used once again.

For this experiments the cooling circuit needed to be built, in order to do so, a refrigeration unit, pipes and the copper coil were needed. The copper tubes needed for the chosen solution were smaller than the ones easily available for the time that the experiment was carried out, thus copper tubes with an outer diameter of $\varnothing = 4$ mm and inner diameter of $\varnothing = 1$ mm were bought and finally used on these trials.

The following picture shows the available refrigeration unit that was used on these experiments, with the pipes used for the connections already in. See *Figure 40*.

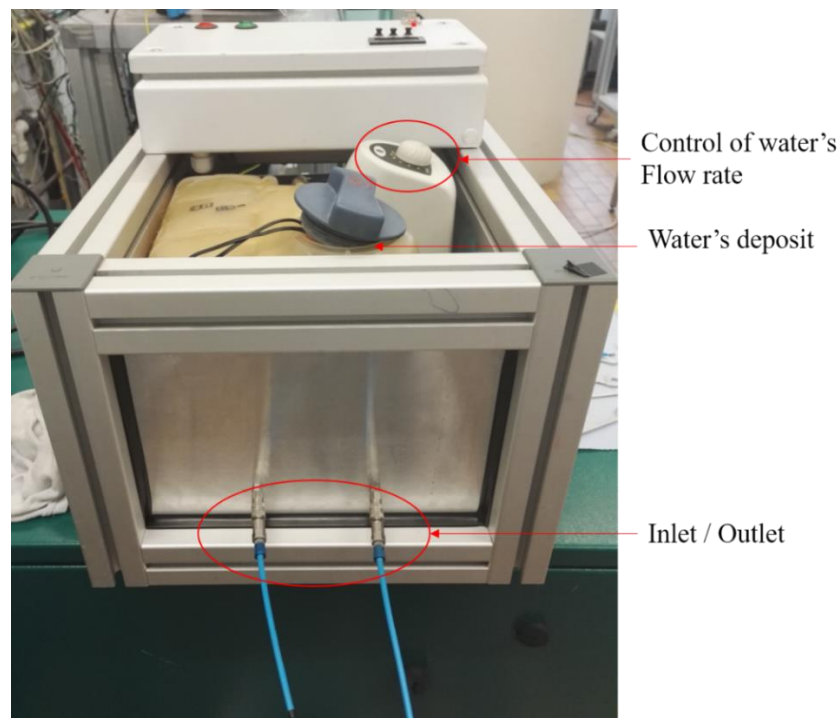


Figure 40. Refrigeration unit used for the trials

The copper tubes were bended over a 20 mm diameter metallic bar in order to simulate the external surface of the adapter, once this was done the copper coil was placed on the adapter and tightened to be on contact with the adapter as much as possible. See *Figure 41*.

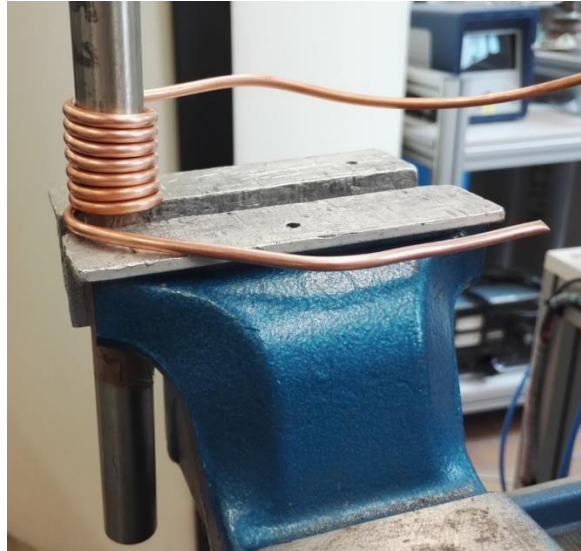


Figure 41. Copper tubes being coiled around the metallic bar

Once the copper coil was properly adjusted to the adapter's body all the connections were made and the experiments could start. See *Figure 42*.

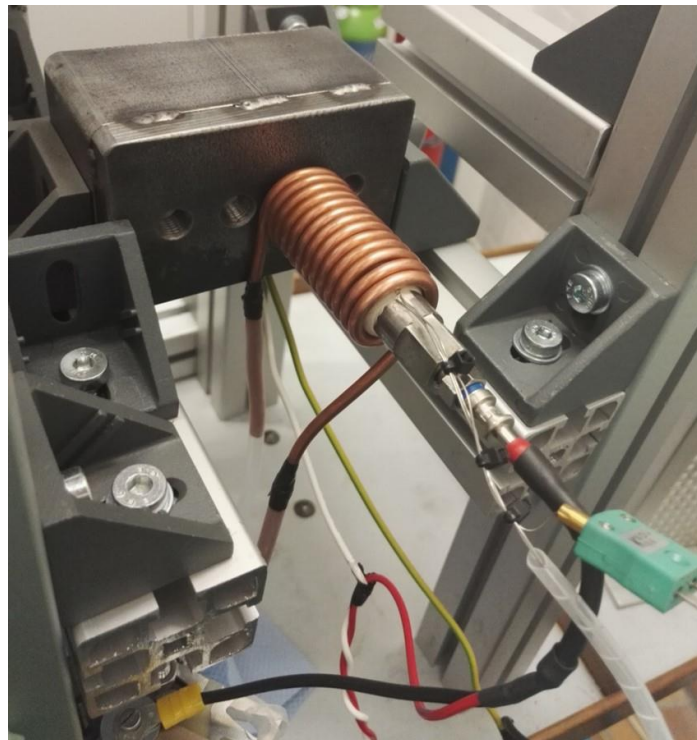


Figure 42. Adapter with the copper coil being tested

In order to test the minimum temperature that we could achieve under operation conditions for the adapter, or in other words which was the maximum variation of temperature for the adapter that could be obtained, the maximum flow rate of the pump was selected.

In order to calculate the maximum flow rate of the pump taking into account the losses that we had on our circuit, and the circuit's pressure the following experimental calculation was carried out:

- First a recipient was filled with water during 1 exact minute while the pump was working with its maximum flow rate. This was made three times in order to get the average volume that the pump gave.
- In order to measure exactly the liters of water that were pumped out of the pump, the water that was on the recipient was moved to a test tube like the one shown in the following figure.



Figure 43. Test tube used for measuring the volume of water

- Once the three volumes were measured the following calculation was carried out:

$$V_1 = 0.572 \text{ L} ; V_2 = 0.562 \text{ L} ; V_3 = 0.565 \text{ L}$$

The average volume obtained was then: $V_m = 0.5663 \text{ L}$ and thus the max flow rate would be:

$$\dot{v}_{max} = \frac{V_m}{t} = \frac{0.566333 \text{ L}}{60\text{s}} = 0.00944 \frac{\text{L}}{\text{s}} = 9.44 \times 10^{-6} \frac{\text{m}^3}{\text{s}}$$

$$\dot{m}_{max} = v_{max} * \rho_{water} = 9.44 \times 10^{-3} \frac{\text{m}^3}{\text{s}}$$

With the maximum flow rate calculated, the heat produced by the water could be obtained by measuring the temperature at the inlet of the circuit and that at the outlet of it.

In order to evaluate the effectiveness of the water cooling method, the following tests were carried out.

Three voltages were designated to have three different set of temperatures to work with, being these 3 V , 4 V and the working voltage 5.4 V. For each voltage the starting conditions were written down, then the voltage was applied until achieving steady state conditions, at that point the pump was turned on with its maximum flow rate, after some minutes steady state conditions were achieved being these conditions the ones with minimum achieved temperature that are shown in the next table.

For these experiments T_{adap_front} and T_{adap_back} were used as references, and as it has been mentioned before, being T_{adap_front} the temperature that these cooling system would need to decrease as much as possible. After the trials were completed the following data was extracted:

Comment	T_{adap_front} (°C)	T_{adap_back} (°C)	R_{HSI} (mohm)
3V_start_conditions	46,4	38,6	
3V_Max_temperatures	100,4	72,74	513,6
3V_Min_temperatures	95,1	51,5	510
4V_start_conditions	37,3	35,8	
4V_Max_temperatures	133,4	89,9	636
4V_Min_temperatures	124,9	58,2	631,7
5.4V_start_conditions	34,5	33,1	
5.4V_Max_temperatures	181,2	114,5	789,3
5.4V_Min_temperatures	167,5	67,1	782,1

Table 7. Result of the copper coil, as cooling method ,test

R_{HSI} was measured in order to see the electrical behaviour change when the adapter was cooled, and since power is defined as $P_{HSI} = \frac{U_{HSI}^2}{R_{HSI}}$ when the electrical resistance of the CGP decreases due to the water flowing through the copper coil, the power consumed by the CGP increases, being the voltage applied to it constant. After extracting all the data the following graphs were created to clearly see the decrease on temperature that was achieved at each voltage measured.

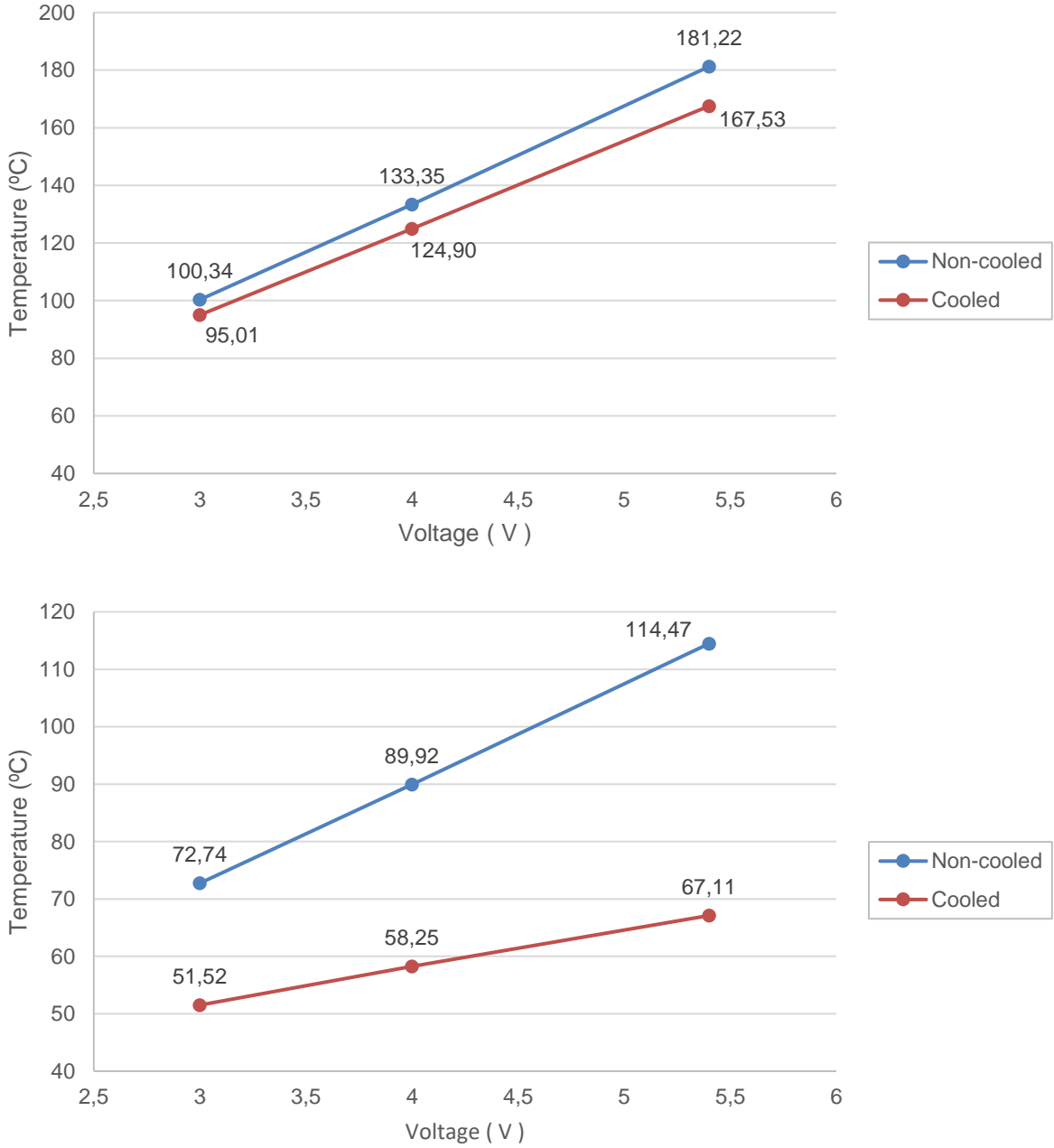


Figure 44. Result of the copper coil, as cooling method, test; on the upper graph results for the front part of the adapter; on the lower graph results for the rear part of the adapter

As expected, the cooling system works better for higher temperatures where the difference of temperature between the inlet and the outlet of the water at the circuit is the maximum. The results for the T_{adapt_back} were acceptable, decreasing the temperature almost 50 °C when working with 5.4V; but those for T_{adapt_front} , as can be seen, were really poor, the decrease on temperature achieved was far from being the one desired, only around 15 °C when working with 5.4 V, the expected value for this temperature was around 100 °C which is way far from the 167 °C achieved, but, before saying that this method does not meet the needed results for

the project another test was carried out. The outer walls of the copper coil were cool while the experiment was carried out, this means that the flow rate of the pump was not the problem. Since the copper tubes used for the previous experiment were bigger than the ones that were going to be used on the real model, the contact surface between the Adapter and the copper coil was less than the one achieved at the actual model; in order to be closer to reality, copper paste was put all over the adapter's body and the copper coil, this way the contact surface will be the maximum available, even bigger than the one that would be achieved in the actual model if manufactured with the smaller copper tubes. This experiment would give us the maximum decrease on temperature that could be achieved with this method, if the results with this method were not good at all, another cooling system should need to be study.

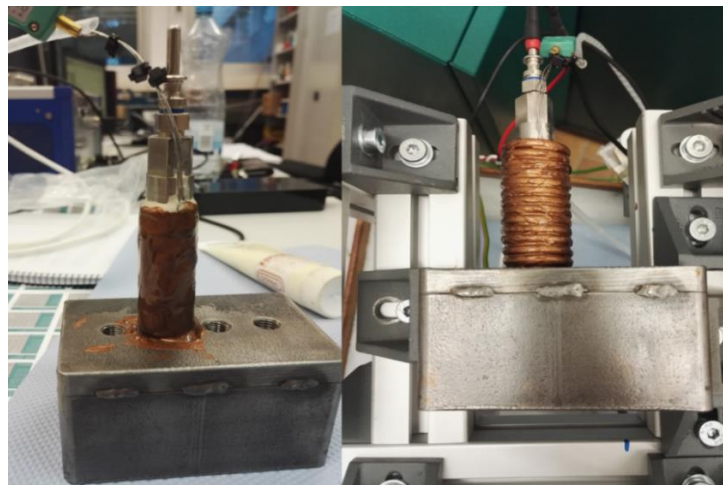


Figure 45. Copper paste being applied on the left; adapter mounted on the metallic block with the copper paste applied

In order to trully prove this increase of surface contact, the experiment was carried out with the maximum possible temperature of T_{adap_front} achieved by applying 3V , 4V and 5.4 V to the CGP, as done before. The results obtained this time were:

Comment	T_{adap_front} (°C)	T_{adap_back} (°C)	R_{HSI} (mohm)
3V_start_conditions	47,3	37,4	
3V_Max_temperatures	100,4	68,2	512,3
3V_Min_temperatures	87,8	38,3	505,8
4V_start_conditions	39,6	36,6	
4V_Max_temperatures	133,3	84,5	634,9
4V_Min_temperatures	113,4	39,9	626,4
5.4V_start_conditions	35,9	34,7	
5.4V_Max_temperatures	181,1	105,8	779,5
5.4V_Min_temperatures	155,3	45,6	775,3

Table 8. Results of the water cooling when applying copper paste (Maximum contact surface)

In order to evaluate the results easily the following grphs were created:

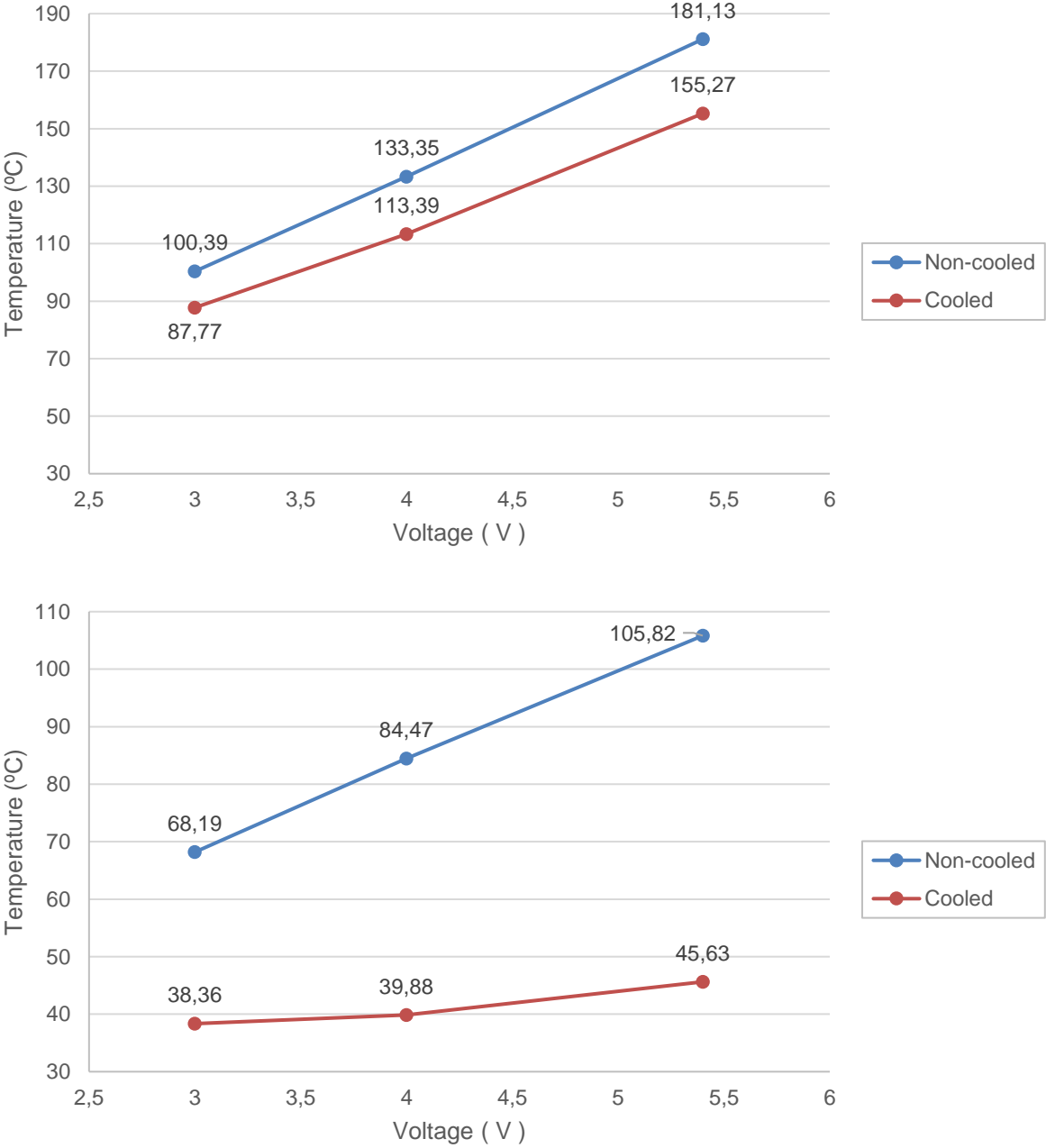


Figure 46. Results of the water cooling when applying copper paste (Maximum contact surface); on the upper graph results for the front part of the adapter; on the lower graph results for the rear part

As it can be seen, when compared with Figure 44, the results were way better , this time T_{adapt_front} was decreased 26 °C when working at 5.4 V , so the contact surface had a big influence when cooling the adapter; but as mentioned before the results still were not the ones expected, far from the desired temperature when applying the cooling method, while a

temperature of around 100 °C the achieved one was 155 °C, and these results were better than the ones that could have been achieved when using the real copper tubes, since this contact surface was the maximum available. The heat dissipated by the water while carrying out the test at 5.4 V was:

$$Q_{water} = \dot{m}_w * c_{p,water} * T_{outlet} - T_{inlet}$$

Being ($T_{outlet} - T_{inlet}$) the difference of temperature between the inlet of the circuit (outlet of the pump) and the outlet of the circuit (inlet of the pump); the temperatures measured were:

$$T_{outlet} - T_{inlet} = 29.1 \text{ } ^\circ\text{C} - 24 \text{ } ^\circ\text{C} = 5.1 \text{ } ^\circ\text{C}$$

With: $\dot{m}_w = v_{max} * \rho_{water}$; being $\rho_{water} = 1000 \frac{kg}{m^3}$ and $c_{p,water} = 4186 \frac{J}{kg * ^\circ\text{C}}$

This results in:

$$Q_{water} = 1000 \frac{kg}{m^3} * 9.44 \times 10^{-6} \frac{m^3}{s} * 4186 \frac{J}{kg * ^\circ\text{C}} * 5.1^\circ\text{C} = \mathbf{201.531 \text{ W}}$$

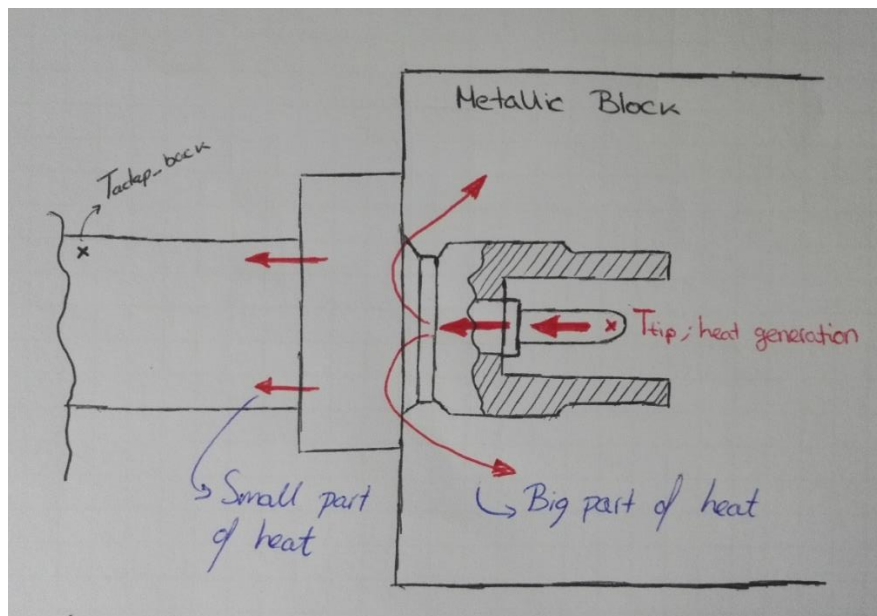


Figure 47. Heat distribution in the adapter when placed on the metallic block

The last figure shows the heat distribution of the CGP and adapter when placed on the metallic block of the test bench, that simulates the engine block. As it is explained on the drawing, only a small fraction of the heat goes into the area where T_{adap_back} is located, this is caused by the

low thermal resistance that the metallic block has, R_{block} , which causes that the biggest part of the heat generated in the front part where the tip is, goes out of the adapter through the area that is in contact with the metallic block, as can be seen in the drawing. So, no matter if the area of the adapter where T_{adap_back} is placed, is cooled, the R_{block} will be still lower than the thermal resistance of the adapter, so the heat distribution of the drawing will still be valid what would cause that the temperature on that area, T_{adap_front} , will always be a lot higher than that of the back part of the adapter. So the copper coil with water as cooling medium would not decrease more than the one showed before; furthermore the temperatures measured while operating on the engine block for T_{adap_front} were somewhere in between 200 °C and 300 °C, way higher than the ones achieved in the metallic block (due to the engine block being located in a closed space instead of an open room as the test bench), this will cause than the temperatures after applying this cooling method would be even bigger than the ones obtained during the development of these experiments.

3.3.2 Cooling medium tests: Air

Once the tests for the water were concluded the ones for the compressed air could start. For the realization of these tests a compressed air pistol was used and directly placed facing the adapter when it was placed on the metallic block just as before, so we had a comparable situation.

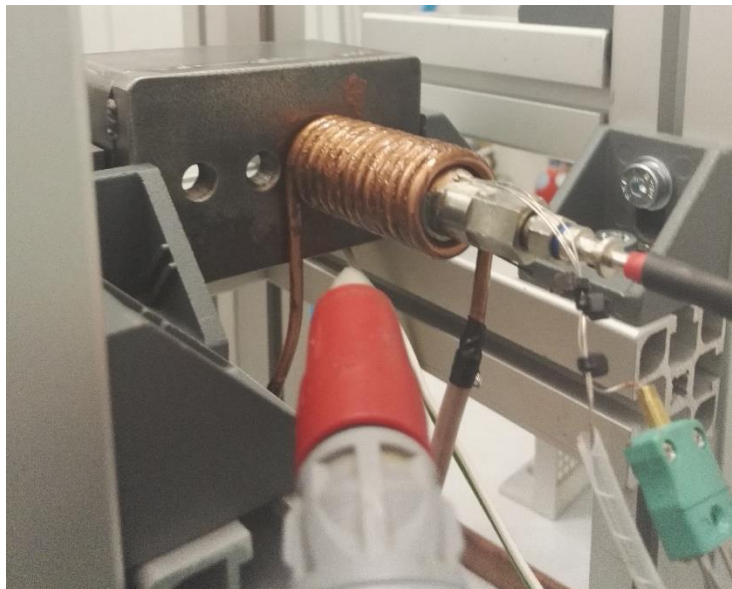


Figure 48. Compressed air pistol facing the adapter during the development of this experiment

For this experiment, the starting conditions were once again recorded, at that point 5.4 V were applied to the CGP, since we were trying to prove if the compressed air would work better than the water, just this voltage was used because being the one that generated the highest temperatures. Once steady state conditions were reached the maximum temperatures were recorded, at that point the compressed air pistol were activated with the maximum flow rate

available, from that moment over a thousand points were recorded while the temperature was dropping until steady state conditions were reached again.

Since the compressed air pistol generated a lot of vibrations on the system, the minimum temperature was fluctuating even when steady state conditions were achieved because the vibrations caused that the point where the compressed air met the adapter was varying a bit its position, thus the last 100 points were taken as steady state conditions and its average value was calculated and considered the minimum values, generating the table that is shown below.

Comment	T_{adap_front} (°C)	T_{adap_back} (°C)	R_{HSI} (mohm)
StartConditions_air	33,5	33,5	
Max_Temperatures_air	182,1	107,1	786,3
Min_temperatures_air	113,2	46,5	740,9

Table 9. Compressed air test results; 5.4 V applied

Once again the results are shown in a graph to easily be compared:

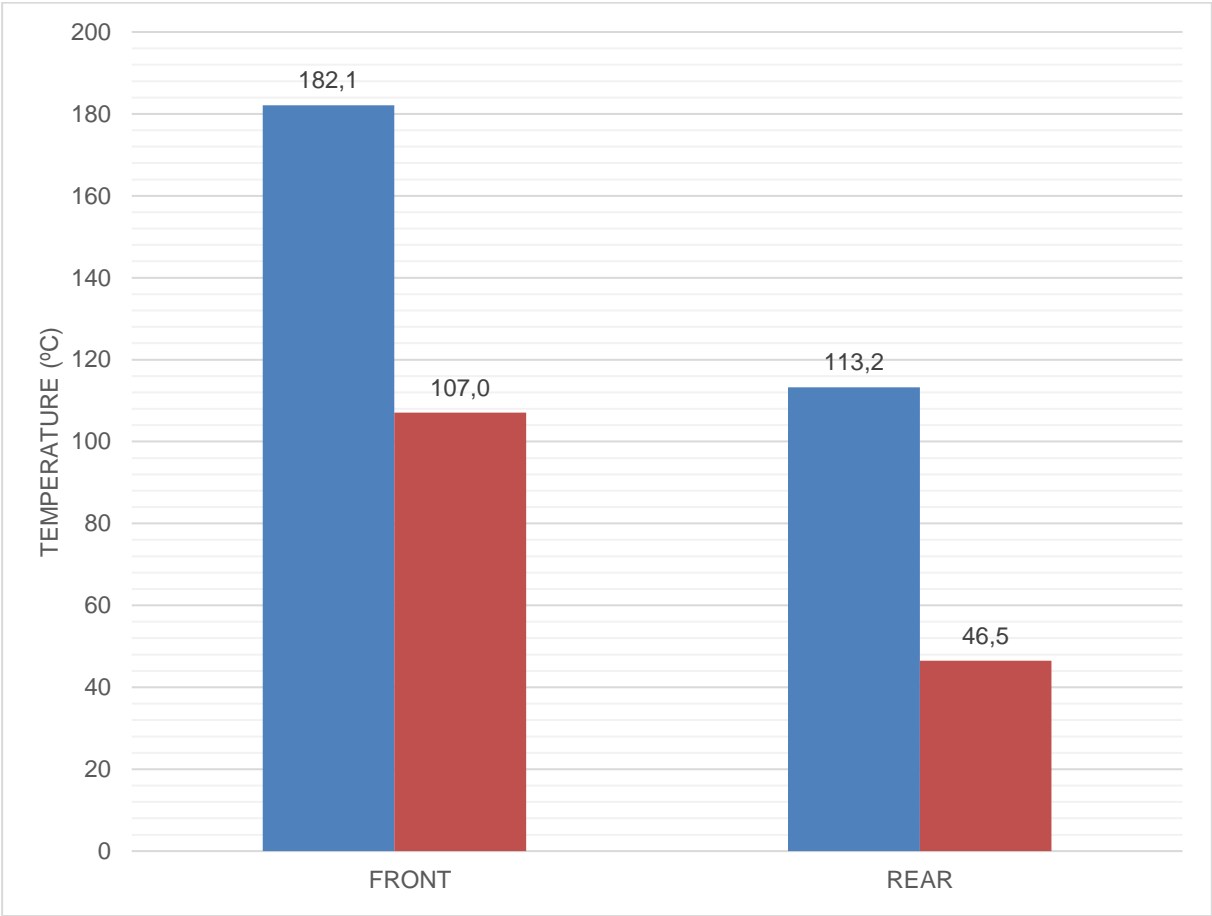


Figure 49. Compressed air test results with 5.4 V applied; on the left set maximum and minimum temperatures for the front part of the adapter; on the right values for the rear part.

If the results of the Graph above are compared with those of *Figure 46*, it can be seen that the compressed air achieved a higher decrease on the T_{adap_front} , exactly of around 69 °C achieving a minimum temperature equal to 113 °C way lower than the 155 °C achieved before, which is the aim of the cooling system. While the desired temperature of 100 °C was not achieved, this test shows the maximum reduction of temperature that we could achieve with the cooling medium that we had available, so it has been shown that the desired temperature could not be achieved neither with water or compressed air.

3.4 Chosen Design

Due to not having enough space to design a cooling system placed closer to the area of T_{adap_front} the experimental results that haven been just shown were considered to be the maximum reduction of temperature that we could achieve. The only way to look for a better solution, with air or water applied directly at that area, would be to suppress both the sapphire and the thermocouples, which are one of the key points of this project.

It was scientifically shown that the water cooling for this project was not a suitable option, so the cooling system with compressed air as cooling medium was finally chosen (*Air cooled: Model N°6*).

By using compressed air, the thermocouples and optical fiber for the sapphire would need a protective sleeve as the one that was designed for the previous adapter, named as shell. Also, since space for the cooling system was not needed on the adapter more thermocouples could be added, coming up with the idea shown in the next figure which is based on the Model N°6.

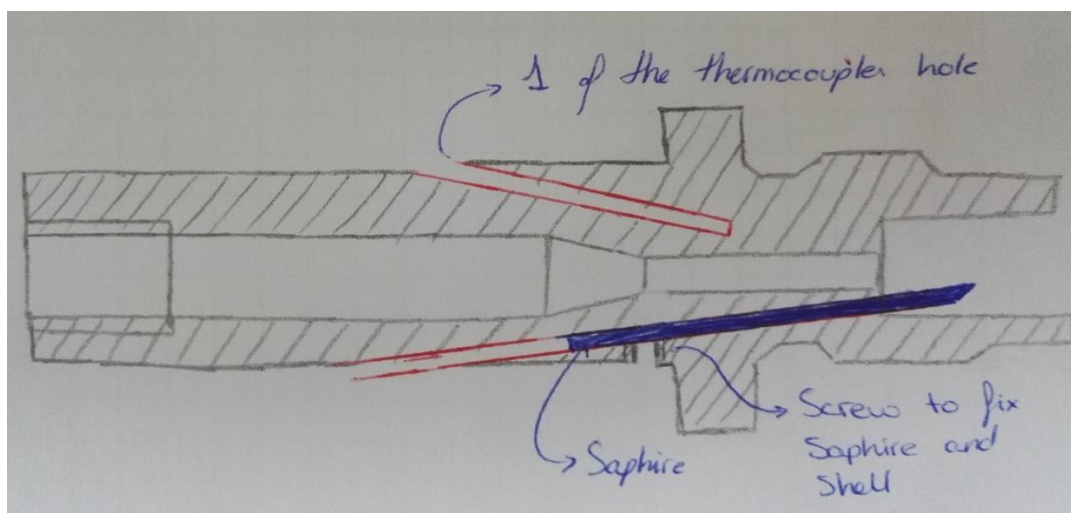


Figure 50. Initial sketch of the final solution

Since this time we had more space to play with, the thermocouples chosen for this design were the ones with a diameter of 1.5 mm instead of the ones used on the old design which had

0.5 mm, thanks to this the thermocouples would not break as easily as before, when placing the adapter on the engine block. Furthermore, more cavities for thermocouples were added, each having different depth being able this way to create a gradient of temperatures over the desired area of the adapter.

For the sapphire a bigger cavity was designed, while the sapphire selected had a diameter of 1.2 mm its cavity would have 1.5 mm having more space for the glue needed to place the sapphire and, furthermore, in order to ensure that the sapphire could not be moved due to the vibrations of the engine block, a small hole was made in order to place a little screw that would fix both the sapphire but also the shell. Taking advantage of this fact, another small hole was made on the adapter's body, so another little screw could be placed to completely fix the shell when mounted on the adapter, avoiding this way the use of glue like the older adapter, and thus being easier to assembly and disassembly the whole set of pieces.

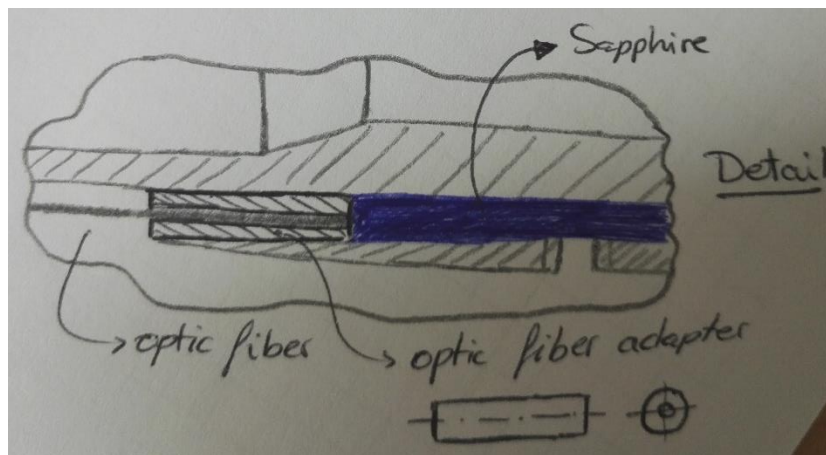


Figure 51. Concept for the optical fiber's adapter that would be inserted on the hole

The following pictures show the 3D model of the adapter and the rest of the parts once they were designed:

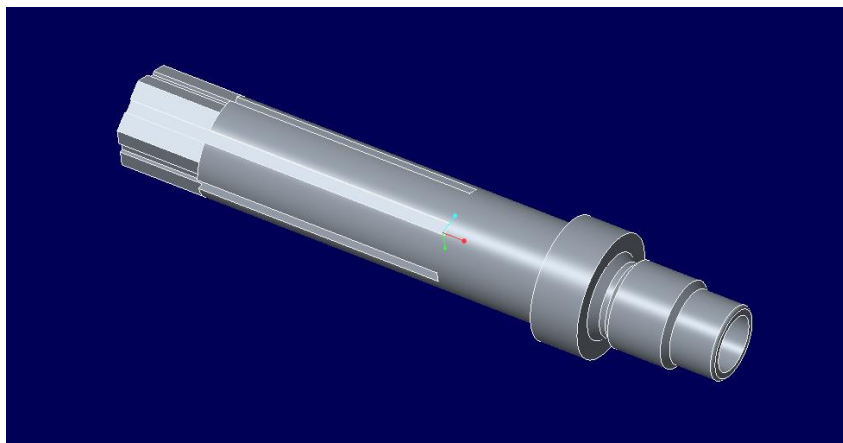


Figure 52. 3D model of the designed adapter

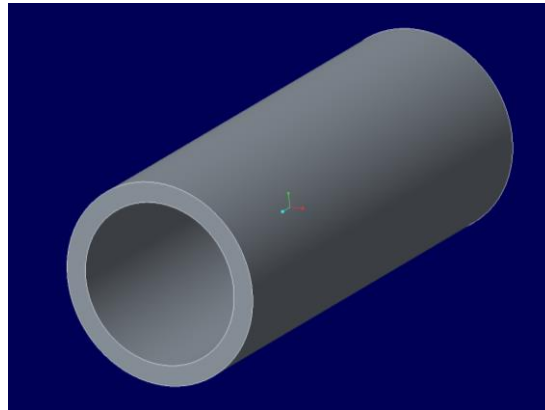


Figure 53. 3D model of the shell for the adapter

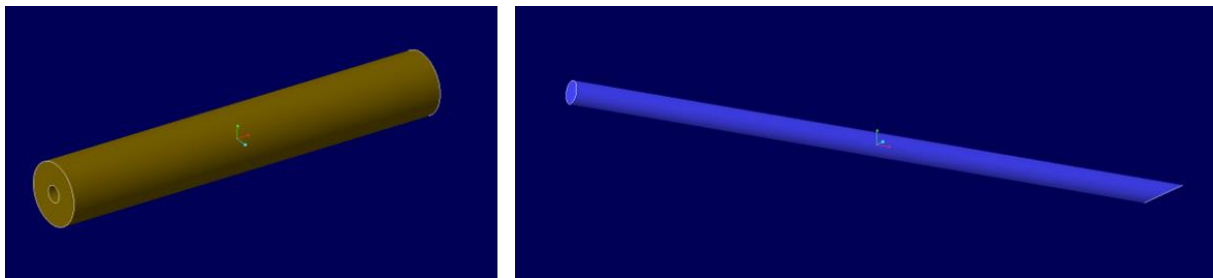


Figure 54. 3D model of the optical fiber adapter on the left; 3D model of the sapphire on the right

The only extra parts needed for the cooling system will be the compressed air supply, already available at the laboratory, the pipes and the FCV ; since the compressed air would be directly applied at the adapter while working on the engine block as it was previously discussed.

4 Manufacturing Plan

With the best possible solution for the new adapter's design chosen, the manufacturing processes needed to be chosen. While deciding the best strategy for manufacturing the adapter, failures could be found and thus corrected, since the adapter was not manufactured yet and changes could be added.

The adapter was divided in to two different parts, the adapter without „measuring techniques“ and the adapter itself, being the difference between them that the adapter without „measuring techniques“ would not have the holes for the thermocouples, the hole for the sapphire or the holes needed for the Shell; or in other words, this adapter would not have any of the characteristics needed to complete the final assembly. This was done in order to have an adapter that could be machined if the manufacturing process of the measurement characteristics was not the one expected. So, in order to manufacture the desired pieces, first the adapter without „measurement techniques“ would be machined and then it would be machined once more, to finally obtain the adapter itself with all the characteristics needed.

4.1 Adapter without the measuring techniques

The adapter shown in *Chosen Design* was further developed, and as it has been mentioned before split in to two parts.

The adapter without measuring techniques is shown in the next figure.

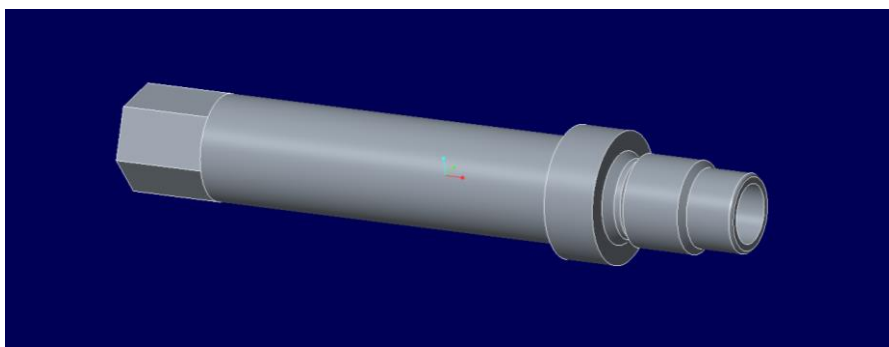


Figure 55. 3D model of the adapter without "measuring techniques"

As it was explained, this part would be the first step in order to manufacture the final version of the Adapter with all of its characteristics. The technical drawing for this part is shown in *Appendix A. 1* and *Appendix A. 2* ; as it can be seen the manufacturing process needed for this part were not too special, starting from a metallic bar some standard process needed to be used, like turning, milling and drilling. The manufacturing plan generated for this part is shown in *Appendix B. 1*.

The only difficulty for this manufacturing process would be the process described there as: iterative drilling. One of the mandatory requirements for the manufactured adapter, would be

the 10 mm distance that is shown on that document. In order to achieve this length, the glow plug should be screwed with the torque $M= 10 Nm$ required into the inner holes that were previously machined as described, once it was screwed, the length between the tip of the glow plug and the surface indicated should be measured, and if the 10 mm were not achieved, the drill should be repeated again, this time with a higher depth, repeating this process until the 10 mm were achieved, by drilling in small steps.

As can be seen in *Appendix A. 2*, the concentricity of the inner characteristics was imposed with a geometrical tolerance, and thus it should be manufactured following that standard, to avoid the problems previously mentioned on this project.

Once the adapter without „measurement techniques“ was completely manufactured, the following parts could be manufactured as well.

4.2 Extra Parts for the final assembly

The first extra part needed for the final assembly would be the protective sleeve that covers the adapter's body and thus the thermocouples and optical fiber, named the Shell of the adapter. The final design for this part is shown in the next figure. As a remark, the colors added on the surfaces of these parts were given to differentiate better the different parts in the final assembly of the adapter. See *Figure 56*.

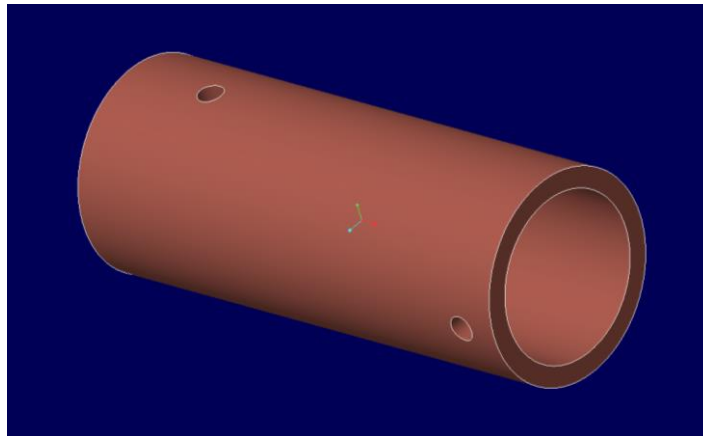


Figure 56. Final 3D model of the adapter's shell

Two extra holes were added to the design of the shell in order to fix it to the adapter body without using glue. The technical drawing for this part is included in *Appendix A. 3*; as it can be seen this part had not any difficulty for its manufacturing process, so no specific plan was created for it. Just starting from a metallic bar, some holes needed to be drilled and afterwards the finishing operation to achieve the fit tolerances required, as the technical drawing shows.

As an important remark, the two small holes that are drilled on the shell, need to be drilled before having the adapter with all its characteristics, thus they can be used as pattern to drill the same required holes in the adapter itself.

The following extra part that would need to be manufactured, is the small adapter that would connect the optical fiber with the surface of the sapphire, making this way the connection with the pyrometer possible. The technical drawing for this part is included in *Appendix A. 4A* as it has been said with the shell, this part would not need any specific manufacturing process and thus any specific manufacturing plan was created. As an important note, the small hole that needs to be drilled need to have really tight tolerances since it would be the one incharged to place the optical fiber. The final extra part needed for the whole assembly would be the sapphire, which in this case would be manufacture by an external company.

Both 3D models for these parts can be seen in *Figure 54*.

4.3 Adapter with all the required characteristics

Once the initial part for the adapter is manufactured, and the Shell has the small holes on it, the manufacturing process for the final adapter could start.

Since it has been shown through the different pictures of the solution, the holes for the thermocouples and the sapphire have some degree of inclination with respect the axis of the adapter, making them this way hard to be manufactured. At first, EDM (electrical discharge machining) process was selected for the machining of the holes, but this manufacturing process would be really expensive since it must be done out of the University, at the Industry; thus standard drilling was the process selected in order to achieve these holes, but as can be deduced, to manufacture such small holes with 6° of inclination would not be an easy task.

In order to check if the drilling machine available at the University was able to manufacture these holes without collapsing with the adapter's body, a 3D model of the drill chuck was created. See *Figure 57*.



Figure 57. Drill chuck of the drilling machine

After the 3D model of the drill chuck was created, drill bits were tested in order to find the needed length for the drill bit that would ensure that it would not collision with the adapter's body while the manufacturing of the holes were taking part.

After several trials, it was found that the standard length of the drill bit that would make the holes was 100 mm, with a diameter of 1.5 mm. And in order to facilitate things, the hole needed for the sapphire should be manufactured from above. See *Figure 58*.

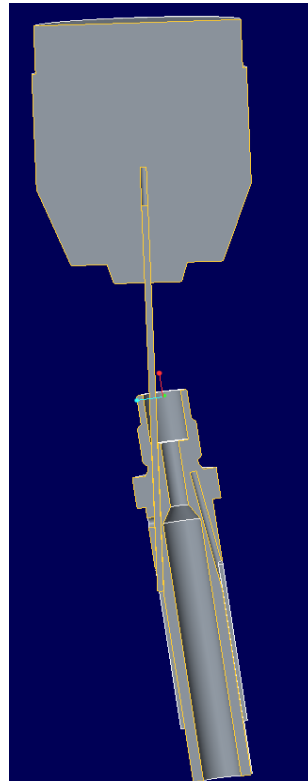


Figure 58. Example on how the hole for the sapphire should be manufactured

The following step would be to check if the thermocouples could be manufactured with the same drill bit as the sapphire.

When discussing the manufacturing process with the workshop at the University, it was concluded that some extra features should be included on the adapter's design in order to be able of centering the drill bit encharged of manufacturing the thermocouples' holes. For this reason a milled surface was added to the initial design to create a 90° plane with respect to the axis of those thermocouples' holes. By machining these surfaces, the drill encharged to manufacture the holes for centering the drill bit would have enough space to be placed. See *Figure 59*.

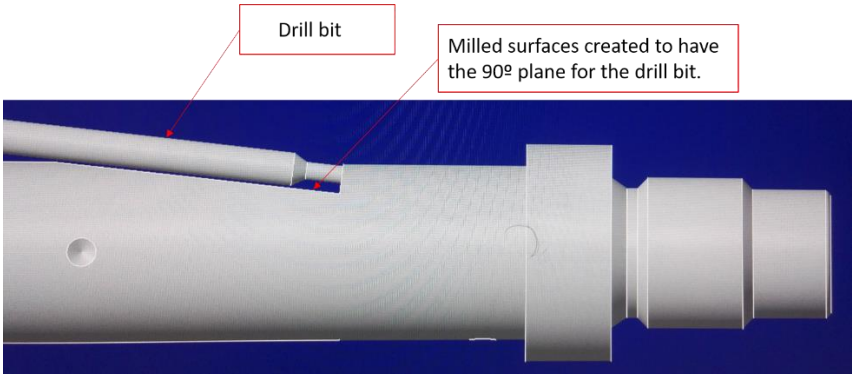


Figure 59. 3D model showing the drill bit correctly placed thanks to the new milled surfaces

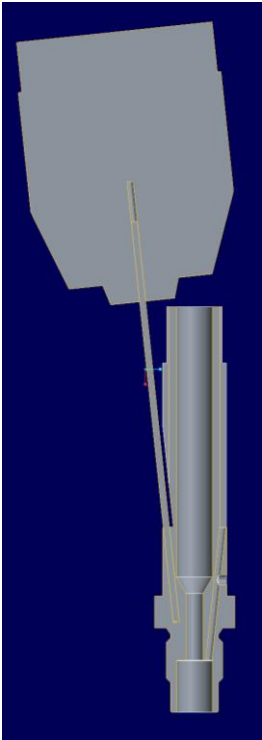


Figure 60. 3D simulation of how to manufacture the thermocouples holes

Once this was checked with the 3D model, as can be seen above, the final design for the adapter was obtained by adding these new milled surfaces.

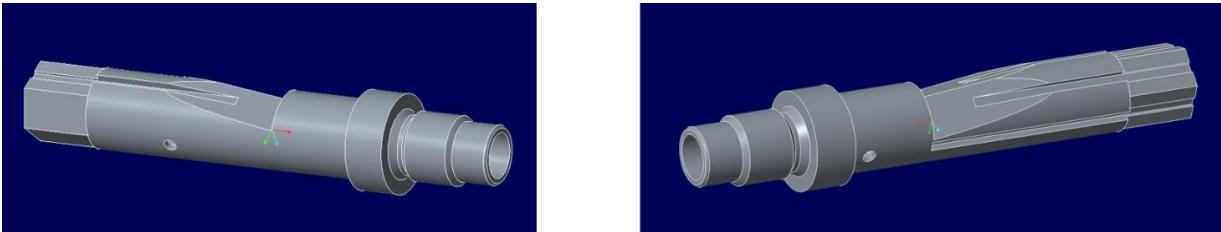


Figure 61. Different views of the final adapter's design 3D model

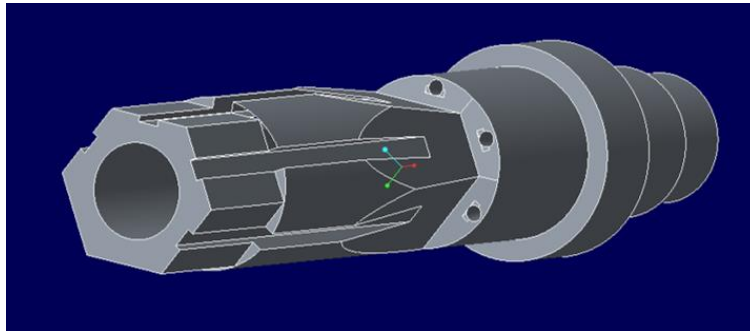


Figure 62. Rear view of the final adapter's design 3D model

The manufacturing plan for this last version of the adapter is included in *Appendix B. 2*. As can be seen in this document the only important remark now to take into account, would be to use the holes of the shell as a pattern to create the same holes on the adapter, if it were not done like this, some manufacturing failure could occur, for example that the center of one hole of the shell was not exactly at the same place as the same hole in the adapter, which would mean that the adapter could not be assemble. The technical drawing of this final version for the adapter is included in *Appendix A. 5*, *Appendix A. 6* and *Appendix A. 7*

5 Assembly of the adapter

Once all the individual parts are manufactured, the assembly of the entire adapter should be carried out. In order to successfully assemble it, the following steps should be carefully followed:

- 1- Insert the glow plug in the adapter using the torque wrench with $M=10\text{ Nm}$, to place the tip of the CGP 10 mm away from the surface mentioned in its manufacturing plan. See *Figure 63*.

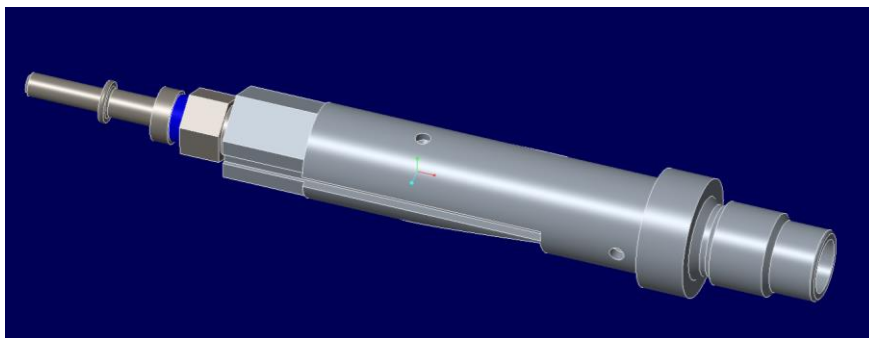


Figure 63. First step for the assembly of the adapter

- 2- In order to be able to place the sapphire in its hole, some high temperature resistant glue should be inserted on this hole.
- 3- With the help of a small block, insert and place the sapphire in the desired position as can be seen in the next figure. Thanks to this block, the adapter will be centered while the sapphire is placed and any failure due to this would be avoided. See *Figure 64*.

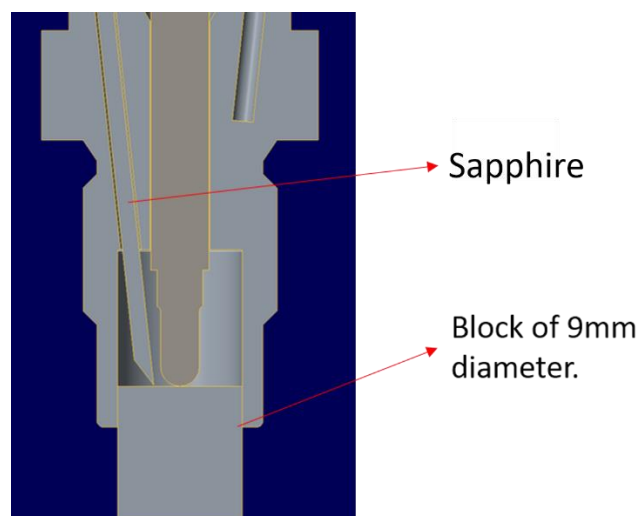


Figure 64. Third step for the assembly; Section view to show how perfectly place the sapphire on its position with the help of the block shown in the figure

- 4- If needed, insert more glue into the sapphire's hole using the small side-hole manufactured for the screw that will fix both, sapphire and shell.
- 5- Insert the thermocouples carefully on its correspondent hole; since these holes have different depths, label the thermocouples when inserted so they can be easily recognised.
- 6- Insert the adapter of the optical fiber at its location on the sapphire's hole, afterwards, introduce the optical fiber to complete the contact between it and the sapphire, creating this way the connection with the pyrometer. See *Figure 65*.

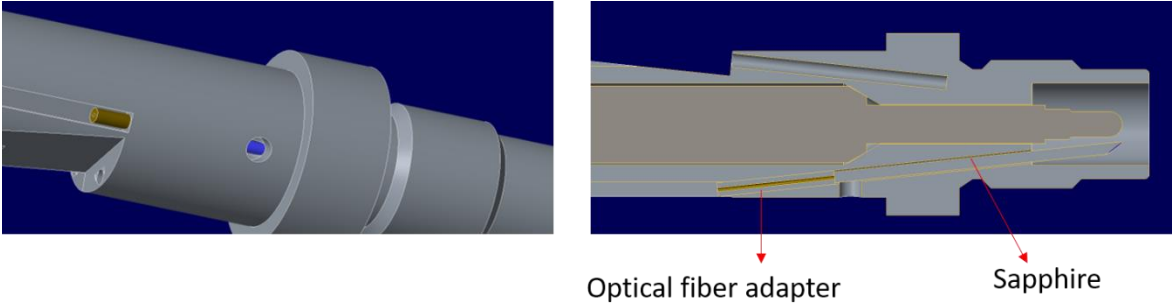


Figure 65. Sixth step of the assembly: on the right , cut view to show the contact between the saphrire and the optical fiber adapter

- 7- Place the shell on its position carefully and screw the two small screws. Once this has been achieved the whole assembly of the adapter would be completed. See *Figure 66*.

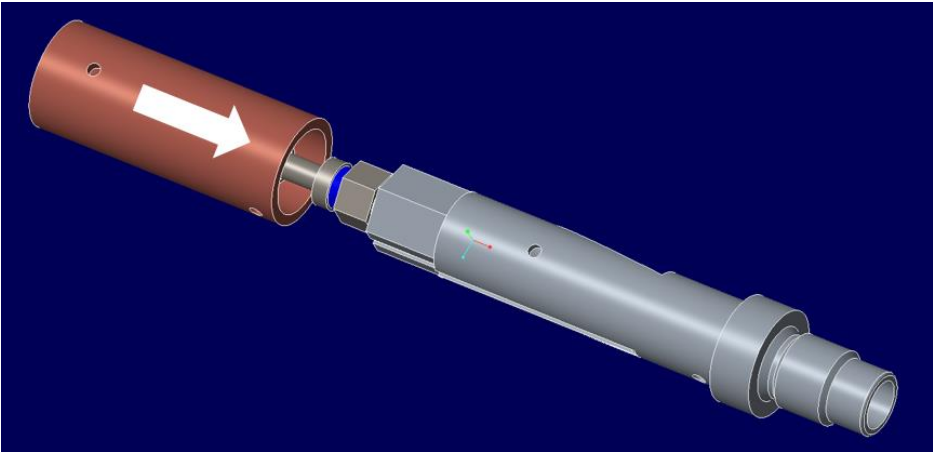


Figure 66. Shell of the adapter being placed on its position

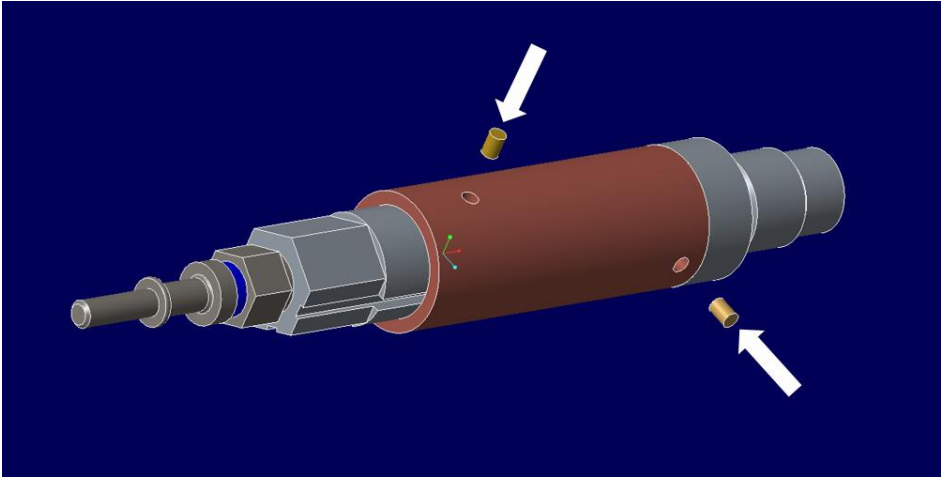


Figure 67. Last step of the assembly; Screws being placed on their position

The complete final assembly of the adapter is shown in the next figure, and as it can be seen, a ring is placed on the threaded part of the adapter in order to ensure its assembly on the engine block. This assembly is shown as well in Appendix A. 8.

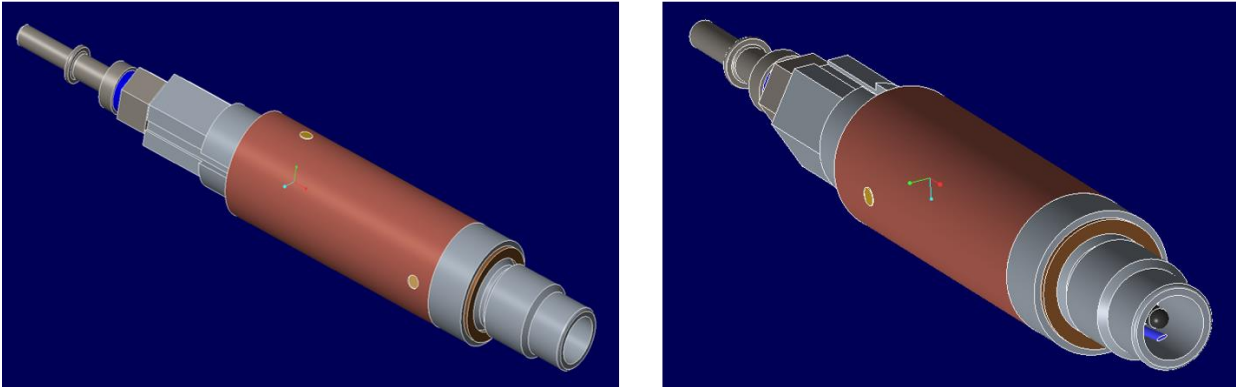


Figure 68. 3D model of the final assembly of the adapter

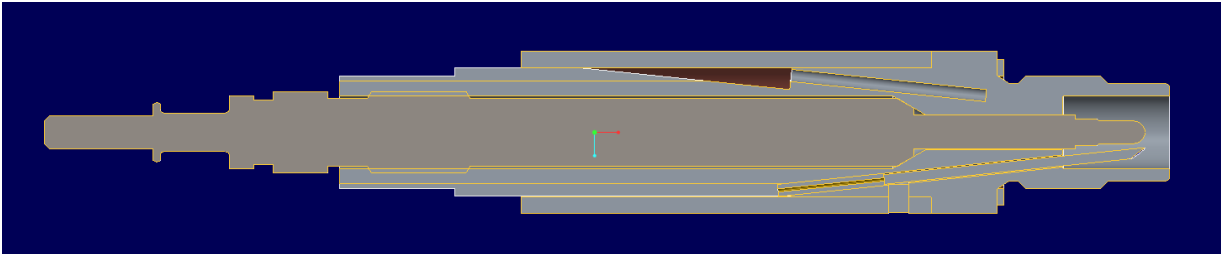


Figure 69. Cut view of the final assembly of the adapter

6 Conclusions

The research concerning the thermo-electrical behaviour of the different glow plugs gave a sufficient amount of data to develop the design of the new adapter and further experiments. The new adapter design includes a cooling system as it was required for the development of this project, but it has been shown that the expectations regarding the decrease on temperatures of the adapter can not be achieved due to the limitation of space that this project has worked with. Due to this fact, the water cooling was not a valid option for this project because it generated not enough disipation of heat, so the air was chosen as cooling medium.

With compressed air applied directly to the adapter when it is inserted in the engine's block, the achieved cooling would be significantly bigger as that achieved if water was used. With this cooling system one of the goals of this project was completely fulfilled.

Thanks to the design phase of this project, not only the cooling system was ensured, but a good measuring system for the temperatures as well. With the new design for the sapphire and thermocouples holes, sufficient amount of data would be extracted for following researches, and due to the final design chosen, it would be relatively easy to change the optical fiber if needed thanks to the adapter added for it, which will ensure the connection needed between it, the sapphire and the pyrometer too. Due to the fact that the shell is screwed to be fixed to the adapter, the maintenance of this device would be easily done, which would help to detect possible failures of this conditioned sensing adapter before they occurred, increasing this way the useful life of the adapter.

Since the sapphire is not longer completely enclosed on the adapter's body, the deposition of particles would not longer be a problem, and the temperature at the tip of the glow plug would be accurately measured thanks to the sapphire being placed right next to this area; furthermore, since the concentricity of the inner diameters is ensured with this design, the problem with some glow plugs being stuck on the adapter (causing the marks, previously exposed) would be completely solved, so the adapter would ensure a long time of operation without having problems as the ones that had occurred before the development of this project.

It has been shown that the limitation of space causes that not too many cooling systems can be studied, for future researches it would be an option to develop two different adapters, one having the measuring system for one kind of experiments, and the other one having the cooling system for another type of them, this way the cooling system could be included right next to the area of heat generation which was impossible in this project due to the thermocouples and sapphire internal holes.

Summary

The aim of this bachelor's thesis is to design a conditioned sensing adapter for Hot Surface Ignition (HSI) Systems, which will be used to test different ceramic glow plugs (CGP) while they are under operation inside the engine. This new adapter must be able to measure both the temperature of the CGP's tip and the temperature at the inside of the adapter, while having a cooling system at the same time. In order to measure the temperature at the CGP's tip a pyrometer will be used, so the adapter must include a sapphire, it being the lens for the measuring device.

As a first step for this thesis, a literature survey was carried out in order to get a general overview of what are glow plugs used for and which are the main differences between them. Once this survey was finished the experimental research to understand the thermo-electrical behaviour of the glow plugs could start, this experimental research was part of a research project *Analysis of the Thermo-electrical Behaviour of Ceramic Glow Plugs by Alejandro Lombardía González*, this research project was the source of all the experiments presented in this thesis before the start of the design phase for the new adapter and started with building a test bench that ensured the repeatability of the results. With this experimental research, the cold resistances of all the glow plugs available at the laboratory were determined, it was shown also the main source of resistance in a glow plug being this, its ceramical part; the relationship between the temperature of the adapter and the cold resistance of the glow plug was also studied. The aim of this experimental research was to extract all the information possible for the adapter's new design, so an experiment to show the temperature distribution along a glow plug was carried out to fully understand how the heat generation occurs and how the temperatures are distributed. For this last experiment, a thermal camera was used to obtain as much thermal images as possible.

Once this experimental research was finished, it was understood that the part closer to the tip of the glow plug was the one that had to be cooled, due to the fact that the temperatures on the rear part of the glow plug were not as high. As a first step for the designing phase of the new adapter, the old design was analyzed to detect the possible improvements that could be done in order to get a better version of this device. After analyzing the old adapter, a new concept for the measurement of the tip's temperature involving the sapphire and its location and shape was sketched for further implementation; since the last adapter had caused several problems in some glow plugs due to the lack of concentricity of its internal diameters this part of the adapter was subjected to study to change everything that was necessary so this will not happen again.

Several options for each characteristic of the adapter were derived after this first study of the old one, by a combination of these different options several models for the new adapter were developed being those divided in models which worked with water as cooling medium and models which worked with compressed air as cooling medium, being those two the only available cooling systems at the laboratory at the time of this thesis development.

After all the models were presented, an evaluation to decide which water model was the most suitable for this project was carried out, being the model nº5 the one selected, which concept included a copper coil with water flowing at its inside as cooling system. The other model chosen as possible solution was the compressed air one, which had as cooling system a pipe connected to a flow control valve and the air supply, aiming directly at the adapter's body when it is placed in the engine block. Since there were two cooling mediums involved in this design, both were submitted to experiments to find out which would be the best solution for the cooling system of the new adapter.

For the experiments that had to do with water as cooling medium, the results were not as good as the ones expected, because the decrease on temperature achieved was not really high even when applying copper paste to the copper coil and adapter's body to maximize the contact surface between them. After the experiments with compressed air as cooling medium were carried out, this model was selected as final solution, due to the fact that the results were better than those obtained with water.

These results obtained with water could not be improved, due to the fact that the metallic block that simulates the engine block has a low thermal resistance causing that the biggest part of the heat passes through this area and thus being this part of the adapter the area with biggest temperatures, no matter how cooled was the rear part of it, furthermore the results obtained on this thesis would be better than those obtained if tested in the engine block, because the temperatures there would be much bigger than those obtained on these experiments, which would cause that the water system will work even worse than expected. This adapter model needed two extra parts for the complete assembly of the adapter, being these a shell to protect the thermocouples and optical fiber placed on the outer surface of the adapter, and an optical fiber adapter to ensure the contact between the sapphire and the optical fiber itself.

With the compressed air model chosen as solution for the adapter's design, the manufacturing phase of the project could start. As a first step of this phase, the adapter was split in two parts the adapter without „measuring techniques“ and the adapter itself, being this adapter without „measuring techniques“ the first to be manufactured and afterwards, it would be submitted to machining to obtain the final adapter. The manufacturing plan for the adapter without „measuring techniques“ was developed without having major problems, afterwards the shell and optical fiber adapter would be manufactured.

Due to the fact that electro discharge machining could not be used to manufacture the holes for the thermocouples and sapphire of the adapter, they had to be manufactured by drilling, which would be really difficult due to the lengths of these holes and their small diameters. In order to drill these holes the outer surface of the adapter needed to have some extra milled surfaces so the drill bit encharged of center the holes could do its work, so the final design of the adapter was modified to this end as shown in this thesis.

Once the manufacturing plan for all the parts was successfully created, the steps for the correct assembly of the adapter were defined and presented at the end of this project.

Bibliography

- [1] Aalco;
http://www.aalco.co.uk/datasheets/Stainless-Steel-14301-Bar-and-Section_34.ashx
- [2] A. Veneziani, L. Formaggia, S. Micheletti, R. Sacco; Mathematical modelling and numerical simulation of a glow-plug, November 2006.
- [3] BERU; BERU Keramische Glühkerze, Ceramic Glow Plug CGP, July 2011.
- [4] BERU;
<http://beru.federalmogul.com/diesel-cold-start-technology/product-description/diesel-cold-start-products/glow-plugs/ceramic-glow-plug-cgp>
- [5] BERU;
<http://beru.federalmogul.com/diesel-cold-start-technology/product-description/diesel-cold-start-products/glow-plugs/ceramic-glow-plug-cgp>
- [6] Clemens Gühmann, Ramita Suteekarn, Marin Sackmann; High-Precision, Robust Cascade Model for Closed-Loop Control of Ceramic Glow Plug Surface Temperature in a Diesel Engine.
- [7] James S. Wallace, Stewart Xu Cheng; Transient Behavior of Glow Plugs in Direct-Injection Natural Gas Engines.
- [8] FLIR Systems;
<http://www.flir.de/>
- [9] Lombardía González Alejandro; Thermo-electrical Behaviour of Ceramic Glow Plugs, Karlsruhe 2017
- [10] NGK Manufacturer;
<https://www.ngk.de/en/products-technologies/glow-plugs/glow-plug-technologies/>
- [11] NGK Manufacturer;
<https://www.ngk.de/en/technology-in-detail/glow-plugs/glow-plugs-basic-principles/>

- [12] Patent; Method for manufacturing ceramic glow plugs US 7160584 B2;
<https://www.google.com/patents/US7160584>
- [13] Río Sastre, Javier; Entwicklung von Auswertestrategien und Durchführung von Versuchen unter Verwendung von kontrollierter Oberflächen-zündung in stationären Erdgasmotoren
- [14] Robert Bosch GmbH;
<https://www.boschautoparts.com/en/auto/diesel-parts/glow-plugs>
- [15] Robert Bosch GmbH;
http://www.boschaa.com.cn/media/parts/engine_systems__auto_parts/diesel__engine_systems/pdf_1/Gluehstiftkerzenfolder.pdf
- [16] Steinel Professional;
<http://www.steinell-professional.de/de/heissluft-kleben/heissluftgeblaese/hg-2120-e-faltschachtel.html>
- [17] VDM-Metals;
http://www.vdm-metals.com/fileadmin/user_upload/Downloads/Data_Sheets/Data_Sheet_VDM_Nickel_200.pdf

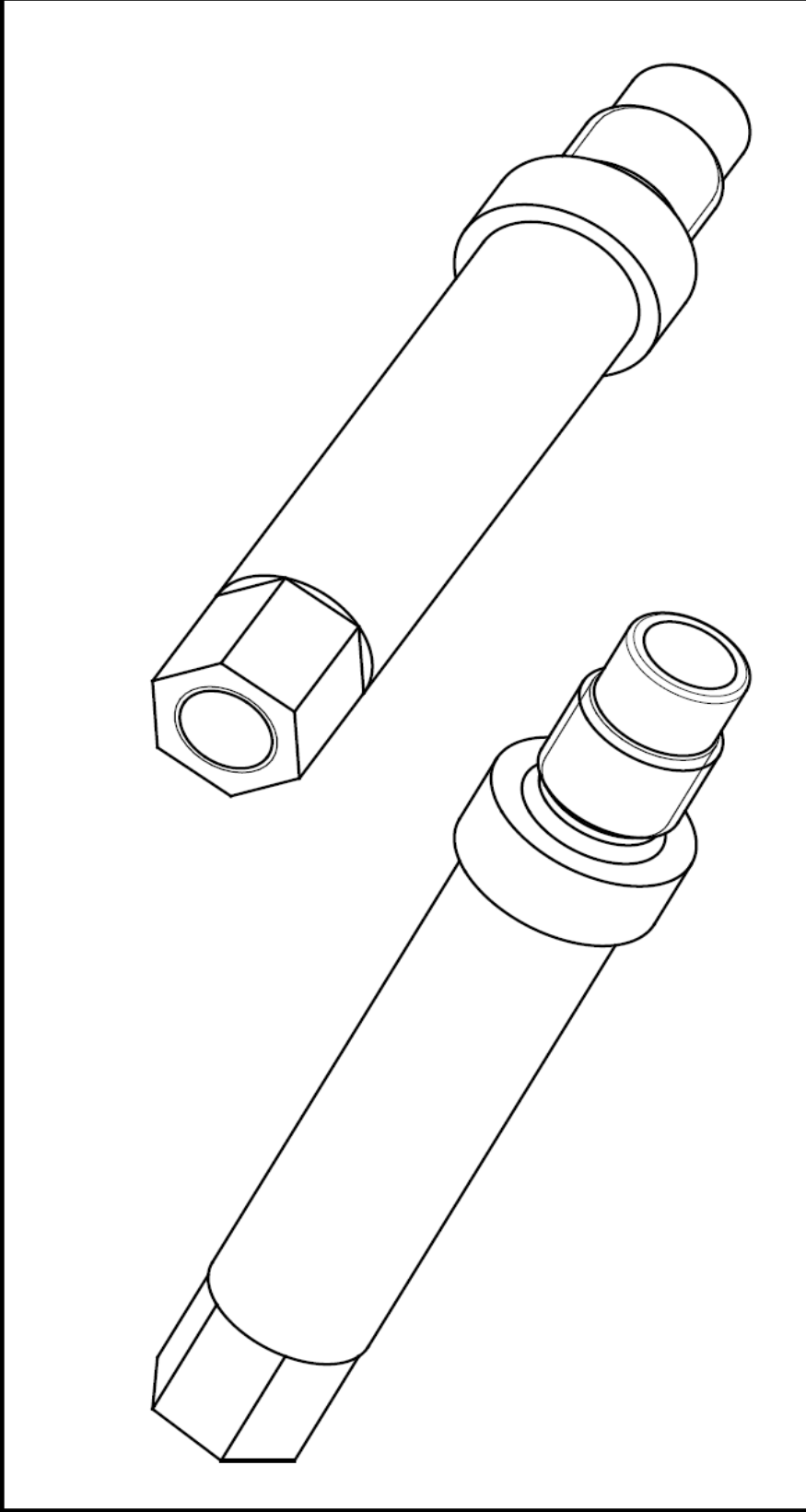
Table of Figures

Figure 1. General structure in product development.....	27
Figure 2. Different examples of locations for a glow plug [11].....	28
Figure 3. Example of a Glow Plug [10]	28
Figure 4. Exploded view of a Metal Glow Plug [10]	29
Figure 5. Exploded view of a SRC -CGP [10].....	31
Figure 6. Scheme of the circuit [9].....	32
Figure 7. Three views of the Test Bench used [9]	33
Figure 8. On the left, ADwin-Gold II, On the Right, ADWin-PRO II [9].....	34
Figure 9. Ceramic part of a CGP located at the inside of this shell [9].....	35
Figure 10. Inner metallic lead of a CGP [9]	35
Figure 11. Inner Metallic Lead connected for the tests.....	36
Figure 12. Hot air tool used on the experiments; Steinel Professional HG 2120E [16]	36
Figure 13. Location of the three measuring points.....	37
Figure 14. Hot air tool heating up the adapter.....	38
Figure 15. Ro variation with temperature of the adapter [9].....	40
Figure 16. Ro variation when adapter's temperatures decreases [9]	41
Figure 17. Thermal camera FLIR T460 used on this project [8]	42
Figure 18. Experiment set up for the thermal camera [9]	43
Figure 19. Thermal images of the CGP working showing the four used temperature points [9]	43
Figure 20. Thermal images at 5.4V: on the left CGP #10, on the right CGP #19 [9].....	44
Figure 21. Electrical resistance variation with the temperature of the CGPs for both glow plugs tested [9].....	45
Figure 22. Biggest Temperatures' generation area shown in an old adapter.....	46
Figure 23. 3D model of the adapter's assembly used until this project [13].....	47
Figure 24. Method used for measure the tip's temperature in the old Adapter [13].....	48
Figure 25. Scheme of the old sapphire's design with the deposition of particles problem	48
Figure 26. New concept for the sapphire design	49
Figure 27. Old adapter placed in an engine block.....	50
Figure 28. Scheme of adapter placed in the engine block.....	50
Figure 29. Important features of the CGP to take into account when designing the adapter...	51
Figure 30. Marks on the CGP after operation in the Adapter	51
Figure 31. Diameter that was changed to ensure that the marks will not happen again	52
Figure 32. Options for each characteristic studied for the design of the new adapter	53
Figure 33. Model N°1; On the right part the different parts of the adapter can be seen, on the lower part the water flow sketch can be seen.....	54
Figure 34. Model N°2; Extra parts for this model.....	55

Figure 35. Model N°3; On the upper part the adapter with the copper coil; on the lower part the shell needed and the sketch for the sapphire's hole	56
Figure 36. Model N°4; On the upper part the adapter with the copper coil is shown; on the lower part the machined surface of the adapter without the copper coil.....	57
Figure 37. Model N°5; On the upper part the adapter with the copper coil is shown; on the lower part the measurement techniques	58
Figure 38. Model N°6; in the upper part the pipe with the FCV is shown entering the engine block's cavity; on the lower part the possible design for the adapter is shown.....	59
Figure 39. Comparisson of models which water as cooling medium	61
Figure 40. Refrigeration unit used for the trials	62
Figure 41. Copper tubes being coiled around the metallic bar.....	63
Figure 42. Adapter with the copper coil being tested	63
Figure 43. Test tube used for measuring the volume of water	64
Figure 44. Result of the copper coil, as cooling method, test; on the upper graph results for the front part of the adapter; on the lower graph results for the rear part of the adapter	66
Figure 45. Copper paste being applied on the left; adapter mounted on the metallic block with the copper paste applied	67
Figure 46. Results of the water cooling when applying copper paste (Maximum contact surface); on the upper graph results for the front part of the adapter; on the lower graph results for the rear part	68
Figure 47. Heat distribution in the adapter when placed on the metallic block.....	69
Figure 48. Compressed air pistol facing the adapter during the development of this experiment	70
Figure 49. Compressed air test results with 5.4 V applied; on the left set maximum and minimum temperatures for the front part of the adapter; on the right values for the rear part.	71
Figure 50. Initial sketch of the final solution	72
Figure 51. Concept for the optical fiber's adapter that would be inserted on the hole.....	73
Figure 52. 3D model of the designed adapter	73
Figure 53. 3D model of the shell for the adapter	74
Figure 54. 3D model of the optical fiber adapter on the left; 3D model of the sahppire on the right	74
Figure 55. 3D model of the adapter without "measuring techniques"	75
Figure 56. Final 3D model of the adapter's shell	76
Figure 57. Drill chuck of the drilling machine.....	77
Figure 58. Example on how the hole for the sapphire should be manufactured.....	78
Figure 59. 3D model showing the drill bit correctly placed thanks to the new milled surfaces	79
Figure 60. 3D simulation of how to manufacture the thermocouples holes	79
Figure 61. Different views of the final adapter's design 3D model.....	79
Figure 62. Rear view of the final adapter's design 3D model	80

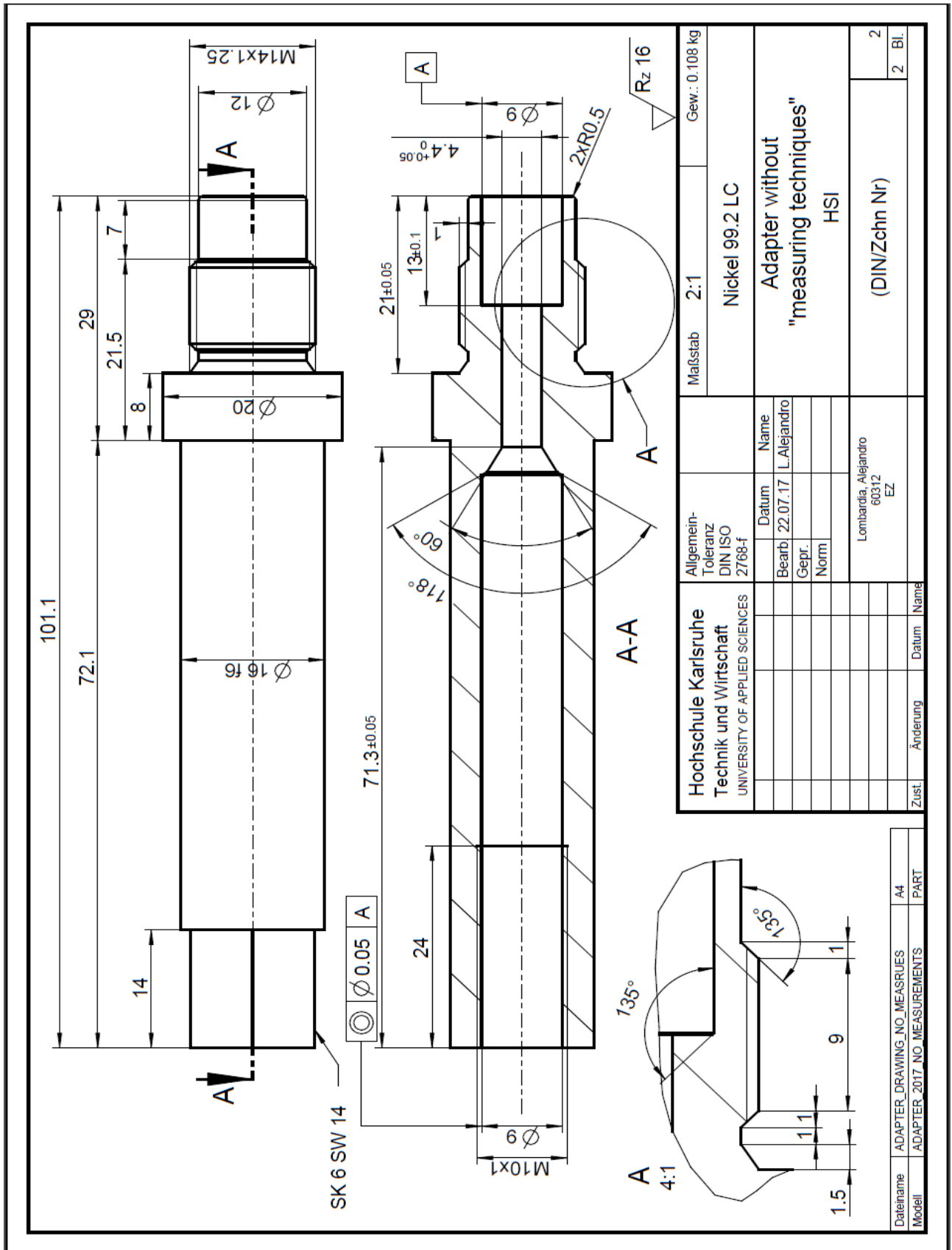
Figure 63. First step for the assembly of the adapter	81
Figure 64. Third step for the assembly; Section view to show how perfectly place the sapphire on its position with the help of the block shown in the figure	81
Figure 65. Sixth step of the assembly: on the right , cut view to show the contact between the sapphire and the optical fiber adapter	82
Figure 66. Shell of the adapter being placed on its position	82
Figure 67. Last step of the assembly; Screws being placed on their position.....	83
Figure 68. 3D model of the final assembly of the adapter	83
Figure 69. Cut view of the final assembly of the adapter	83

Appendix A: Technical drawings

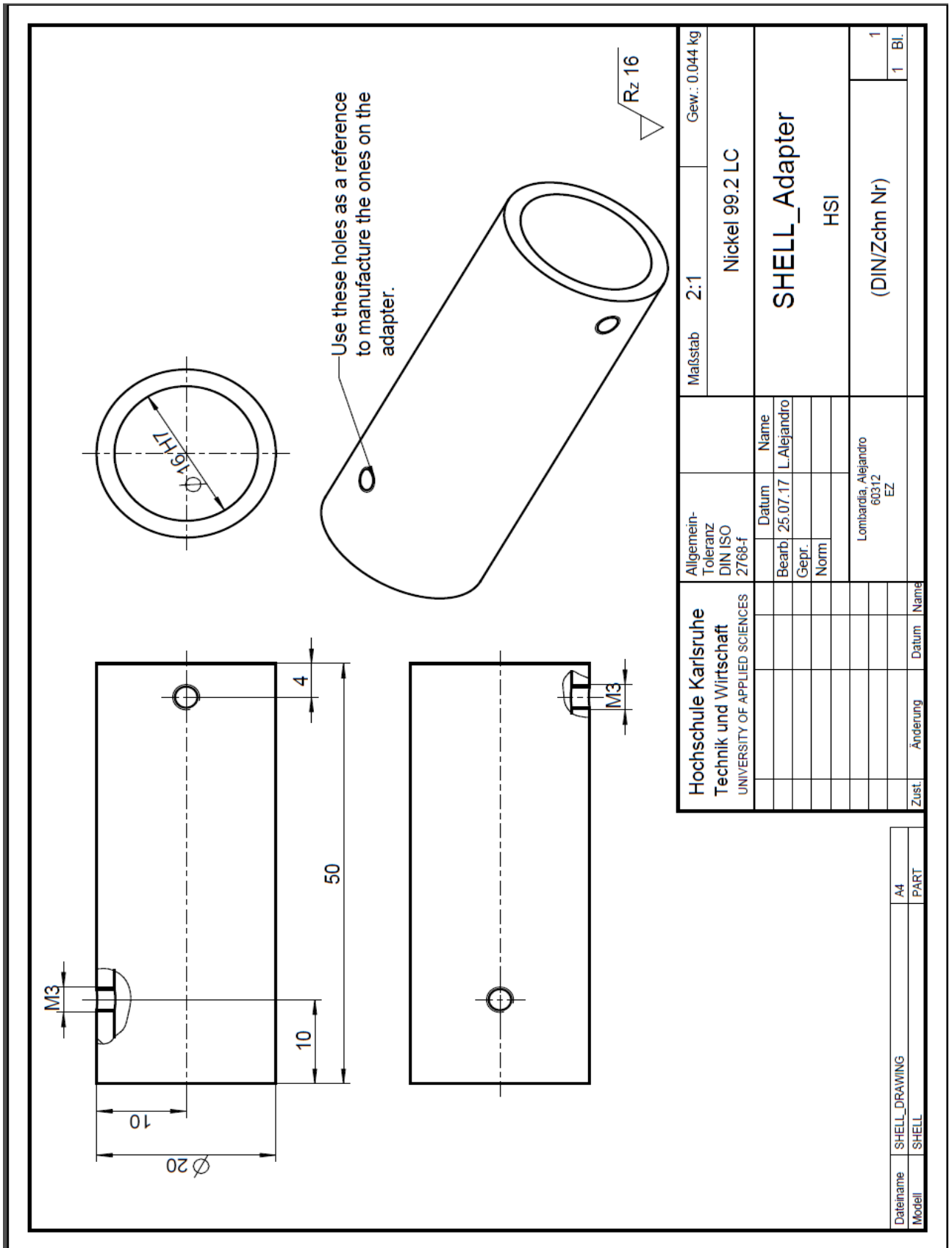


Hochschule Karlsruhe Technik und Wirtschaft UNIVERSITY OF APPLIED SCIENCES		Allgemein- Toleranz DIN ISO 2768-f		Maßstab 2:1		Gew.: 0.108 kg	
Datum		Name		Nickel 99.2 LC			
Bearb.		L.Alejandro		Adapter without "measuring techniques"			
Gepr.				HSI			
Norm				(DIN/Zehn Nr)			
Lombardia, Alejandro 60312 EZ				1		2 Bl.	
Zust.	Aenderung	Datum	Name				

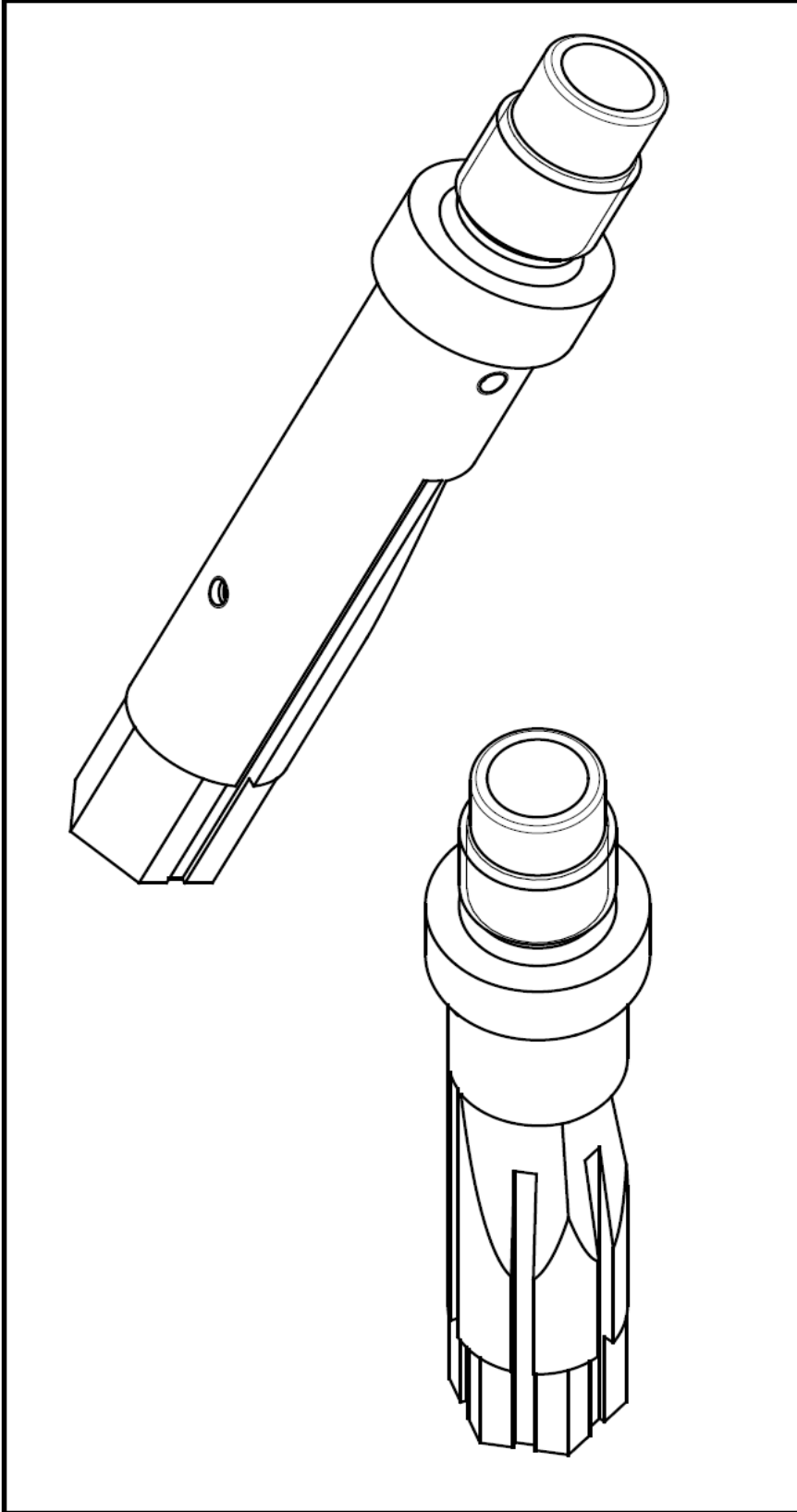
Dateiname	ADAPTER_DRAWING_NO_MEASURES	A4
Modell	ADAPTER_2017_NO_MEASUREMENTS	PART



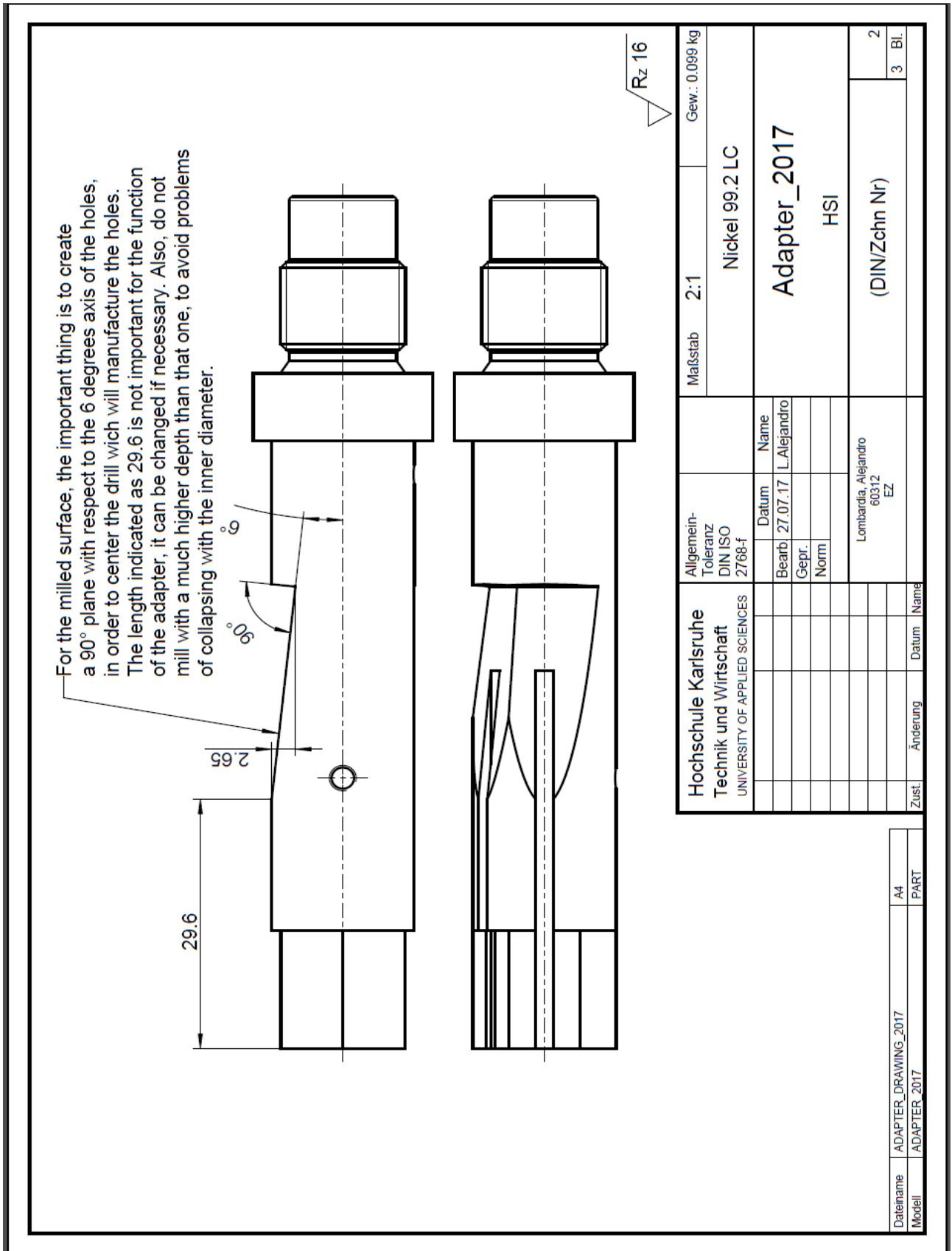
Appendix A. 2. Adapter without "measuring techniques" page 2 out of 2

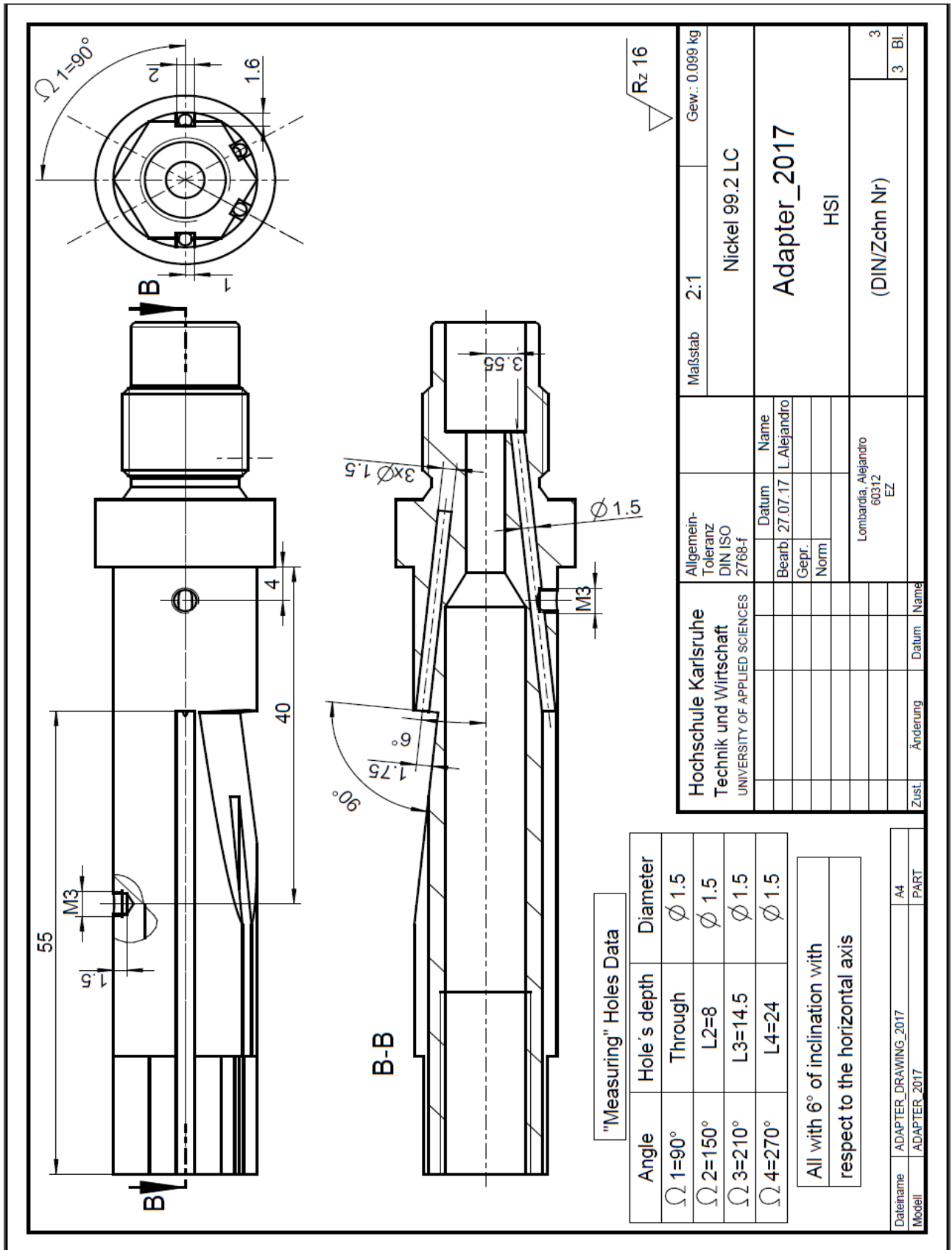


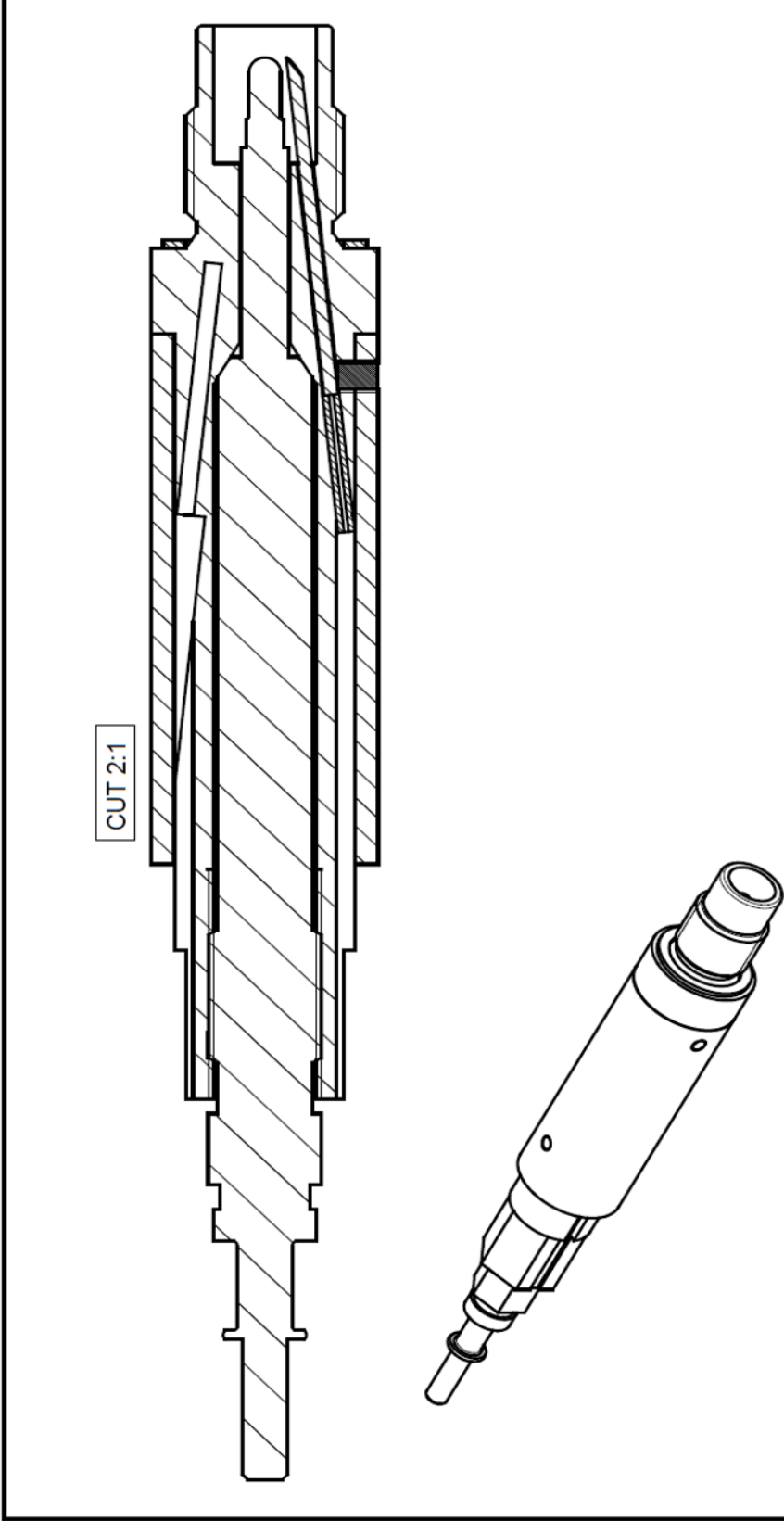
Appendix A. 3. Shell of the adapter page 1 out of 1



Hochschule Karlsruhe Technik und Wirtschaft UNIVERSITY OF APPLIED SCIENCES		Allgemein- Toleranz DIN ISO 2768-f		Maßstab 2:1		Gew.: 0.099 kg	
		Datum		Nickel 99.2 LC			
		Bearb: 27.07.17		Adapter_2017			
		Gepr.		HSI			
		Norm		(DIN/Zchn Nr)		1	
		Lombardia, Alejandro 60312 EZ				3 Bl.	
		Name					
		L.Alejandro					
		Datum					
		Name					
		Lombardia, Alejandro					
		60312					
		EZ					
		Name					
		Lombardia, Alejandro					
		60312					
		EZ					
		Name					
		Lombardia, Alejandro					
		60312					
		EZ					
		Name					
		Lombardia, Alejandro					
		60312					
		EZ					
		Name					
		Lombardia, Alejandro					
		60312					
		EZ					
		Name					
		Lombardia, Alejandro					
		60312					
		EZ					
		Name					
		Lombardia, Alejandro					
		60312					
		EZ					
		Name					
		Lombardia, Alejandro					
		60312					
		EZ					
		Name					
		Lombardia, Alejandro					
		60312					
		EZ					
		Name					
		Lombardia, Alejandro					
		60312					
		EZ					
		Name					
		Lombardia, Alejandro					
		60312					
		EZ					
		Name					
		Lombardia, Alejandro					
		60312					
		EZ					
		Name					
		Lombardia, Alejandro					
		60312					
		EZ					
		Name					
		Lombardia, Alejandro					
		60312					
		EZ					
		Name					
		Lombardia, Alejandro					
		60312					
		EZ					
		Name					
		Lombardia, Alejandro					
		60312					
		EZ					
		Name					
		Lombardia, Alejandro					
		60312					
		EZ					
		Name					
		Lombardia, Alejandro					
		60312					
		EZ					
		Name					
		Lombardia, Alejandro					
		60312					
		EZ					
		Name					
		Lombardia, Alejandro					
		60312					
		EZ					
		Name					
		Lombardia, Alejandro					
		60312					
		EZ					
		Name					
		Lombardia, Alejandro					
		60312					
		EZ					
		Name					
		Lombardia, Alejandro					
		60312					
		EZ					
		Name					
		Lombardia, Alejandro					
		60312					
		EZ					
		Name					
		Lombardia, Alejandro					
		60312					
		EZ					
		Name					
		Lombardia, Alejandro					
		60312					
		EZ					
		Name					
		Lombardia, Alejandro					
		60312					
		EZ					
		Name					
		Lombardia, Alejandro					
		60312					
		EZ					
		Name					
		Lombardia, Alejandro					
		60312					
		EZ					
		Name					
		Lombardia, Alejandro					
		60312					
		EZ					
		Name					
		Lombardia, Alejandro					
		60312					
		EZ					
		Name					
		Lombardia, Alejandro					
		60312					
		EZ					
		Name					
		Lombardia, Alejandro					
		60312					
		EZ					
		Name					
		Lombardia, Alejandro					
		60312					
		EZ					
		Name					
		Lombardia, Alejandro					
		60312					
		EZ					
		Name					
		Lombardia, Alejandro					
		60312					
		EZ					
		Name					
		Lombardia, Alejandro					
		60312					
		EZ					
		Name					
		Lombardia, Alejandro					
		60312					
		EZ					
		Name					
		Lombardia, Alejandro					
		60312					
		EZ					
		Name					
		Lombardia, Alejandro					
		60312					
		EZ					
		Name					
		Lombardia, Alejandro					
		60312					
		EZ					
		Name					
		Lombardia, Alejandro					
		60312					
		EZ					
		Name					
		Lombardia, Alejandro					
		60312					
		EZ					
		Name					
		Lombardia, Alejandro					
		60312					
		EZ					
		Name					
		Lombardia, Alejandro					
		60312					
		EZ					
		Name					
		Lombardia, Alejandro					
		60312					
		EZ					
		Name					
		Lombardia, Alejandro					
		60312					
		EZ					
		Name					
		Lombardia, Alejandro					
		60312					
		EZ					
		Name					
		Lombardia, Alejandro					
		60312					
		EZ					
		Name					
		Lombardia, Alejandro					
		60312					
		EZ					
		Name					
		Lombardia, Alejandro					
		60312					
		EZ					
		Name					
		Lombardia, Alejandro					
		60312					
		EZ					
		Name					
		Lombardia, Alejandro					
		60312					
		EZ					
		Name					
		Lombardia, Alejandro					
		60312					
		EZ					
		Name					
		Lombardia, Alejandro					
		60312					
		EZ					
		Name					
		Lombardia, Alejandro					
		60312					
		EZ					
		Name					
		Lombardia, Alejandro					
		60312					
		EZ					
		Name					
		Lombardia, Alejandro					
		60312					
		EZ					
		Name					
		Lombardia, Alejandro					
		60312					
		EZ					
		Name					
		Lombardia, Alejandro					
		60312					
		EZ					
		Name					
		Lombardia, Alejandro					
		60312					
		EZ					
		Name					
		Lombardia, Alejandro					
		60312					
		EZ					
		Name					
		Lombardia, Alejandro					
		60312					
		EZ					
		Name					
		Lombardia, Alejandro					
		60312					
		EZ					
		Name					
		Lombardia, Alejandro					
		60312					
		EZ					
		Name					
		Lombardia, Alejandro					
		60312					
		EZ					
		Name					
		Lombardia, Alejandro					
		60312					
		EZ					
		Name					
		Lombardia, Alejandro					
		60312					
		EZ					







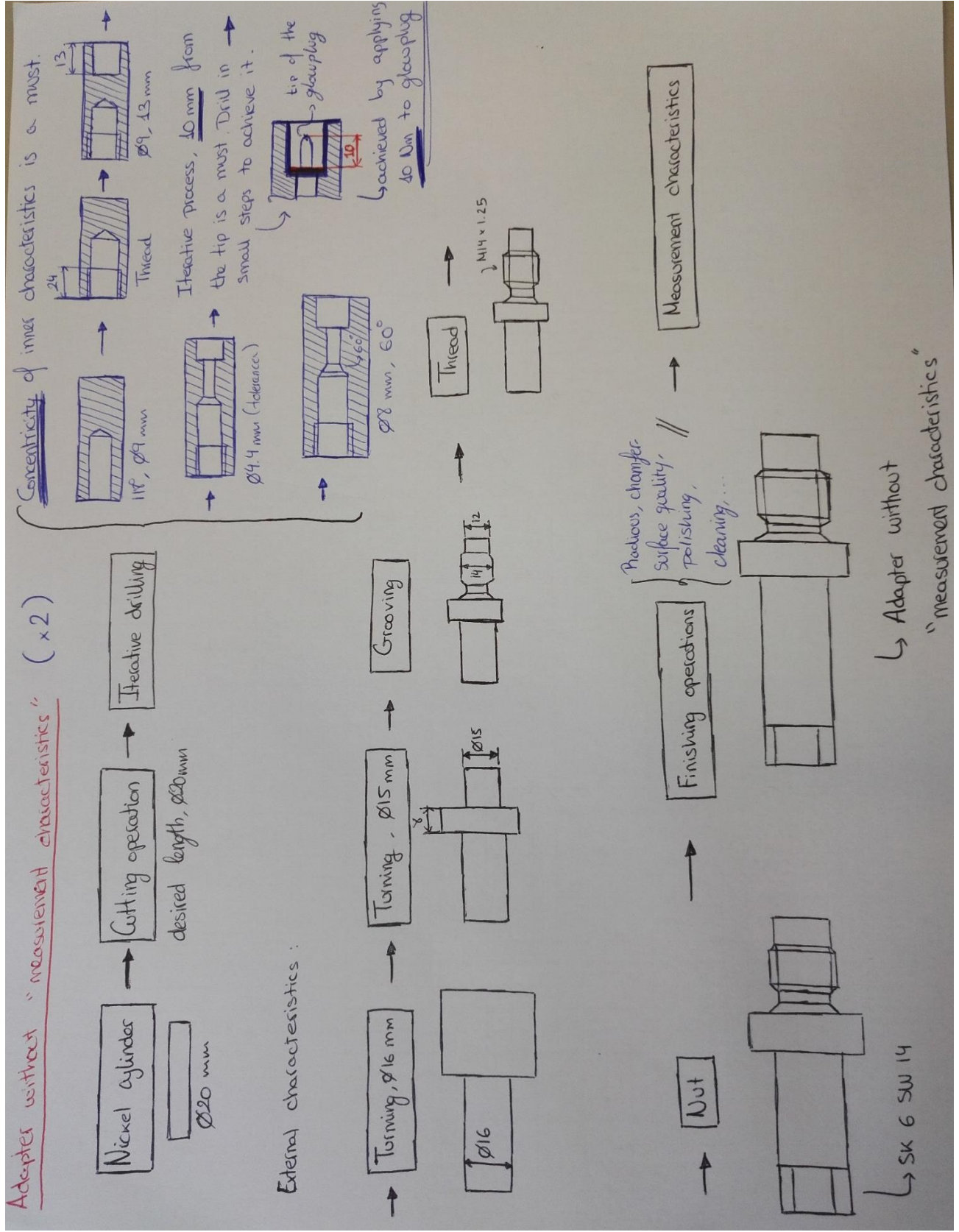
CUT 2:1

Hochschule Karlsruhe Technik und Wirtschaft UNIVERSITY OF APPLIED SCIENCES		Bearb.	Datum	Name	Maßstab	Gew.:
		1.08.17	L. Alejandro	1:1	0.190 kg	
					Assembly_Adapter	
					HSI	
					(DIN/Zchn Nr)	
					1	1
					1	Bl.

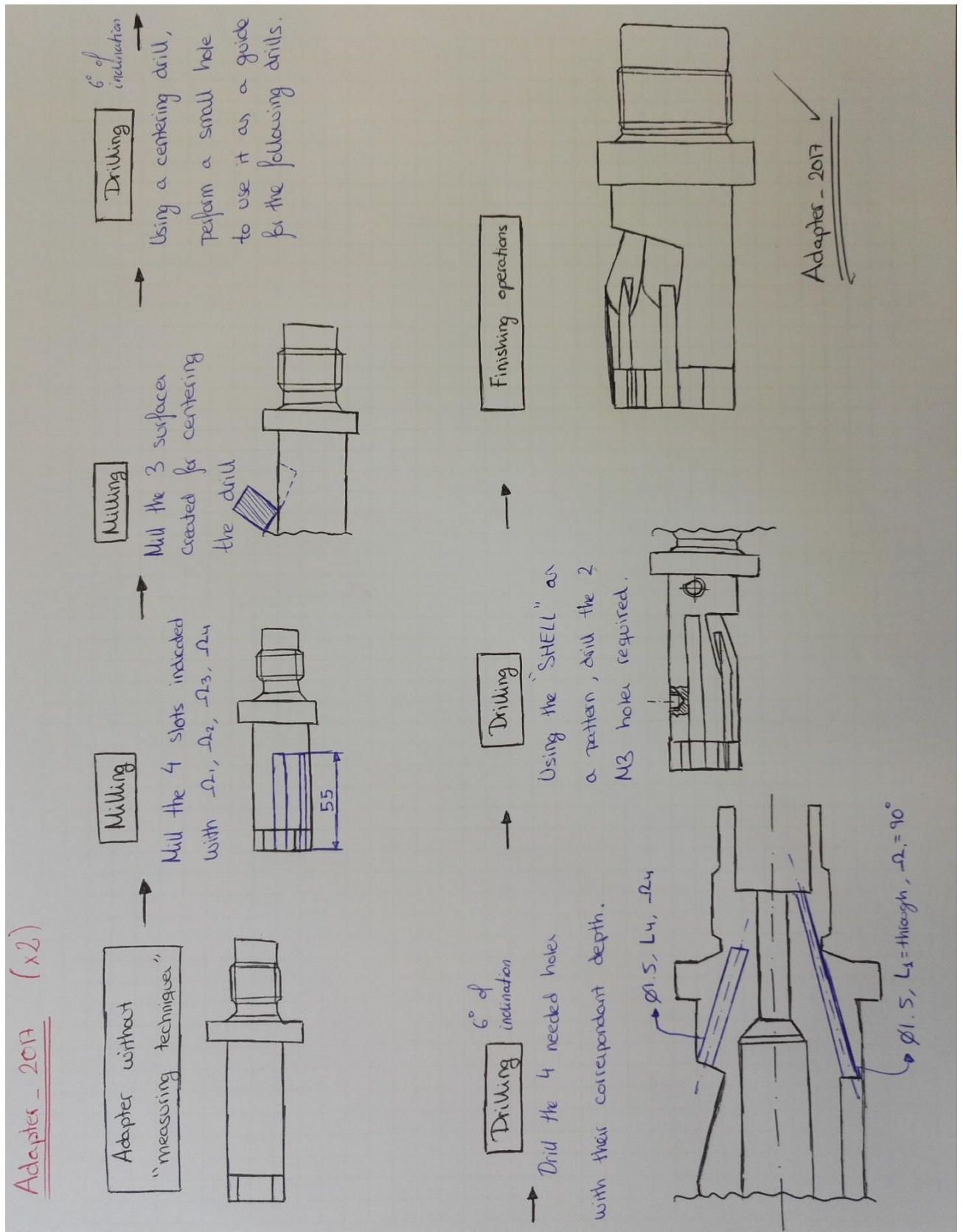
Dateiname	ASSEMBLY_DRAWING	A4
Modell	ASSEMBLY_ADAPTER	ASSEM

Appendix A. 8. Complete Assembly of the adapter, page 1 out of 1

Appendix B: Manufacturing Plan



Appendix B. 1. Manufacturing Plan for the adapter without "measurement techniques"



Appendix B. 2. Manufacturing plan for the adaper with all the characteristics